Austrian Journal of Technical and Natural Sciences

№ 1–2 2019
January–February

PREMIER
Publishing

Vienna
2019

Austrian Journal of Technical and Natural Sciences

Scientific journal

№ 1–2 2019 (January–February)

ISSN 2310-5607

Editorial office Premier Publishing s.r.o.
Praha 8 – Karlín, Lyčkovo nám. 508/7, PSČ 18600

E-mail: pub@ppublishing.org

Homepage: ppublishing.org

Austrian Journal of Technical and Natural Sciences is an international, German/English/Russian language, peer-reviewed journal. It is published bimonthly with circulation of 1000 copies.

The decisive criterion for accepting a manuscript for publication is scientific quality. All research articles published in this journal have undergone a rigorous peer review. Based on initial screening by the editors, each paper is anonymized and reviewed by at least two anonymous referees. Recommending the articles for publishing, the reviewers confirm that in their opinion the submitted article contains important or new scientific results.

Premier Publishing s.r.o. is not responsible for the stylistic content of the article. The responsibility for the stylistic content lies on an author of an article.

Instructions for authors

Full instructions for manuscript preparation and submission can be found through the Premier Publishing s.r.o. home page at:
http://www. ppublishing.org.

Material disclaimer

The opinions expressed in the conference proceedings do not necessarily reflect those of the Premier Publishing s.r.o., the editor, the editorial board, or the organization to which the authors are affiliated.

Premier Publishing s.r.o. is not responsible for the stylistic content of the article. The responsibility for the stylistic content lies on an author of an article.

Included to the open access repositories:

Typeset in Berling by Ziegler Buchdruckerei, Linz, Austria.
Printed by Premier Publishing s.r.o., Vienna, Austria on acid-free paper.

Section 1. Architecture

Inogomov Bakhtiyor,
E-mail: baziz.journal@gmail.com

SOCIO-ECONOMIC PRECONDITIONS OF THE FORMATION OF MAHALLA OF A NEW TYPE

Abstract. This article illustrates socio-economic and formation importance of traditional microdistrics, such as mahalla, simultaneously regarding their new types.

Keywords: mahalla, reforms, microdistricts, implementation, multiple advantage, hakimiyat, morpho-types.

With the acquisition of independence of Uzbekistan, the mahalla (A special part of uzbek district like microdistricts) organization attaches great importance as an integral part of citizens' self-governing bodies. It was the mahalla that a number of plenipotentiary functions were transferred, including the system of social support for the population, the implementation of market reforms, the promotion of entrepreneurship, the increase in employment, the development of social infrastructure, the maintenance and improvement of residential development, etc.

The Oliy Majlis of the Republic of Uzbekistan adopted the Law of the Republic of Uzbekistan "On Citizens' Self-Government" (14.04.1999), in which it is determined that "the self-1government of citizens is guaranteed by the Constitutions and laws of the Republic of Uzbekistan independent activity of citizens to solve local issues based on their interests, historical features of development, as well as national and spiritual values, local customs and traditions "(Article 1.).

The main principles of the activities of self-government bodies are democracy, publicity, social justice, humanism, independence in resolving issues of local importance, and self-government of citizens is carried out throughout the territory of the Republic of Uzbekistan. Education, merger, division and abolition of mahallas, as well as the establishment and change of its borders are carried out by local government bodies at the initiative of citizens' self-government bodies.

The list of powers of citizens 'assemblies of the mahalla includes measures for social protection and support for the inhabitants of mahallas, protection of public order, protection of the rights of ginsengs and children, increase in employment, etc. The mahalla organization has very great powers in the area of mahalla development management, among them:

– making a decision on the development of social infrastructure in the territory of mahalla:

– opening, reorganization and liquidation of small enterprises, hairdressing salons, workshops on repair and tailoring of footwear, workshops of folk crafts, etc.

– organization on a voluntary basis of works on improvement of the territory, construction, repair of roads, irrigation and utility networks, historical and cultural monuments, cemeteries, etc. using funds allocated by the state, as well as own funds, as well as contributions from residents of the mahallas;

– carrying out activities aimed at the economical use and reduction of losses of fuel, electric and thermal energy and water;

– implementation of public control over the use and protection of land in the relevant territory;

– assistance in exercising control over the work of trade and consumer enterprises;

– assistance in monitoring the sanitary and environmental condition of settlements, water sources, thermal protection of schools and other service establishments;

– implementation of public control over the observance of the rules of building and maintenance of yard and house territories;

– rendering assistance to citizens in the operation of the housing stock and ensuring its safety;

– The mahalla organizes and monitors, together with public utilities, the completeness and timeliness of payment by citizens of operating costs and utilities.

The financial basis for the activities of citizens' self-government bodies consists of own funds, budget funds allocated by government bodies, voluntary donations of legal entities and individuals, etc.

One of the important aspects of the activities of the mahalla is currently the issues of social protection of the population. It is this aspect that was the object of close attention of foreign researchers (E. Kuduel, S. Marsh) who note that such an approach gives positive results.

Uzbekistan has created a unique system that is the most effective way to solve the problem of targeted social protection of the population. It determines the families that really need social assistance, through the institution of citizens' self-government, recognized by and respected by all segments of the population, the mahallas, through the same mechanism, benefits are also given to families with children. The system has a multiple advantage: first, it relies on the existing and authoritative structure of the population. Secondly, it provides a transparent process of addressing the distribution of material assistance to those who really need it. Third, it is significantly less laborious and burdensome, both for decision makers and for families seeking help.

At present, the task is to raise the status of the mahalla, to increase the number of functions it performs. These measures should suggest.

A) strengthening the financial base of self-government bodies of citizens. It is not only about the use of budgetary funds aimed at social support of the population through these bodies, but also about enhancing the development of entrepreneurship, creating small enterprises and service facilities that allocate sponsorship funds for land improvement and various social programs of the mahalla. Self-government bodies should also make more active use of the small business support program currently operating in the republic;

B) the transfer of part of the authority from state bodies to local governments.

An example of the transfer of some powers from state bodies to self-government bodies is the creation of the Mahalla Posboni public formations to assist the internal affairs bodies in ensuring the protection of public order. In each mahalla, conciliation commissions were created from among aksakals, veterans, women and youth, representatives of culture and clergy for public educational influence on previously convicted persons, etc.

The extension of the official status of the mahalla to all types of residential development was a positive factor ensuring the effectiveness of the management of the territory and the expenditure of budget funds for social assistance, land improvement, etc. At the same time, it should not be forgotten that the modern mahalla is first and foremost an administrative unit in the city's governance structure, in contrast to the mahalla, the neighboring community, which is spontaneous. The size, boundaries, number of population of the administrative mahalla is established by regional hakimiyat with the aim of the most economical use of funds for the maintenance of the mahalla apparatus.

If the previously established boundaries of the historical mahalla were formed according to their features, then at the present time the boundaries of

the mahalla and assemblies are defined by purely administrative methods, not associating with some town-planning principles and the subordination of elements of social life.

Practically, many borders of the mahalla conflict with the trends of the master plan for the formation of planning areas on a natural-planning basis and transport and communication links, which adversely affect the implementation of the master plan.

Historical and town-planning factors correcting the assessment of the territory according to objective indicators occupied a special place. This includes the genesis of the environment and the inherent time of the formation of the planning structure of the building. All these factors in a certain way affect the way of life of the population in various morpho-types of buildings. In addition, in the current hierarchy of the urban development environment, the psychological aspect in the relationship of a person with the environment is important. In his relationship with the environment, a person conveys a certain organization to this environment, ranks on separate levels depending on the materiality and proximity of a person. This phenomenon is called personalization environment.

Thus, the personalization of the environment is:

– the basic formation of individual and group identity;

– a means of organizing social relationships;

– fixation of the territory, which gives a person the opportunity to determine his own activities in the implementation of this activity.

Studies have shown that the various structural levels of an urban village vary significantly in their social characteristics, in their behavior and communication, in public spaces. These features determine certain requirements for the functional – spatial organization of the structural elements of the village of different levels, each of which represents a certain socio-territorial integrity. From this position, it is possible to single out the levels relating to the mahalla. The first level is characterized as a neighbor since it is represented by primary housing, a group of residential buildings, a unified system of open spaces used by a permanent contingent – residents of this group of neighboring houses. The second level – administratively – public, presented to microdistricts, by a quarter or a gathering of citizens – by the primary units of the administrative structure of the city.

Thus, it is necessary to return the humane character and the cozy isolation of the inner yard courtyard space to the residential development. It is about introducing into the mass development of new residential areas a more precise structural differentiation and individual isolation of internal spaces, correlating them with real needs and the established forms of daily social activity of the population. In addition, the need to strengthen and highlight in the development of the primary level – Mahalla – the neighboring community, as the first step of the transition from its own residential cell to the vast space of the city is emphasized. A clearer structural differentiation will help to more successfully solve problems of a social nature, such as working with children and adolescents, protecting women's rights, organizing leisure activities, etc.

References:

1. Vilkovsky M. Sociology of architecture.– M. Russian Avant-garde Foundation.
2. Khachaturyants K. K. Fundamentals of social typology of housing.– Minsk. 1983.
3. Glazychev V. L. Socio-ecological interpretation of the urban environment.– M., 1984.

Section 2. Biology

Arabova Nodira,
Ph D., in Botany, the Faculty of fruit and olericulture and viniculture
Tashkent state agrarian university
E-mail: nilufar.yozieva@mail.ru

FEATURES OF EXPANSION OF SPECIES OF *LAMIACEAE* FAMILY IN THE NATURE OF UZBEKISTAN

Abstract. This paper presents data about the family of Lamiaceae Lindl., plants of which were ecologically investigated on the level of frequency in vertical zones, different edaphic locations and it was defined which groups they belong to. In the process of research such books as "Flora of Uzbekistan", monograph of I. V. Belolipov "Introduction to herbaceous plants by nature of Central Asia (ecological-introductory analysis)", "Vegetation cover of Uzbekistan and ways of its rational use".

Keywords: *Lamiaceae*, *Eremostachys*, ecological analysis, upland gypsophytes, petrophytes, tropophytes.

1. Introduction

Flora of Uzbekistan is reach and fertile. It includes around 4350 species of vascular plants. *Lamiaceae* Lindl., with 206 species, is considered one of the largest families of the region's flora, which is in the first ten systematic spectrum [1, 263–416].

Majority of plain territories of Uzbekistan lies under the same width with southern France, Italy, Spain, northern Africa. However, climate of the plain territories is unusually severe for these widths. It can be explained by inland location of Central Asia, lying almost in the centre of European-Asian continent and remote distance from seas and oceans.

Geographic and climate conditions of Uzbekistan are various: large irrigation areas, broad deserts and sands, also mountain massifs. Rivers (Sirdarya, Amudarya, Zarafshan and etc.), lakes and Aral sea form basins, rich with vegetation. Therefore, in the territory of the republic one can find vegetation characteristics of mountainous and high-mountainous areas, deserts and sands, irrigated lands and oases, floodplains of rivers and tugais. The classification of mountain and alpine vegetation in Central Asia is still debatable. In recent decades, a number of vegetation classifications have been created, based on traditional physiognomic ecological and morphological principles [2–5], taking into account the climate and edaphic features of environmental factors affecting the process of adaptation of species and the formation of ecobiomorphs [6–9].

2. Results and discussion

The climate of the Central Asian deserts is characterized by a sharp continentality, due to the inland position at a great distance from the seas and oceans; extremely small and uneven precipitation; high temperatures during the hot summer months (around 40 °C), an acute shortage of moisture in the soil and air; low temperature in winter (–30–35 °C) [8, 24].

K. Z. Zakirov and P. K. Zakirov [7, 135–156] distinguish five edapotypes in the vegetation cover of

steppes, of which there are three main ones: halophyta, psammophyta and gypsophyta.

In the sandy deserts occur *Eremostachys transoxana, Eremostachys Boissieriana, Eremostachys Regeliana*; In stony-clay deserts *Eremostachys desertorum* grows; On fixed sands *Eremostachys aralensis* grows; in clay deserts-*Eremostachys tuberosa*; On gray-brown soils in the desert-*Eremostachys eriolarynx*; In the artemisia and saltwort deserts-*Lagochilus acutilobus*; On sands and crushed-sand soils-*Chamaesphacos ilicifolius*; From deserts to middle zone of mountains, particularly in the foothills species of ephemers-*Lallemantia Royleana* [1, 316, 319–345].

According to Kh. Shomurodov [9, 27, 40–41], fodder flora of Kyzylkum consists of 908 vascular plant species belonging to 345 genera and 68 families. Leading position in the spectrum of fodder flora of Kyzylkum are possessed by such families as *Chenopodiaceae* (148 species), *Asteraceae* (112), *Poaceae* (106), *Fabaceae* (67), *Lamiaceae* (24). Rare species of *Eremostachys eriolarynx* identified, which is growing in sandy places of Kyzylkum.

On the saline soils of Kyzylkum, not a single representative of such large families as *Boraginaceae, Lamiaceae, Apiaceae* [9, 43] was identified.

Adyr (foothills) – hilly foothills and low mountains, a characteristic part of the natural landscapes of Central Asia. Adyr is a natural-historical zone that surrounds all the mountains of Central Asia with a wide belt. They occupy the space between two contrasting ecological regions – xerothermic desert, on the one hand, and mesothermal tau, on the other.

Precipitation falls unevenly, mainly confined to the autumn-winter-spring period. Summer is hot, comes quickly. Precipitation is very rare, and soil drought is increasing rapidly. All this has developed a special rhythm of plant development. The main type of vegetation is ephemeral. Many ephemeras and ephemeroids are part of the formation of shliblaka-xerophylic shrub and wood vegetation [8, 42; 10, 3].

The representative plants of adyr include species of genera *Phlomis. Phlomis thapsoides* is distributed on adyrs between Zarafshan and Karshi plains, as well as on the rivers of Kashkadarya accompanying the valley. To the south within the Surkhandarya region at the same height, this species is replaced by another genera *Phlomis bucharica.* In the north foothills of the Western Tien-Shan *Phlomis salicifolia* distributed, which is found in the southern regions as well, grows on fine-gravelly soils. In the described band of adyr there are several species of the *Eremostachys* genus, particularly common are *E. labiosa, E. napuligera,* in the higher parts of adyr on fine-earth and fine-gravelly slopes – *E. sogdiana, E. labiosissima, E. eriocalix,* in the upper parts of adyr – *E. speciosa* [10, 44]. As mentioned I. V. Belolipov [8, 40–44], in adyr zones there are ephemeres of such species as *Ziziphora tenuior, Ziziphora persica,* and perennial, vegetative herbs – *Phlomis thapsoides, Phlomis bucharica.*

The description of the main features of the habitat of upland gypsophytes in Central Asia is given in various monographic works [2; 8]. Upland gypsophyte plants from these areas have a narrow ecological range. The peculiarities of the natural habitats of upland gypsophytes (abundance of gypsum, high salinity of the substrate, high flight temperatures and dry air) have quite specific effects on the biology and ecology of plants [8, 46].

On the slopes of lowlands, sometimes 2000 meters above the sea levels, there are variegated outcrops of red, violet, green, orange, and other colors of clay richly impregnated with salts of different chemical composition, mainly carbonate. Many variegated plants are strictly confined to a particular substrate. Upland gypsophytes are highlighted heliophytes. A small number of plants of the *Lamiaceae* family includes variegated gypsum rocks as: *Otostegia bucharica, Ajuga turkestanica, Lagochilus Nevskii, Salvia bucharica.* I. V. Belolipov [8, 46–56] engaged in the introduction of these plants, and divided them into two groups: optional gypsophyte and obligatory gypsophyte.

In the vegetation cover of the mountains of Central Asia, E. P. Korovin [2] distinguishes 11 types of vegetation: half-savannahs or turanian dry grass

steppes; mountain steppes; upland xerophytes; deciduous mountain forests; coniferous mountain forests; overgrown valleys; mountain meadows, petrophilic and cryophilic types of vegetation; vegetation of water bodies.

In the lower tau there are tropophytes, such as *Scutellaria bucharica, Ziziphora persica, Salvia glabricaulis, Salvia Margaritae, Nepeta Olgae, Scutellaria haematochlora.* In the upper tau genus of *Scutellaria, Nepeta, Ziziphora* can be found.

In the rocks of the upper mountain zones – *Scutellaria holosericea; In the upper mountain zones – Scutellaria filicaulis;* On taluses and in the rocks of the upper mountain zones – *Scutellaria microphysa;* On taluses of the upper mountain zones – *Nepeta Lipskyi;* On gravelly and stony slopes of the upper mountain zones – *Ziziphora pamiralaica* (figure-1); On the stony slopes of the upper zone of mountains – *Lagochilus Nevskii* [1, 263–416].

Upland xerophytes are sharply presented heliophytes. An equally important ecological factor in the habitats of upland xerophytes is the extreme erosion of the mountain slopes. These are steeps, stony-gravelly mountain slopes, mostly of southern exposure, where a very special and harsh ecological regime is taking shape. Plants on such slopes are exposed to wind, water, and physical erosions.

According to I.V. Belolipov [8, 69–77], some representatives of upland xerophytes of Uzbekistan flora are *Scutellaria glabra, S. intermedia, S. microdasis, S. squarrosa, Lagochilus platycalyx, Salvia drobovii, S. komarovii, S. korolkovii, S. submutica.* They are considered representatives of upland xerophytic tomillarii for adaptation to harsh habitats [10, 77–86].

In the mountain conditions on the rocks, stony outcrops, talus and pebbles are found such petrophyte species as *Stachys hissarica, Hyssopus zeravschanicus, Perovskia scrophulariifolia, Nepeta Olgae* [8, 78–86].

Figure 1. Hissor. Locality Village Kaltakul 1000 meters above the sea level: a) *Phlomis salicifolia;* b) *Ziziphora pamiralaica*. Picture: N.Z. Arabova (2017)

Conclusion

In the study of taxonomy, geography and ecological features of *Lamiaceae* in Uzbekistan, much attention was paid to the study of mid-mountain and alpine plants.

1. In the deserts of the representatives of the species *Lamiaceae* is rare. In the sandy deserts psammophytes including *Eremostachys transoxana, Eremostachys Boissieriana, Eremostachys Regeliana* and etc are found.

2. The representative plants of adyrs include species of the genera of *Phlomis, Eremostachys*. Some species pertaining to this genus are reffered to as edificatory species. In the adyr zones, among the ephemeres there are species like *Ziziphora tenuior, Ziziphora persica*.

3. In the lower tau (mid-mountain zone) there are tropophytes comprising *Scutellaria bucharica, Ziziphora persica, Salvia glabricaulis, Salvia Margaritae, Nepeta Olgae, Scutellaria haematochlora*; Upland gypsophytes – *Otostegia bucharica, Ajuga turkestanica, Lagochilus Nevskii, Salvia bucharica;* upland xerophytic tomillarii – *Perovskia angustifolia, Perovskia scrophulariifolia, Thymus zeravschanicus, Dracocephalum integrifolium, Scutellaria adenostegia, Scutellaria comosa, Scutellaria intermedia, Salvia bucharica, Ajuga turkestanica*; petrophytes – *Stachys hissarica, Hyssopus zeravschanicus, Perovskia scrophulariifolia, Nepeta Olgae.*

References:

1. Flora Uzbekistana.– T. 5.– Tashkent: AN Uz SSR, 1961.– P. 263–416.
2. Korovin E. P. Rastitelnost Sredney Azii i yujnogo Kazakhstana.– Tashkent: AN SSR, 1962.– 547 p.
3. Ladigina G. M. Tipy visokogornoy rastitelnosti Sredney Azii // V kn. Rastitelniy pokrov visokogoriy.– L.: Nauca, 1986.– P. 137–141.
4. Khudoyberdiev T. Gubotsvetnie v rastitelnom pokrove Ferganskoy doliny (floristicheskaya, fitotsenoticheskaya, ekologicheskaya, resursovedcheskaya kharakteristiki, ratsionalnoe ispolzovanie i ix okhrana) // Avtoreferat diss. na soiskanie uchenoy stepeni dok. biol. nauk.– Tashkent, 1997.– 45 p.
5. Tadjibaev K. Sh. Flora Yugo-zapadnogo Tyan-Shanya // Diss. dokt. biol. nauk. – Tashkent, 2010.– 41 p.
6. Bilolov B. V. Gubotsvetnie Kopet-Daga, ix biologiya i prakticheskoe znachenie // Avtoreferat diss. na soiskanie uchenoy stepeni dok. biol. nauk.– Ashabad, 1968.– 20 p.
7. Zakirov K. Z., Zakirov P. K. Zakonomernosti raspredeleniya rastitelnogo pokrova i printsipy visotnoy zonalnosti // Rastitelniy pokrov Uzbekistana I puti ego ratsionalnogo ispolzovaniya. Tom 1.– Tashkent: Fan, 1971.– P. 135–156.
8. Belolipov I. V. Introduktsiya travyanistyx rasteniy prirodnoy flory Sredney Azii (ecologo-introduktsionniy analiz).– Tashkent: Fan, 1989.– 152 p.
9. Shomurodov H. F. Kormovie rasteniya Kyzylkuma i perspektivy ix ispolzovaniya // Avtoreferat dissertatsii doktora (DSc) po biologicheskim naukam.– Tashkent, 2018.– 62 p.
10. Rastitelniy pokrov Uzbekistana I puti ego ratsionalnogo ispolzovaniya // Red. Kol. V. A. Burigin, A. Ya. Butkov, I. I. Granitov, K. Z. Zakirov I dr – Tashkent: Fan Uz SSR,– Tom III,– 287 p.

Section 3. Machinery construction

Vasenin Valery Ivanovitch,
Perm National Research Polytechnic University,
associate professor, candidate of technical sciences,
department of "Materials, technologies and design of machinary"
E-mail: vaseninvaleriy@mail.ru
Bogomjagkov Aleksey Vasilievitch,
senior teacher
Sharov Konstantin Vladimirovitch,
senior teacher

STUDY OF THE COMBINED OPERATION OF THE RING-SHAPED GATING SYSTEM AND THE STEP GATING SYSTEM

Abstract. The article theoretically and experimentally investigated the most complex multi-gate gating system (GS), consisting of horizontal ring-shaped and vertical step systems. The experimental version of such system is described. A method for calculating the velocity and fluid flow rate, dependent on the number of simultaneously operating gates, has been developed. The main method of the calculation is based on the setting of the fluid velocities ratio in the basins after the flow branches in the lower section of the sprue and calculation by bringing the difference between the target and the resulting ratio to the desired value. The method takes the branching and mergers of flows in GS and the location of gates at different heights into account. Taking into account the previously studied GS, we can consider the possibility of using the Bernoulli's equation for calculating flow sections with different flow rates – multi-gate gating systems. Still, it is not proven theoretically.

Keywords: pouring basin, sprue, sprue basin, gate, resistance coefficient, flow coefficient, flow velocity, fluid flow rate.

Introduction

Previously, single and multi-gate gating systems were theoretically and experimentally studied: L-shaped, P-shaped, branched, combined, cross, step, single and two-ring, L-shaped system with a variable section sprue basin, a system with two sprues. Vertical step GS with different number of gates was also studied. In the calculations of multi-gate GS, the Bernoulli's equation was used, although it was derived for a constant flow rate (mass) [1, p. 10; 2, p. 205], which means it should be used for GS with a single gate. Consequently, the BE works for the flow with variable flow rate, although it is not clear why it works. And the possibility of using the BE in the calculation of GS with a variable from maximum to zero flow rate in the sprue basin (runner) is not theoretically proven. Therefore, it seems expedient experimentally and by calculations to investigate, apparently, the most complex multi-gate GS: horizontal ring-shaped and vertical step systems.

Research methods

The system (Fig. 1) consists of a pouring basin, sprue, sprue basins and six identical gates I – VI. Gates I – III form a horizontal ring-shaped GS, gates IV – VI form a vertical step GS. The internal diameter of the pouring basin is 272 mm, the height of the water in the basin is 103.5 mm. Fluid level H – the vertical distance from section 1–1 in the pouring basin to section 0–0 in the sprue basin and sprue – was maintained constant by continuously pouring water into the basin and draining it over the special slot in the basin: $H = 0.6135$ m. Fluid pours out from the top of gates into castings. The fluid flow time from each gates was 50–200 s – depending on the number of simultaneously running gates, and the volume of fluid flown from each gate was about 9 litres. These time and volume limitations ensured a deviation from the average speed of ± 0.005 m/s. The fluid flow rate from each gate was determined at least 6 times.

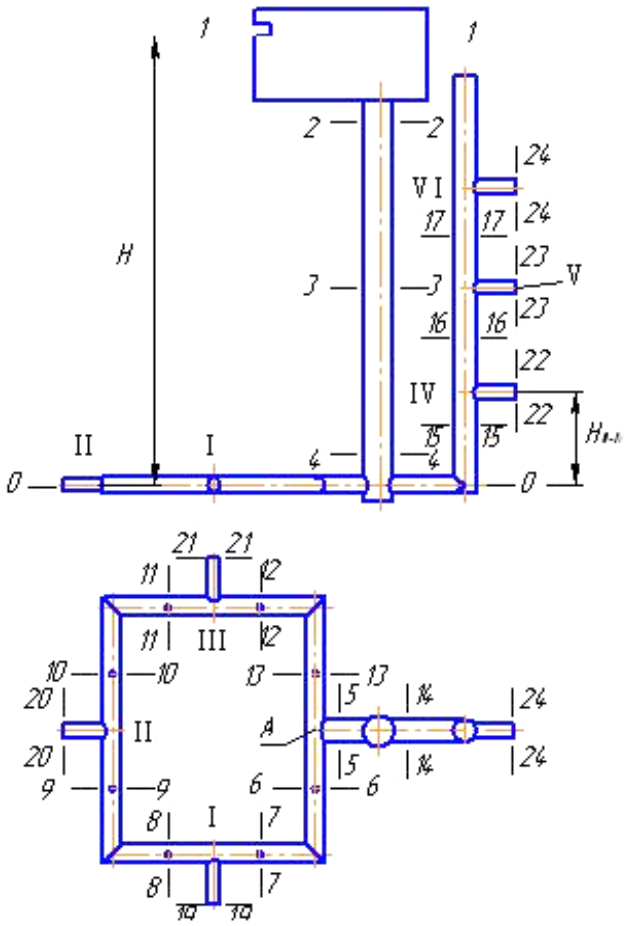

Figure 1. Gating system

Main body

First, we calculate the parameters of the GS when only one gate II is operated for the case when the hydraulic system is open in section *10–10* (no ring). Let us write the BE for sections *1–1* and *20–20* of GS:

$$H = \alpha \frac{v_{20}^2}{2g} + h_{1-20}, \qquad (1)$$

where α is the coefficient of uneven velocity distribution over the flow section (Coriolis coefficient); let us assume $\alpha = 1.1$ [2, p. 108]; v_{20} – metal velocity in cross section *20–20*, m/s; g – acceleration of gravity; $g = 9.81$ m/s^2; γ is the specific weight of the molten metal, N/m^3; h_{1-20} are the losses of head at fluid

movement from section 1–1 to section 20–20, m. These losses of head:

$$h_{1-20} = \left(\zeta_s + \lambda\frac{l_s}{d_s}\right)\alpha\frac{v_s^2}{2g} + \left(\zeta_{sb} + 3\zeta + \lambda\frac{l_{s-II}}{d_{sb}}\right)\alpha\frac{v_5^2}{2g} + \left(\zeta_g + \lambda\frac{l_g}{d_g}\right)\alpha\frac{v_{20}^2}{2g}, \quad (2)$$

where ζ_s, ζ_{sb} and ζ_g are the local resistances coefficients of the metal entrance from the pouring basin to the sprue, turn from the sprue to the sprue basin and turn from the sprue basin to the gate II; ζ is the local resistance coefficient at 90° turn from section 5–5 to section 6–6, from section 6–6 to section 7–7 and from section 8–8 to section 9–9 (without changes in the collector sections area); λ is the coefficient of friction loss; l_s – length (height) of the sprue, m; $l_s = 0.518$ m; d_s, d_{sb} and d_g are hydraulic diameters of the sprue, sprue basin and gate II, m; v_s and v_5 are the fluid velocities in the sprue and in the sprue basin in the cross section of 5–5, m/s; l_{s-II} is the distance from the sprue to the gate II, m; $l_{s-II} = 0.623$ m; l_g is the gate length, m; $l_g = 0.0495$. Flow rate in GS when pouring from the top is determined by the metal velocity v_{20} and the exit section 20–20 of the gate II and its cross-sectional area: $Q = v_{20}S_g$. The remaining fluid velocities in GS channels are determined from the flow continuity equation:

$$Q = v_sS_s = v_5S_{sb} = v_6S_{sb} = v_7S_{sb} = v_8S_{sb} = v_9S_{sb} = v_{20}S_g, \quad (3)$$

where S_s, S_{sb} are the cross-sectional areas of the sprue and sprue basin, m^2. $v_5 = v_6 = v_7 = v_8 = v_9$. Express all metal velocities in (2) in terms of the velocity v_{20}, sing the flow continuity equation (3):

$$h_{1-20(20)} = \alpha\frac{v_{20}^2}{2g}\left[\left(\zeta_s + \lambda\frac{l_s}{d_s}\right)\left(\frac{S_g}{S_s}\right)^2 + \left(\zeta_{sb} + 3\zeta + \lambda\frac{l_{s-II}}{d_к}\right)\left(\frac{S_g}{S_{sb}}\right)^2 + \zeta_g + \lambda\frac{l_g}{d_g}\right] \quad (4)$$

Let us denote the expression in square brackets as $\zeta_{1-20(20)}$: the resistance coefficient of the system from section 1–1 to section 20–20, reduced to the fluid velocity in section 20–20.

$$\zeta_{1-20(20)} = \left(\zeta_s + \lambda\frac{l_s}{d_s}\right)\left(\frac{S_g}{S_s}\right)^2 + \left(\zeta_{sb} + 3\zeta + \lambda\frac{l_{s-II}}{d_{sb}}\right)\left(\frac{S_g}{S_{sb}}\right)^2 + \zeta_g + \lambda\frac{l_g}{d_g}. \quad (5)$$

Now (1) can be written as:

$$H = \alpha v_{20}^2(1 + \zeta_{1-20(20)})/2g. \quad (6)$$

And system flow coefficient from section 1–1 to section 20–20, reduced to velocity v_{20}:

$$\mu_{1-20(20)} = \left(1 + \zeta_{1-20(20)}\right)^{-1/2}. \quad (7)$$

Velocity:

$$v_{20} = \mu_{1-20(20)}\sqrt{2gH/\alpha}. \quad (8)$$

Flow rate Q is calculated using (3). The diameters of the gate, the sprue basin and the sprue: $d_g = 0.00903$ m, $d_{sb} = d_5 = ... = d_{17} = 0.01603$ m, $d_s = 0.02408$ m. We adopt, as in [3; 4], that the coefficient of friction loss: $\lambda = 0.03$. The local resistance coefficient of the entrance from the pouring basin to the sprue, dependent on the chamfering radius of the entry edge, is determined according to [5, p. 126]: $\zeta_s = 0.12$. Local resistance coefficients [6]: $\zeta = 0.885$, $\zeta_{sb} = 0.396$, $\zeta_g = 0.334$. The results of calculations based on (5), (7), (8) and (3): $\zeta_{1-20(20)} = 0.938220$, $\mu_{1-20(20)} = 0.718288$, $v_{20} = 2.376068$ m/s, $Q_{20} = 152{,}168321 \cdot 10^{-6}$ m^3/s.

When the gate II is in the ring, the losses of head in the parallel pipes 6–7–8–9 and 13–12–11–10 are not cumulative, and equal to each other. The BE for sections 1–1 and 20–20 is already written down – (1). Losses of head at fluid flow through sections 1–1, 5–5, 6–6 and 9–9:

$$h_{1-20(20)} = \left(\zeta_s + \lambda\frac{l_s}{d_s}\right)\alpha\frac{v_s^2}{2g} + \left(\zeta_{sb} + \lambda\frac{l_{s-A}}{d_{sb}}\right)\alpha\frac{v_5^2}{2g} + \left(\zeta_{5-6(6)}^b + \lambda\frac{l_{A-II}}{d_{sb}} + 2\zeta\right)\alpha\frac{v_6^2}{2g} + \left(\zeta_{tr} + \lambda\frac{l_g}{d_g}\right)\alpha\frac{v_{20}^2}{2g},$$

where l_{s-A} is the distance from the sprue to point A on the longitudinal axis of the sprue basin, m; $l_{s-A} = 0.135$ m; l_{A-II} is the distance from point A to gate II, m; $l_{A-II} = 0.448$ m; ζ_{tr} is the local resistance coefficient at turn from the sprue basin to the gate II when the fluid is supplied to the gate from two sides; $\zeta_{tr} = 0.218$ [7].

Here $\zeta^b_{5-6(6)}$ is the resistance coefficient to the flow branching in section 5–5 between sections 6–6 and 13–13, reduced to the velocity of the metal in section 6–6. $\zeta^b_{5-13(13)}$ is the resistance coefficient at flow branching in section 5–5 between sections 6–6 and 13–13, reduced to the velocity of the liquid in section 13–13. These coefficients are determined by the following equation [5, p. 277]:

$$\zeta^b = \left[1+\varphi\left(v_b / v\right)^2\right] / \left(v_b / v\right)^2, \qquad (9)$$

where φ is the coefficient, that depends on the chamfering of the edge at the point of flow branching; with a large chamfering radius $\varphi = 0.3$; with zero chamfering radius $\varphi = 1.5$; for our GS $\varphi = 1.5$; v – fluid velocity before branching of the flow, m/s; v_b is the fluid velocity in one of the channels after branching, m/s.

It is obvious that $v_6 = v_{13}$. $Q = v_s S_s = v_5 S_{sb} = . + v_{13} S_{sb} = 2 v_6 S_{sb} = v_{20} S_g$ $v_6 / v_5 = S_{sb} / 2 S_{sb} = 0.5$. Using (9) we calculate: $\zeta^b_{5-6(6)} = \zeta^b_{5-13(13)} = 5.5$.

$v_s S_s = v_{20} S_g / S_s$, $v_5 = v_{20} S_g / S_{sb}$, $v_6 = v_{20} S_g / 2 S_{sb}$. Resistance coefficient in GS from section 1–1 to section 20–20, reduced to velocity v_{20} in gate II:

$$\zeta_{1-20(20)} = \left(\zeta_s + \lambda \frac{l_s}{d_s}\right)\left(\frac{S_g}{S_s}\right)^2 + \left(\zeta_{sb} + \lambda \frac{l_{s-A}}{d_{sb}}\right)\left(\frac{S_g}{S_{sb}}\right)^2 + \left(\zeta^b_{5-6(6)} + \lambda \frac{l_{A-II}}{d_{sb}} + 2\zeta\right)\left(\frac{S_g}{2S_{sb}}\right)^2 + \zeta_{tr} + \lambda \frac{l_g}{d_g}.$$

Substituting the known values in equation, we find: $\zeta_{1-20(20)} = 0.668913$, $\mu_{1-20(20)} = 0.774075$, $v_{20} = 2.560611$ m/s, $Q_{20} = 163.986856 \cdot 10^{-6}$ m^3/s.

As one can see, closing the ring around the gate II led to a decrease in the resistance coefficient $\zeta_{1-20(20)}$ from 0.938 to 0.669. The addition of a parallel sprue basin led to a drop in fluid velocities in each of the channels, decrease in friction losses and in local resistances, which caused a decrease in $\zeta_{1-20(20)}$, increase in $\mu_{1-20(20)}$, v_{20} and Q_{20} compared to the case where gate II operated when the liquid ring was open in section 10–10.

When only the feeder IV is operating, the BE for sections 1–1 and 22–22 will be written as:

$$H - H_{0-IV} = \alpha \frac{v^2_{22}}{2g} + h_{1-22}, \qquad (10)$$

where H_{0-IV} is the vertical distance from the sprue basin axis 0–0 to the longitudinal axis of the gate IV, m; $H_{0-IV} = 0.116$ m; v_{22} s the metal velocity in section 22–22 of gate IV, m/s; h_{1-22} are the losses of head when fluid moves from section 1–1 to section 22–22, m. These losses of head:

$$h_{1-22} = \left(\zeta_s + \lambda \frac{l_s}{d_s}\right)\alpha \frac{v^2_s}{2g} + \left(\zeta_{sb} + \zeta + \lambda \frac{l_{s-IV}}{d_{sb}}\right)\alpha \frac{v^2_{14}}{2g} + \left(\zeta_g + \lambda \frac{l_g}{d_g}\right)\alpha \frac{v^2_{22}}{2g},$$

where l_{s-IV} is the distance from the sprue to the longitudinal axis of the gate IV, m; $l_{s-IV} = 0.251$ m.

$Q = v_s S_s = v_{14} S_{sb} = v_{15} S_{sb} = v_{22} S_g$, $v_{14} = v_{15}$. And the system resistance coefficient from section 1–1 to section 22–22, reduced to the fluid velocity in section 22–22:

$$\zeta_{1-22(22)} = \left(\zeta_s + \lambda \frac{l_s}{d_s}\right)\left(\frac{S_g}{S_s}\right)^2 + \left(\zeta_{sb} + \zeta + \lambda \frac{l_{s-IV}}{d_{sb}}\right)\left(\frac{S_g}{S_{sb}}\right)^2 + \zeta_g + \lambda \frac{l_g}{d_g}.$$

Flow coefficient: $\mu_{1-22(22)} = \left(1+\zeta_{1-22(22)}\right)^{-1/2}$, velocity: $v_{22} = \mu_{1-22(22)} \sqrt{2g\left(H - H_{0-IV}\right)/\alpha}$, flow rate: $Q = v_{22} S_g$. Calculation results: $\zeta_{1-22(22)} = 0.689882$, $\mu_{1-22(22)} = 0.769258$, $v_{22} = 2.291509$ m/s, $Q_{22} = 146.752979 \cdot 10^{-6}$ m^3/s.

Let us calculate the combined operation of the feeders II and IV. Expressions (1) and (10) are valid. We need to combine them. Let us proceed as follows: velocities v_{20} and v_{22} will be different, same with velocities v_5 and v_{14}. It is necessary to specify the velocity ratio $z = v_5 / v_{14}$ and ensure that, after calculations, it corresponds to the ratio $x = v_{20} / v_{22}$.

Loss of head at fluid flow through sections 1–1, 5–5, 6–6 and 9–9 to gate II:

$$h_{1-20} = \left(\zeta_s + \lambda \frac{l_s}{d_s}\right)\alpha \frac{v^2_s}{2g} + \left(\zeta^b_{4-5(5)} + \lambda \frac{l_{s-A}}{d_{sb}}\right)\alpha \frac{v^2_5}{2g} + \left(\zeta^b_{5-6(6)} + \lambda \frac{l_{A-II}}{d_{sb}} + 2\zeta\right)\alpha \frac{v^2_6}{2g} + \left(\zeta_{tr} + \lambda \frac{l_g}{d_g}\right)\alpha \frac{v^2_{20}}{2g}. \qquad (11)$$

where $\zeta^b_{4-5(5)}$ is the resistance coefficient to the branching of flow in the sprue in section 4–4 between

sections 5–5 and 14–14, reduced to the velocity of the metal in section 5–5. $\zeta^{b}_{4-14(14)}$ is the resistance coefficient to the flow branching in the sprue in section 4–4 between sections 5–5 and 14–14, reduced to the velocity of the liquid in section 14–14. These coefficients can be calculated by using (9):

$Q = v_s S_s = (v_5 + v_{14}) S_{sb} = (v_5 + v_5 / z) S_{sb} = v_5 S_{sb} (1 + 1/z)$.

Or $Q = v_{14} S_{sb} (1 + z)$.

$v_5 = v_s S_s / S_{sb} / (1 + 1/z)$, $v_{14} = v_s S_s / v_{sb} / (1 + z)$, $v_5 = v_{20} S_g / S_{sb}$, $v_6 = v_{20} S_g / 2S_{sb}$, $v_s = v_5 S_{sb} (1 + 1/z) / S_s = = v_{20} S_g / S_s (1 + 1/z)$.

And the expression (11) is converted to:

$$h_{1-20(20)} = \alpha \frac{v_{20}^2}{2g} \left[\begin{array}{l} \left(\zeta_s + \lambda \frac{l_s}{d_s} \right) \left(\frac{S_g}{S_s} (1 + 1/z) \right)^2 + \\ + \left(\zeta^{b}_{4-5(5)} + \lambda \frac{l_{s-A}}{d_{sb}} \right) \left(\frac{S_g}{S_{sb}} \right)^2 + \\ + \left(\zeta^{b}_{5-6(6)} + \lambda \frac{l_{A-II}}{d_{sb}} + 2\zeta \right) \left(\frac{S_g}{2S_{sb}} \right)^2 + \\ + \zeta_{tr} + \lambda \frac{l_g}{d_g} \end{array} \right]. \quad (12)$$

The relation in square brackets is the resistance coefficient $\zeta_{1-20(20)}$. Loss of head at fluid flow through sections 1–1, 14–14 and 15–15 to gate IV:

$$h_{1-22} = \left(\zeta_s + \lambda \frac{l_s}{d_s} \right) \alpha \frac{v_s^2}{2g} + \left(\zeta^{b}_{4-14(14)} + \lambda \frac{l_{s-IV}}{d_{sb}} + \zeta \right) \times \times \alpha \frac{v_{14}^2}{2g} + \left(\zeta_g + \lambda \frac{l_g}{d_g} \right) \alpha \frac{v_{22}^2}{2g}. \quad (13)$$

$v_{14} = v_{22} S_g / S_{sb}$, $v_s = v_{14} S_{sb} (1 + z) / S_s = v_{22} (1 + z) S_g / S_s$.

Now equation (13) can be written as:

$$h_{1-22(22)} = \alpha \frac{v_{22}^2}{2g} \left[\begin{array}{l} \left(\zeta_s + \lambda \frac{l_s}{d_s} \right) \left(\frac{S_g}{S_s} (1 + z) \right)^2 + \\ + \left(\zeta^{b}_{4-14(14)} + \lambda \frac{l_{s-IV}}{d_{sb}} + \zeta \right) \left(\frac{S_g}{S_{sb}} \right)^2 + \zeta_g + \lambda \frac{l_g}{d_g} \end{array} \right]. \quad (14)$$

The dependence in square brackets is the resistance coefficient $\zeta_{1-22(22)}$.

Let us start by taking $z = v_5 / v_{14} = 1$. When $z = 1$ $v_5 / v_4 = v_{14} / v_4 = 1.128277$, and $\zeta^{b}_{4-5(5)} = \zeta^{b}_{4-14(14)} = 2.285540$.

Calculation results:

$\zeta_{1-20(20)} = 0.904589$, $\mu_{1-20(20)} = 0.724602$, $v_{20} = 2.396955$ m/s, $Q_{20} = 153.505947 \cdot 10^{-6}$ m^3/s;

$\zeta_{1-22(22)} = 0.925558$, $\mu_{1-22(22)} = 0.720646$, $v_{22} = 2.146700$ m/s, $Q_{22} = 137.479128 \cdot 10^{-6}$ m^3/s; $x = v_{20} / v_{22} = 1.116577$. It can be seen that $x = 1.116577 > z = 1$. Let us establish $z = 1.116577$, we repeat the calculation and we obtain $x = 1.125627$. By such approximations we determine that $z = 1.126352$ $x = 1.1263523$. After that, we can stop calculating z and x, due to the fact that the difference between their values is only 0.0000003. The results of calculations and experiments (reciprocally) are given in the Table 1.

When calculating the fluid flow from gates I, III and IV, velocities v_{19} and v_{21} are equal, and the flow rate in the system: $Q = v_s S_s = (v_5 + v_{14}) S_{sb} = (2v_{19} + v_{22}) S_g$. Flow rate in the section 5–5 $Q_5 = (v_6 + v_{13}) S_{sb} = 2v_6 S_{sb} = = (v_{19} + v_{21}) S_g = 2v_{19} S_g$. Loss of head for gate IV is already known – (14). Loss of head for gate I:

$$h_{1-19(19)} = \alpha \frac{v_{19}^2}{2g} \left[\begin{array}{l} \left(\zeta_s + \lambda \frac{l_s}{d_s} \right) \left(\frac{2S_g}{S_s} (1 + 1/z) \right) + 2 \\ + \left(\zeta^{b}_{4-5(5)} + \lambda \frac{l_{s-A}}{d_{sb}} \right) \left(\frac{2S_g}{S_{sb}} \right)^2 + \\ \left(\zeta^{b}_{5-6(6)} + \lambda \frac{l_{A-I}}{d_{sb}} + \zeta \right) \left(\frac{S_g}{S_{sb}} \right)^2 + \zeta_g + \lambda \frac{l_g}{d_g} \end{array} \right], \quad (15)$$

where l_{A-I} is the distance from point A to gate I; $l_{A-I} = 0.240$ m.

Again, we take $y = v_5 / v_{14} = 1$, perform the calculation and find the ratio $x = 2v_{20} / v_{22}$, which equals 1.658965. By the method of successive approximations we determine: y = 1.769701.

When the gates I – IV are operating, the velocities v_{19} and v_{21} are equal, and the flow rate in the system: $Q = v_s S_s = (v_5 + v_{14}) S_{sb} = (2v_{19} + v_{20} + v_{22}) S_g$. Loss of head for gate IV is already known – (14). We introduce the notation: $t = v_{19} / v_{20}$. Then $v_{19} = t \cdot v_{20}$, and $v_{20} = v_{19} / t$. Flow rate in the section 5–5 $Q_5 = (v_6 + v_{13}) S_{sb} = 2v_6 S_{sb} = (2v_{19} + v_{20}) S_g = = v_{19} S_g (2 + 1/t) = v_{20} S_g (2t + 1)$. Flow rate in the section 6–6 $Q_6 = (v_{19} + 0.5 v_{20}) S_{sb} = (v_{19} + 0.5 v_{19} / t) S_g = = v_{19} S_g (1 + 0.5/t) = v_{20} S_g (t + 0.5)$. Flow rate in the section 8–8 $Q_8 = 0.5 Q_{20}$.

Loss of head for gate I:

$$h_{1-19(19)}=\alpha\frac{v_{19}^2}{2g}\left[\begin{array}{l}\left(\zeta_s+\lambda\frac{l_s}{d_s}\right)\left(\frac{S_g}{S_s}\left(2+1/t\right)\left(1+1/z\right)\right)^2+\left(\zeta^b_{4-5(5)}+\lambda\frac{l_{s-A}}{d_{sb}}\right)\left(\frac{S_g}{S_{sb}}\left(2+1/t\right)\right)^2+\\ \left(\zeta^b_{5-6(6)}+\lambda\frac{l_{A-I}}{d_{sb}}+\zeta\right)\left(\frac{S_g}{S_{sb}}\left(1+0.5/t\right)\right)^2+\zeta_{19}+\lambda\frac{l_g}{d_g}\end{array}\right]. \quad (16)$$

Loss of head for gate II:

$$h_{1-20(20)}=\alpha\frac{v_{20}^2}{2g}\left[\begin{array}{l}\left(\zeta_s+\lambda\frac{l_s}{d_s}\right)\left(\frac{S_g}{S_s}\left(2t+1\right)\left(1+1/z\right)\right)^2+\left(\zeta^b_{4-5(5)}+\lambda\frac{l_{s-A}}{d_{sb}}\right)\left(\frac{S_g}{S_{sb}}\left(2t+1\right)\right)^2+\\ \left(\zeta^b_{5-6(6)}+\lambda\frac{l_{A-I}}{d_{sb}}+\zeta\right)\left(\frac{S_g}{S_{sb}}\left(t+0.5\right)\right)^2+\left(\zeta_8+\lambda\frac{l_{I-II}}{d_{sb}}+\zeta\right)\left(\frac{S_g}{2S_{sb}}\right)^2+\zeta_{tr}+\lambda\frac{l_g}{d_g}\end{array}\right]. \quad (17)$$

Where $l_{I\text{-}II}$ is the distance between the gates I and II, m; $l_{I\text{-}II}=0.248$ m; ζ_{19} is the resistance coefficient to the branch of the flow from section 7–7 to section 19–19 of gate I; ζ_8 is the resistance coefficient to the flow in the sprue basin from section 7–7 to section 8–8 when a part of the flow branches off from section 7–7 to gate I. The resistance coefficients of flow branching from the sprue basin to the gate and the flow pass will be calculated using the formulas for the distributing tee [1, p. 112–115]. The resistance coefficient to the flow in the sprue basin at branching part of the flow to the gate:

$$\zeta_{tr}=0.4\left(1-v_{tr}/v_{sb}\right)^2/\left(v_{tr}/v_{sb}\right)^2, \quad (18)$$

and the resistance coefficient to the branch of the flow in the gate:

$$\zeta_{br}=\left[1+\tau\left(v_g/v_{sb}\right)^2\right]/\left(v_g/v_{sb}\right)^2, \quad (19)$$

where v_{sb} and v_s are the metal velocity in the sprue basin before and after branching part of the flow in the gate, m/s; v_g is the fluid velocity in the gate, m/s; τ is the coefficient. In this case when $S_g/S_{sb}=0.317$ $\tau=0.15$ [8]. The coefficient ζ_{tr} is reduced to the velocity of the passing flow v_{tr}, and ζ_{br} – to the velocity in the gate v_g. As can be seen, the coefficients ζ_{tr} and ζ_{br} depend on the unknown ratios of velocities v_{tr}/v_{sb} and v_g/v_{sb}, more precisely, on v_8/v_7 and v_{19}/v_7.

Ratio $\frac{v_8}{v_7}=\frac{Q_8}{Q_7}=\frac{0.5v_{20}S_g}{v_{19}S_g+0.5v_{20}S_g}=\frac{0.5v_{20}}{t\cdot v_{20}+0.5v_{20}}=\frac{0.5}{t+0.5}$.

Ratio $\frac{Q_{19}}{Q_7}=\frac{v_{19}S_g}{v_7S_{sb}}=\frac{v_{19}S_g}{v_{19}S_g+0.5v_{20}S_g}=\frac{tv_{20}}{tv_{20}+0.5v_{20}}=\frac{t}{t+0.5}$,

$\frac{v_{19}}{v_7}=\frac{t}{t+0.5}\frac{S_{sb}}{S_g}$.

t is unknown value. We take (arbitrarily) $t=0.5$. In this case $v_7/v_6=0.5$, $\zeta_8=0.4$ – according to the formula (18). $v_{19}/v_7=1.575657$, by using (19) we calculate: $\zeta_{19}=0.552788$.

Again, we take $y=v_5/v_{14}=1$, calculate and find: $y=\left(2v_{19}+v_{20}\right)/v_{22}=1.885465$, $t=v_{19}/v_{20}=0.975920$, $v_8/v_7=0.338772$. By the method of successive approximations we determine: $t=0.969982$, $y=2.100715$, $v_8/v_7=0.340140$. The results are given in the Table 2.

For GS composed of gates I–V, for gates I–III, losses of head are already known – (16) and (17) $v_{19}=v_{21}$. Flowrate in the system $Q=v_sS_s=\left(v_5+v_{14}\right)S_{sb}=$ $=\left(2v_{19}+v_{20}+v_{22}+v_{23}\right)S_g$. Losses of head from section *1–1* to gate IV:

$$h_{1-22}=\left(\zeta_s+\lambda\frac{l_s}{d_s}\right)\alpha\frac{v_s^2}{2g}+\left(\zeta^{\partial}_{4-14(14)}+\lambda\frac{l_{s-IV}}{d_{sb}}+\zeta\right)\times$$
$$\times\alpha\frac{v_{14}^2}{2g}+\left(\zeta_{22}+\lambda\frac{l_g}{d_g}\right)\alpha\frac{v_{22}^2}{2g}. \quad (20)$$

Losses of head from section 1–1 to gate V:

$$h_{1-23}=\left(\zeta_s+\lambda\frac{l_s}{d_s}\right)\alpha\frac{v_s^2}{2g}+\left(\zeta^b_{4-14(14)}+\lambda\frac{l_{s-IV}}{d_{sb}}+\zeta\right)\alpha\frac{v_{14}^2}{2g}+$$
$$+\left(\zeta_{16}+\lambda\frac{l}{d_{sb}}\right)\alpha\frac{v_{16}^2}{2g}+\left(\zeta_g+\lambda\frac{l_g}{d_g}\right)\alpha\frac{v_{22}^2}{2g}. \quad (21)$$

where l is the distance between gates IV and V, m; $l=0.119$ m; ζ_{22} is the resistance coefficient to the branch of the flow from section 15–15 to section 22–22 of gate IV; ζ_{16} is the resistance coefficient to the flow in the sprue basin from section 15–15 to section 16–16 when a part of the flow branches off

from section 15–15 of gate IV. These resistance coefficients are calculated by formulas (18) and (19) as shown above. We introduce the following notation: $w_1 = v_{23} / v_{22}$. Then $v_{23} = w_1 \cdot v_{22}$, and $v_{22} = v_{23} / w_1$. Flow rate in section 14–14 $Q_{14} = (v_{22} + v_{23})S_g = v_{22}S_g(1+1/w_1) = v_{23}S_g(1+w_1)$.

We take $y = 1$, $v_{16} / v_{15} = 0.5$, $w_1 = 0.5$. t and v_8 / v_7 are already calculated: $t = 0.969982$, $v_8 / v_7 = 0.340140$. Using the method of successive approximations we find: $y = 1.433532$, $v_{16} / v_{15} = 0.425422$, $w_1 = 0.740407$. The results of calculations and experiments are given in Table 2.

Table 1.– The parameters of GS with 1 or 2 gates operating

System	Gate	ζ	μ	v	Q	Q_{GS}
I*	I*	0.802	0.745	2.464 / 2.43	157.80 / 155.62	
I	I	0.661	0.776	2.567 / 2.52	164.40 / 161.39	
II*	II*	0.938	0.718	2.376 / 2.35	152.17 / 150.50	
II	II	0.669	0.774	2.561 / 2.55	163.99 / 163.61	
IV	IV	0.690	0.769	2.292 / 2.27	146.75 / 145.63	
V	V	0.712	0.764	1.986 / 1.98	127.16 / 126.80	
VI	VI	0.757	0.754	1.623 / 1.59	103.94 / 101.83	
II, IV	II	0.889	0.728	2.407 / 2.41	154.12 / 154.34	290.95 / 291.39
	IV	0.944	0.717	2.137 / 2.14	136.83 / 137.05	
II, V	II	0.873	0.731	2.417 / 2.39	154.79 / 153.06	272.59 / 269.62
	V	0.995	0.708	1.839 / 1.82	117.80 / 116.56	
II, VI	II	0.856	0.734	2.428 / 2.37	155.48 / 151.78	251.78 / 245.92
	VI	1.047	0.699	1.504 / 1.47	96.30 / 94.14	

**The hydraulic system is open in section 10–10*

When calculating the operation of all six gates still $v_{19} = v_{21}$, and the flow rate in the system $Q = v_s S_s = (v_5 + v_{14})S_{sb} = (2v_{19} + v_{20} + v_{22} + v_{23} + v_{24})S_g$. In the expression (21) for the gate V, the coefficient ζ_g must be replaced by ζ_{23} – he resistance coefficient to the branch of the flow from section 16–16 to section 23–23 of gate V. Loss of head from section 1–1 to gate VI:

Table 2. – The parameters of GS with 3, 4 or 5 gates operating

System	Gate	ζ	μ	v	Q	Q_{GS}
I – III	I	2.865	0.509	1.683 / 1.71	107.75 / 109.51	326.60 / 330.45
	II	2.637	0.524	1.735 / 1.76	111.09 / 112.71	
	III	2.865	0.509	1.683 / 1.69	107.75 / 108.23	
I – IV	I	4.559	0.424	1.403 / 1.48	89.86 / 94.78	405.42 / 414.34
	II	4.005	0.447	1.479 / 1.54	94.69 / 98.62	
	III	4.559	0.687	1.403 / 1.46	89.86 / 93.50	
	IV	1.120	0.754	2.046 / 1.99	131.02 / 127.44	
I – V	I	4.672	0.420	1.389 / 1.46	88.95 / 93.50	405.42 / 414.34
	II	4.336	0.433	1.432 / 1.49	91.71 / 95.42	
	III	4.672	0.420	1.389 / 1.44	88.95 / 92.22	
	IV	2.116	0.566	1.687 / 1.64	108.07 / 105.03	
	V	3.325	0.481	1.249 / 1.19	80.01 / 76.21	
I, IV–VI	I	0.947	0.717	2.371 / 2.34	151.84 / 149.86	457.69 / 462.38
	IV	1.951	0.582	1.734 / 1.67	111.04 / 106.95	
	V	6.289	0.370	0.962 / 0.91	61.63 / 58.28	
	VI	20.352	0.216	0.466 / 0.44	29.82 / 28.18	

$$h_{1-24} = \left(\zeta_s + \lambda\frac{l_s}{d_s}\right)\alpha\frac{v_s^2}{2g} + \left(\zeta^b_{4-14(14)} + \lambda\frac{l_{s-\text{IV}}}{d_{sb}} + \zeta\right)\alpha\frac{v_{14}^2}{2g} + \\ + \left(\zeta_{16} + \lambda\frac{l}{d_{sb}}\right)\alpha\frac{v_{16}^2}{2g} + \left(\zeta_{17} + \lambda\frac{l}{d_{sb}}\right)\alpha\frac{v_{17}^2}{2g} + \left(\zeta_g + \lambda\frac{l_g}{d_g}\right)\alpha\frac{v_{23}^2}{2g}, \quad (22)$$

where ζ_{17} is the resistance coefficient to the flow in the collector from section 16–16 to section 17–17 when a part of the flow branches off section 16–16 to gate V.

We introduce the following notation: $w_2 = v_{24} / v_{22}$. Then $v_{24} = w_2 \cdot v_{22}$, a $v_{22} = v_{24} / w_2$. $w_1 = v_{23} / v_{22}$. Flow rate in section 14–14 $Q_{14} = (v_{22} + v_{22} + v_{24}) S_g = v_{22} S_g (1 + w_1 + w_2) = v_{23} S_g (1 + w_1 + w_2) / w_1 = v_{24} S_g (1 + w_1 + w_2) / w_2$. $Q_{16} = (v_{23} + v_{24}) S_g = v_{23} S_g (1 + 1 / w_2) = v_{24} S_g (1 + w_2)$. $v_{17} = v_{24} S_g / S_{sb}$.

However, calculations showed that $v_{24} = 0$, water does not flow from the gate VI. This is a gate located at high altitude, and taking into account the loss of head before it, the head H is no longer enough to lift the fluid to the gate VI.

Results and discussion

The experimental costs in the systems differ from the calculated values from –2.2% to +3.2%, and the velocities in the gates – from 5.2% to +5.9%. The differences are small, so it is difficult to draw any conclusions. In summary, it can be considered that good agreement has been obtained between the theoretical and experimental data. And the Bernoulli equation derived for a particular case – for a systems with a single gate – also works in the most complex systems, such as horizontal ring-shaped and vertical step systems with multiple gates.

To start the calculation, we assign the value to the flow rate ratio Q_5 / Q_{14}, we find the flow rates in each gate Q_5 / Q_{14}, the flow rates ratio Q_5 / Q_{14} and compare it with the value assigned at the beginning of the calculation. Using the method of successive approximations, we achieve the necessary magnitude of the discrepancy between the given and calculated values of the ratio Q_5 / Q_{14}. As can be seen, the ring-shaped and step system are calculated separately from each other, and the "stitching" of these systems occurs for the flow in the lower section of the sprue. That differs from previously studied systems, in which the calculation could be carried out for velocity in any gate.

Let us take a look at GS formed by gates I and VI. In this system, in section 4–4, the flow is branching into 2 unequal parts between sections 5–5 and 14–14, and in section 5–5 the flow is branching into 2 unequal parts between sections 6–6 and 13–13, the flows from which merge in gate I. Gate VI is 354 mm higher than gate I. And this system can be calculated – although the BE derived for GS with one gate. Why this is possible is unknown.

Taking into account the previously studied GS listed in the introduction, we can consider the possibility of using the Bernoulli's equation for calculating flow sections with different flow rates – multi-gate gating systems. Still, it is not proven theoretically.

Conclusion

In summary, for the first time, the most complex multi-gate gating system consisting of horizontal ring-shaped and vertical step systems was theoretically and experimentally investigated. A method has been developed for calculating velocities and flow rate in such GS. The main method of the calculation is based on the setting of the fluid velocities ratio in the basins after the flow branches in the lower section of the sprue and calculation by bringing the difference between the target and the resulting ratio to the desired value. A good agreement was obtained between the calculated and experimental data.

References:

1. Меерович И. Г., Мучник Г. Ф. Гидродинамика коллекторных систем.– М.: Наука, 1986.– 144 с.
2. Чугаев Р. Р. Гидравлика.– М.: изд-во "Бастет", 2008.– 672 с.
3. Токарев Ж. В. К вопросу о гидравлическом сопротивлении отдельных элементов незамкнутых литниковых систем // Улучшение технологии изготовления отливок.– Свердловск: изд-во УПИ, 1966.– С. 32–40.
4. Jonekura Koji (et al.) Calculation of amount of flow in gating systems for some automotive castings // The Journal of the Japan Foundrymen's Society. 1988.– Vol. 60.– No. 8.– P. 326–331.
5. Идельчик И. Е. Справочник по гидравлическим сопротивлениям.– М.: Машиностроение, 1992.– 672 с.

6. Васенин В. И., Васенин Д. В., Богомягков А. В., Шаров К. В. Исследование местных сопротивлений литниковой системы // Вестник Пермского национального исследовательского политехнического университета. Машиностроение, материаловедение. 2012.– Т. 14.– № 2.– С. 46–53.
7. Vasenin V. I., Bogomyagkov A. V., Sharov K. V. Definition of the resistance to liquid flow during confluence and rotation of the streams // Austrian Journal of Technical and Natural Sciences. 2018.– No. 5–6.– P. 11–15.
8. Васенин В. И., Богомягков А. В., Шаров К. В. Исследования L-образных литниковых системы // Вестник Пермского национального исследовательского политехнического университета. Машиностроение, материаловедение. 2012.– Т. 14.– № 4.– С. 108–122.

Tretiak Oleksii,
Candidate of Technical Sciences (Ph. D.),
SE "Plant Electrotyazhmash", Deputy Head of Department,
Senior Lecturer of Aerospace Thermal Engineering Department,
National Aerospace University named after N. Ye. Zhukovsky "KhAI"
E-mail: alex3tretjak@ukr.net

Kobzar Kostyantyn,
Candidate of Technical Sciences (Ph. D.),
SE "Plant" Electrotyazhmash", Chief Designer on Turbogenerators
E-mail: kk7@ukr.net

Kovryga Anton,
SE "Plant" Electrotyazhmash", Head of Department
E-mail: a.kovryga@i.ua

Tribushnoi Nickita,
Student, Design Engineer, National Aerospace University
after N. Ye Zhukovsky, "KhAI", SE Plant Electrotyazhmash
E-mail: leer07770@gmail.com

Piatnytska Yevheniia,
Student, Design Engineer, National Aerospace University
after N. Ye Zhukovsky, "KhAI", SE Plant Electrotyazhmash
E-mail: pyatnitskayaes@bigmir.net

CONTACT TASKS IN ENERGETICS. PRACTICAL AND THEORETICAL RATIONALE FOR USAGE OF NEW FEM METHODS

Abstract. In submitted paper the peculiarities of operation, design and design version of the supporting elements construction of high power electric machines are considered. The possibility of transition from analytical methods of mathematical modeling of the stressed state to three-dimensional is considered in the present paper. A methodology for calculating of rigid supports for high power Hydrogenerators, which includes taking into account the specific features of the contact zone geometry, as well as the influence of the metal structure on the grid parameters of the finite element method was developed.

Keywords: electric machine of high power, the contact stresses, finite element method, metal structure.

Introduction

The history of the electric machines design has more than a century. Our modern civilization is almost entirely based on electrical energy, and the developed and existing constructions of generators, which were in operation since the middle of the last century and up to the present moment, are among the most reliable sources of electricity on the planet.

During the last 20 years, a significant increase in the power of computer equipment has allowed

to proceed to calculation of the strain-stress state of the essential parts of the generators in the three-dimensional formulation. At the same time, the main dogmas of analytical methods were shifted to a three-dimensional calculation without rethinking of possibilities of new approaches.

At the present time, in a number of structures, steels of foreign manufacturers without data on their fatigue characteristics are applied. This requires the use of new calculation methods without the possibility of additional laboratory researches.

One of the most stressed elements of Hydrogenerator is the thrust bearing support, which takes the load of the entire unit. However, this issue in the open press is not fully covered.

Features of Designing, Development and Operation of Electric Machines

The main stages of the life cycle of any product as per GOST P 53791–2010 are as follows:

– rationale of designing;
– development of Technical Task;
– carrying out of research and development;
– manufacturing and tests;
– modernization;
– usage (operation);
– elimination (with elimination of waste by utilization and / or elimination).

At that it is assumed that the types of used resources namely material, raw materials, fuel and energy shall be used in a similar equivalent.

As a rule, when establishing requirements for resource conservation, the Customer shall proceed from the requirements for ensuring quality, reliability, safety, and protection of life, human health, and the environment.

However, if you look in details at the service life cycle of Turbogenerators and Hydrogenerators, you can see that it comprises 40 years (see GOST 533–2000 for Turbogenerators and 5616–1989 for Hydrogenerators). And, as a rule, according to the work of Sazykin V. G. [1], in the average repair, power units shall be withdrawn from operation when they reach the operating time between the average repairs in the previous period, or half the time between the overhauls. Routine repairs are carried out in accordance with the need to eliminate the malfunction and to carry out monitoring and testing, the frequency of which is established in technical conditions and other documents for each type of power equipment (PE).

It is necessary to pay a special attention that one of the most perspective methods for repairing of power equipment is the aggregate-unit diagram for replacing of faulty elements with new ones or repaired ones. Transfer to this method of repairing of complex and critical responsible equipment is based on the provision of replaceable repair units, components and parts in equipment, establishment of optimal terms for their replacement, the development of the nomenclature and the necessary margin of replaceable elements. Such an approach to organization of power equipment repair on the technical condition of power equipment is the option associated with the "development and consumption of repair services".

The essence of the method is in the fact that after a certain period of time as wearing out of the main parts of power equipment increases, it becomes necessary to replace them with new parts or previously repaired parts. This is power equipment demand for a repair service. If the demand is not satisfied, then the worn-out part shall break down after a while with shutdown of the functioning of power equipment unit in the production process and emergency demand for the repair service shall arise. At that, other parts and assemblies may be damaged, up to complete destruction, and power equipment units shall be rejected.

According to the results of the papers of Kobzar K. A. [2] during operation, the following damage pattern is available, submitted in Figure 1. In general, the nature of damages is similar also for Hydrogenerators.

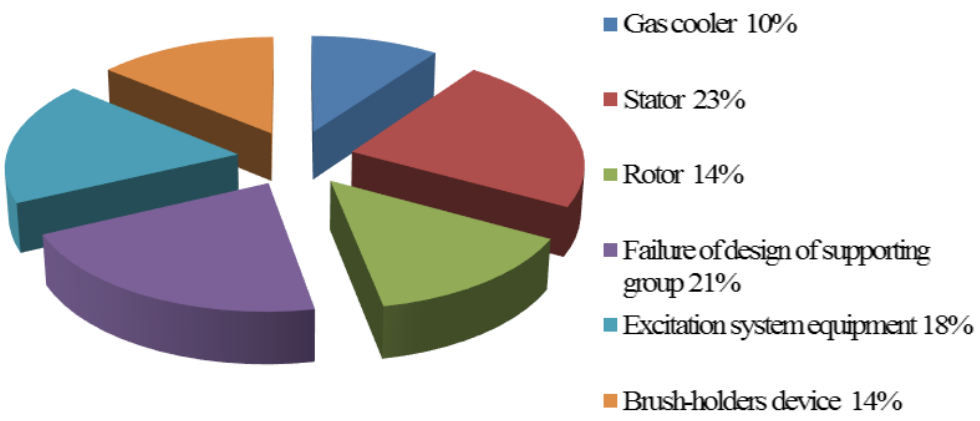

Figure 1. Diagram of Data on Emerge of Typical Emergency Situations of Electric Generators

As per their physical nature structural elements with respect to the mechanical strength calculation methods are distributed as follows:

– shielding;
– large bodies with preload fit;
– plates;
– contact tasks.

For the existing calculation methods in the classical formulation, temperature accounting is almost completely absent.

At that the issue of resource design remains open even with the usage of new methods of calculation and design.

At the turn of the 20th century, there was a tendency to transfer from two-dimensional analytical calculations to three-dimensional ones. At the same time, the classical performances submitted in [3; 4] were repeated and improved.

Studied Design

Studied design of Hydrogenerator is carried out in vertical design version, of suspended type with two guide bearings (1) and the thrust bearing (4), arranged above the rotor (3) with the support on to the spider (2). The excitation of Hydrogenerator shall be carried out from the system of thyristor independent excitation.

The rotor flange is connected to the turbine shaft by means of the flange connection. The stator (6) is installed on the foundation inside the access-shaft of the Hydrogenerator and is attached to the foundation using anchor studs (5). The spider (2) rests on the upper shelf of the stator casing. The overlap of the turbine access-shaft, installed on the beams under the rotor of Hydrogenerator, serves as a platform for maintenance of the brakes (7).

Ventilation of Hydrogenerator is carried out in a closed cycle with partial intake of hot air for heating of the machine room. Air coolers (8) are arranged around the stator casing of Hydrogenerator. The zones of cold and hot air are separated by upper and lower air-separation shields. The general arrangement of Hydrogenerator is shown in Figure 2.

The Reasons of Destruction of the Thrust Bearing Design

In the literature, great attention is paid to the "active parts", to their fastening elements and the rotors of Hydrogenerators. However, attention is not paid to the supporting elements of the aggregates.

The main causes of damage of the thrust bearings is macroroughness. It comprises a separate protrusions and cavities with a distance between them of hundreds of millimeters, located on the mirror surface of the disk, usually in the direction of rotation. When the rotor rotates, these protrusions and cavities create periodic changes in the load on each segment.

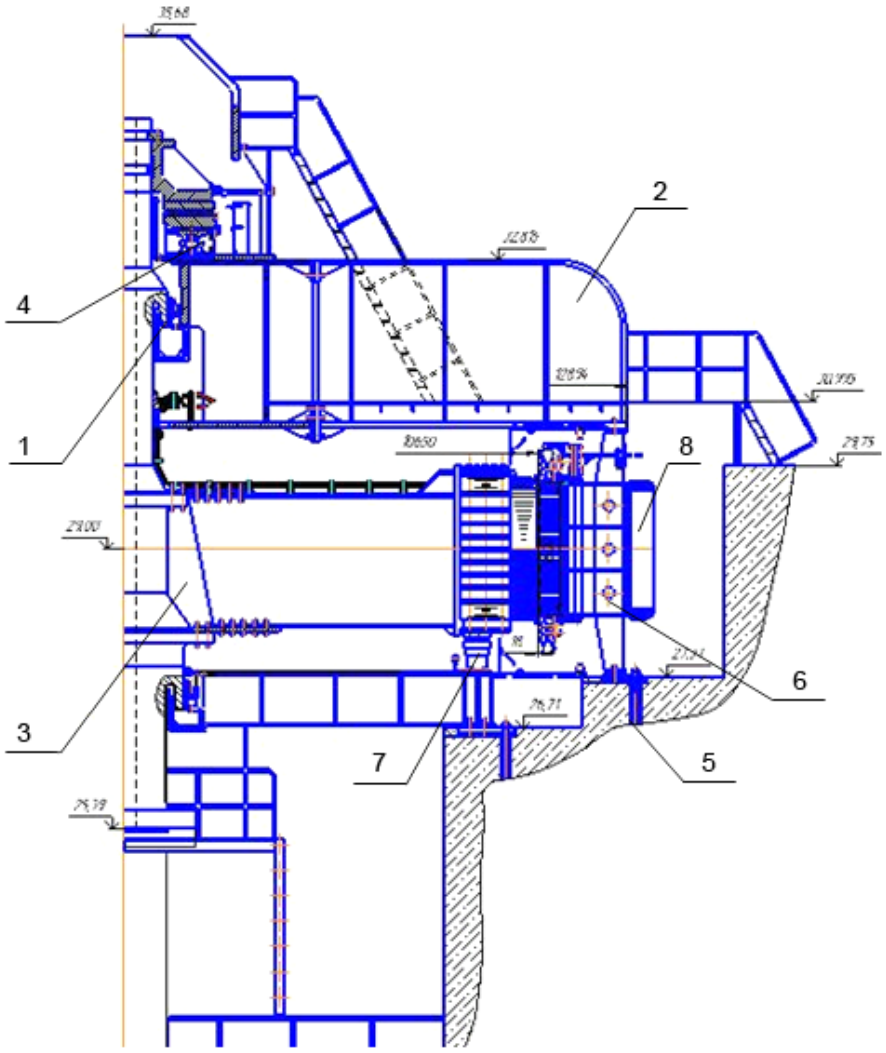

Figure 2. General Arrangement of Hydrogenerator

The reasons of macroroughnesses emerge are as follows namely structural defects or peculiarities, such as a thin bottom of the thrust bearing bush, resulting in it bending under the load between the ribs of the bush, causing emerging of the protrusions and cavities on the thrust bearing disk fastened to it; residual deformations of the thrust bearing bush as a result of its hot fit on the shaft, which, after fastening of the disk to it, causes unevenness on its mirror surface; residual deformations of the disk, which emerged during operation, at installation or before it; destruction of the gaskets installed between the disk and the bush [5].

The increased macroroughness irregularity of the mirror surface of the disk leads primarily to worsened working conditions of the thrust bearing during starts and stops. During start-up, the formation of an oil film separating the friction surface is impeded and slows down. When stopping earlier, i.e. at higher speeds, the oil film is broken. As a result, the process of direct contact of friction surfaces is lengthened, rubbing on the segments emerges, and then the geometry of the fluoroplastic surface of the segments changes, and the thrust bearing loses its serviceability.

Formulation of the Task

Development of the method of calculating of the supporting elements of rigid thrust bearings in a three-dimensional setting with the possibility of taking into account the use of new materials.

Calculation Diagram of the Analytical Method

In Figure 3 the Diagram of calculating of the thrust bearing in a two-dimensional setting is shown. In this case, a significant disadvantage is the assumption of a uniform distribution of the load, which does not reflect reality.

Maximum stresses shall emerge in the center of the support. However, based on this diagram, they emerge at the edges, in the place of availability of concentrators.

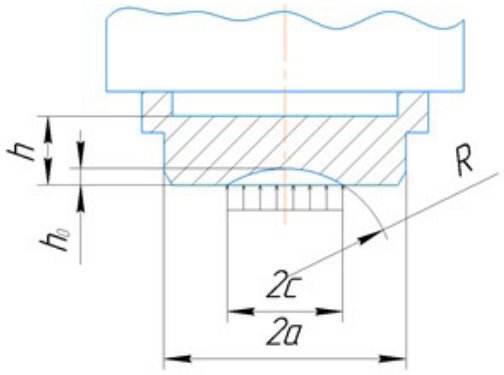

Figure 3. The Design Diagram of Thrust Bearing in Two-Dimensional Setting

Implementation of the Method of Three-Dimensional Calculation

In paper [6], the method of calculating and designing of elastic structural elements was considered, but the calculation of support bolts and plates was not considered there. The support bolt and plates perceive an alternating load at all stages of operation, and failure often results in the need for replacement with disassembly of the entire Hydrogenerator.

Considering the above, it is necessary to develop the method of calculating the thrust bearings of Hydrogenerators in a three-dimensional setting, taking into account the characteristics of the chosen material and supporting elements (bolts and plates).

As calculation material Steel 40XH or Steel 34CrMo4 are used. Their mechanical characteristics are determined as per GOST 8479–70 gr. 5 KP (killed) 590, and availability of internal defects is regulated at supersonic diagnostic as per GOST 24507–80 group 4P.

The macrostructure of steel is sorbitol. It is necessary to pay a special attention to the fact that the availability of lowercase non-metallic inclusions in the steel structure can negatively affect the mechanical strength of the samples.

Controlling the dimension of a grid of solid body includes specifying finite element values in various areas of the model. The smaller dimension of the element in the area improves the accuracy of the results in this area.

At that special attention shall be paid to the type of grid. It is proposed to use the grid at the basis of curvature. SolidWork Simulation currently includes solid continuum elements, curved surface shell elements (thin and thick) and truss and frame line elements [7]. Solid elements have only displacement degrees of freedom. Solid and membrane shell elements use linear and quadratic interpolation for the solution based on whether they have two (see Figure 4.) or three units on an edge. Solid elements have their stresses and strains recovered at a number of tabulated locations inside the elements. Stress or strain results from adjacent solids are averaged at their common nodes.

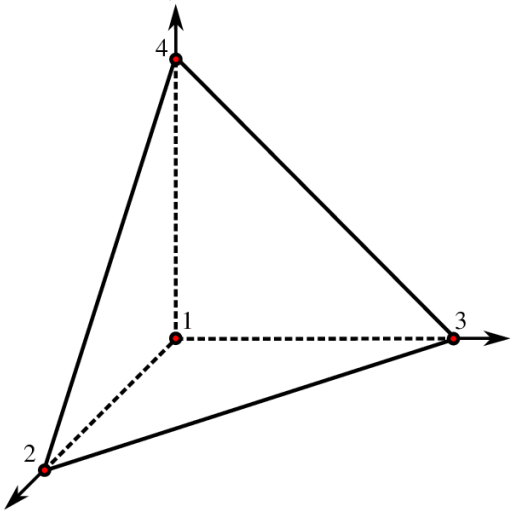

Figure 4. The Grid in General Coordinates

At that the order of the dimension of the minimum element corresponds to the maximum grain dimension of the crystal lattice in the contact zone (see Figure 5).

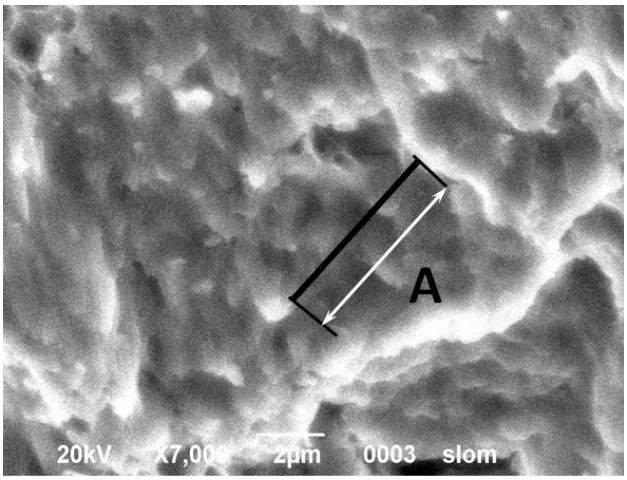

Figure 5. The Grain Dimension of the Crystal Lattice

In Figure 6 the loads acting on the thrust bearing and the boundary conditions are shown. The calculation results of the mechanical stresses acting on the support of the thrust bearing, obtained using SolidWork Simulation, are shown in Figure 7.

The calculated axial force P on the thrust bearing unit, caused by the weight of the Hydroaggregate unit rotor group and the hydraulic force, may comprise about 500 tons and is distributed evenly between the supports.

As the basis of the choice of safety margin for the finite element method is proposed to use the criterion of Cramer-von Mises, which is typical for isotropic materials with a viscous nature of fracture. However, it is necessary to take in to consideration that under pure compression/tension, the both of criteria are identical. And with a pure bend, the strength as per Cramer-von Mises is about 15% more.

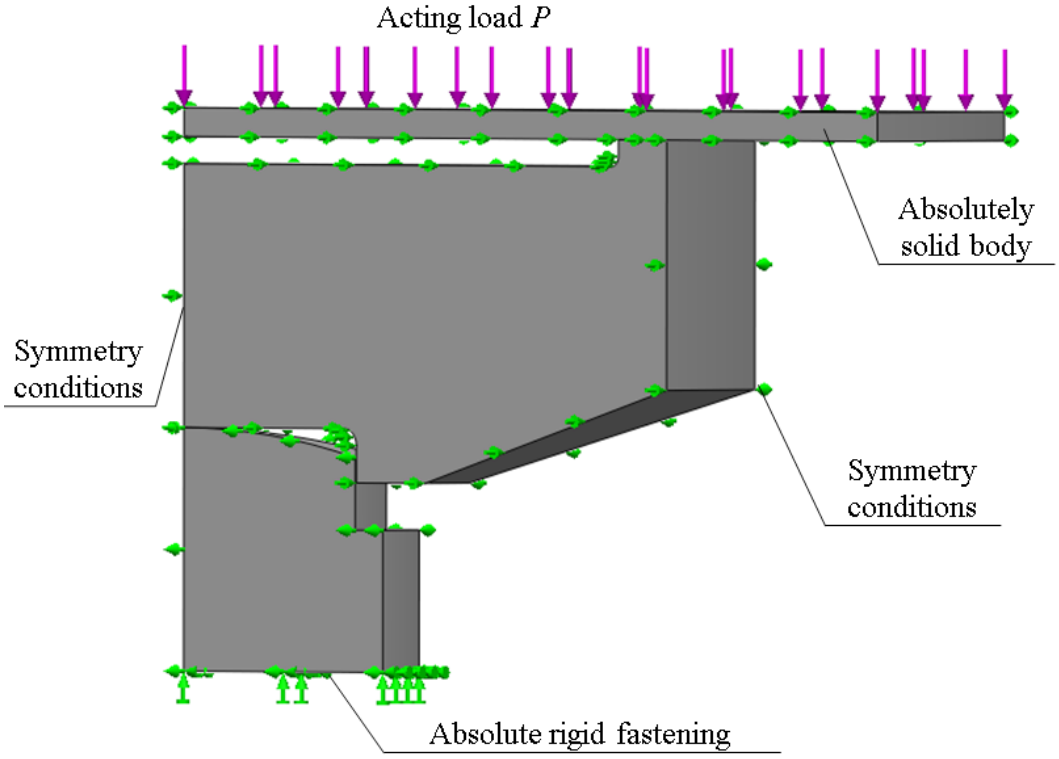

Figure 6. Loads, acting on to the thrust bearing and limiting conditions

However, if we consider the results in details, then the actual strength margin shall be supplemented by a contact stress coefficient.

For a ball with radius R_{ball} and plane $R_n \Rightarrow \infty$ at condition of a touch provided in the form of an ellipse equation $\frac{1}{2R}$ the greatest stress comprises $0.388\sqrt[3]{PE^2\frac{1}{R_{ball}^2}}$ (see Figure 8), where E – is the elasticity modulus of steel.

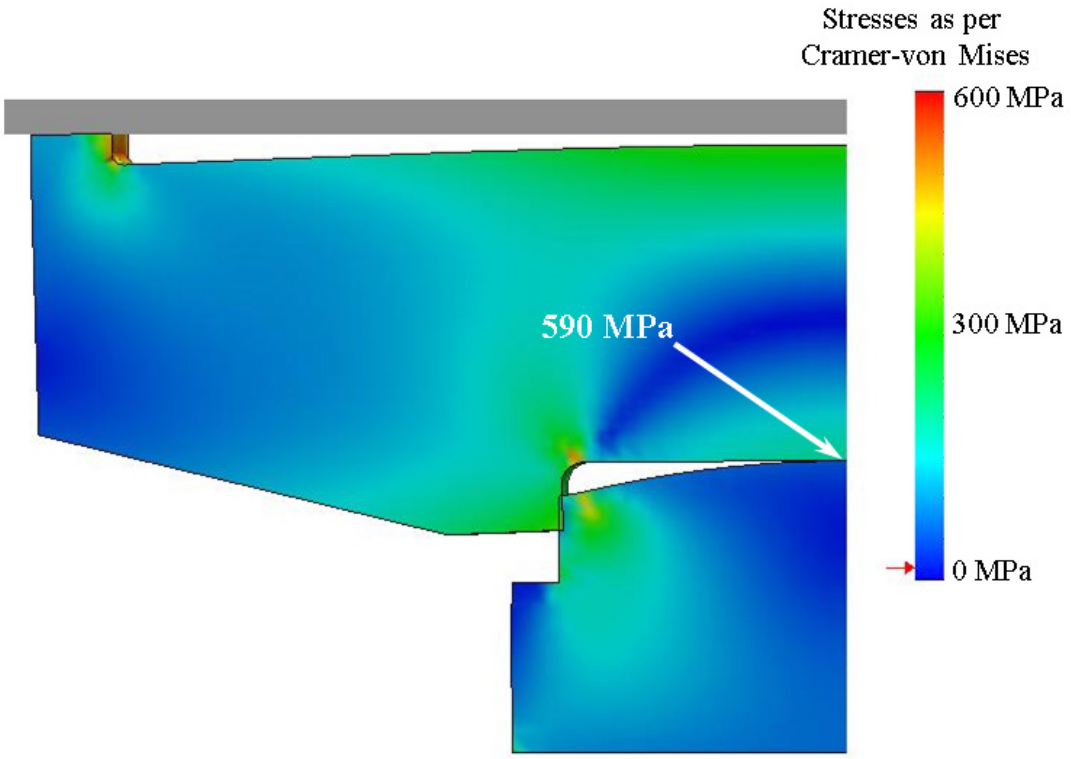

Figure 7. The Results of Calculation

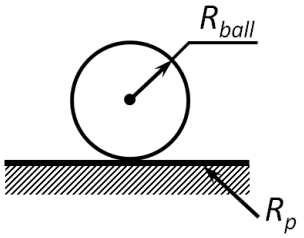

Figure 8. The Diagram of Contact Stress

Got stresses comprise of 590 MPa. At that the average ones do not exceed the admissible ones in accordance with the requirements of GOST 5616–1989, and the maximum ones satisfy the following formulae:

$$0.388\sqrt[3]{PE^2\frac{1}{R_{ball}^2}}.$$

Conclusion

The features of operation, design and design versions of the supporting elements construction of electric machines of high power are considered in given paper. It is shown that the most loaded elements that perceive contact loads are rigid thrust bearings, namely plates and support bolts. The method of mathematical modeling of the stressed state in a three-dimensional formulation was implemented. The permissible stresses in the contact zone are specified taking into account the geometry of the zone of contact between the plate and the bolt, the influence of the metal structure on the grid parameters of the finite element method.

References:

1. Sazykin V. G., Kudryakov A. G., Netrebko S. A., Pron' V. V. Perspectives for efficiency of the electric power complex of Kuban. Electric-geriatrics – improving the operation of worn-out equipment. – Krasnodar: Kub SAU, 2012.– 448 p.
2. Kobzar K. A. Methods and means of making and complex unit-wise modernization of Turbogenerators rated 150–300 MW: author's abstract. diss. … Candidate Tech. Sciences: 05.09.01. National Academy of Sciences of Ukraine Institute of Electric Dynamics.– Kiev, 2015.– 22 p.

3. Milykh V. I. Organization of numerical-field calculations of electric magnetic processes in Turbogenerator with its asymmetrical load. Bulletin of the NTU "KhPI". Series: "Electric machines and electric mechanical energy conversion". 2016.– No. 11 (1183).– P. 3–10.
4. Shevchenko V. V. Determining of the forces acting in the stator core of the Turbogenerator. Electric Power and Electric Mechanics: Collection of Scientific and Technical Papers. International Scientific Conference. Voronezh: Private Educational Institution of Higher Education "International Institute for Computer Technologies", 2015.– P. 52–56.
5. Mamikoniants L. G., Elkind Yu. M., Petrov Yu. V. Detection of defects of Hydrogenerators. – M.: Energoatomizdat, 1985.– 231 p.
6. Tretiak O. Peculiarities of determining of the time between failures of the Hydrogenerator thrust bearing unit by the methods of three-dimensional modeling. Vestnik Kaznrtu. 2018.– No. 5 (129).– P. 113–118.
7. Akin J. Ed Finite Element Analysis Concepts via SolidWorks. Rice University, Houston, Texas: World Scientific, 2009.– 303 p.

Section 4. Food processing industry

Jabbarova Sarvinoz Komiljonovna,
researcher – applicant of the department
"Food technology and industrial ecology"
Bukhara Engineering and Technological Institute
E-mail: sarvi1208@mail.ru

Isabaev Ismail Babadjanovich,
Doctor of Technical Sciences, Professor of the Department
"Food Technology and Industrial Ecology"
Bukhara Engineering and Technological Institute
E-mail: isabaev_63@mail.ru

PRIORITY AREAS FOR IMPROVING THE RANGE OF CONFECTIONERY

Abstract. The article considers the issue of increasing consumer properties, nutritional and biological value of flour confectionery products, reducing their sugar capacity and calorie content. The analysis of the main directions of scientific research on the development of new original formulations of this type of products using natural raw materials and composite mixtures.

Keywords: flour confectionery, sugar substitutes, sugary starch products, dietary fiber, fats, fruit and berry and vegetable raw materials, multicomponent mixtures.

Today, the confectionery industry solves a number of important tasks to improve consumer properties, food and biological value of products, reduce its sugar capacity and caloric content, create highly efficient innovative technologies, reduce the consumption of imported and expensive domestic raw materials, improve the product range by developing new original recipes of confectionery with using functional food ingredients in conditions of tremendous competition with foreign manufacturers.

Of particular interest is the creation of new types of functional products with full or partial replacement of sugar by natural (monelin, miraculin, stevioside, thaumatin, maltose, fructose, galactose, honey, etc.) and synthetic (aspartame, acesulfame K, cyclamate, saccharin, sucralose, sorbitol, xylitol, etc.) sugar substitutes. There are various classifications of sugar substitutes: by origin (natural and synthetic), by degree of sweetness relative to sucrose (bulk sweeteners – the level of sweetness is close to sucrose, and intensive sweeteners – the level of sweetness is many times sweeter than sucrose), by calorie content (calorie (sucrose substitutes) and calorie-free (sweeteners). However, in recent years, economically developed countries have been searching for and developing technologies for producing sugar substitutes of a new generation, that is, possessing not only high technological indicators, pure sweet

taste, harmless to humans, but also capable of giving the product functional properties [1].

Currently, in the face of rising prices for sugar and sweeteners, mainly imported, the use of high-sweet sugary starch products is of undoubted interest. A promising direction is the production of sugary starch products directly from grain starch-containing raw materials, bypassing the extraction of "pure" starch. Sugar products of varying degrees of sweetness have unlimited potential applications in the food industry (tab.) [2].

Table 1. – Main properties and application of starch hydrolysis products

Product type	Properties	Application
Maltodextrins	Low osmolaritygelability	Carbohydrate component for baby food, thickeners, fillers, stabilizers
Maltose syrup	Increased sweetness	Hard pastry and bakery products
High sugar syrup	Low hygroscopicity and viscosity; increased water retention, sweetness and fermentation	Confectionery, soft drinks, fermentation products, jams, canned foods, sauces
Molasses for baby food	Moderate sweetness, reduced crystallisability	Sweeteners for baby food, confectionery, soft drinks, jams, jelly, canned food, ice cream
Glucose Syrups	Increased sweetness	Non-alcoholic beverages, fermentation products, raw materials
Glucose-fructose syrups	High sweetness	Soft drinks, canned food, sauces, canned fruit
Cereal syrups	Moderate sweetness, non-crystallizability, high nutritional value	Flour confectionery and bakery products

Among the functional food ingredients, a large role is played by dietary fibers as traditional (from cereals and bean crops, vegetables, fruits and berries, citrus, nuts, mushroom, seaweed, etc.), so and nontraditional (from cereal and cane stables, herbs, medicinal and softwood, etc.), which have an important physiological significance. New extrusion products from unheaded grains of rye, corn, millet, barley, buckwheat, soybean and other rich in dietary fiber are widely used in the manufacture of confectionery products [1; 3].

Among the insoluble dietary fiber in the production of food, pulp is the most widely used as an additive that prevents caking and clumping. Cellulose is used in the production of bakery products, frozen semi-finished products, extruded products and pasta, etc. The main property on which the use of pectins in food technology is based in the gel-forming ability. Pectins are used in the manufacture of confectionery, baked products, for the preparation of fruit fillings, canned fruit, etc. as thickeners, stabilizers, gelling agents [3; 4]. However, a necessary condition for gelation of low-esterified pectins is the presence of calcium ions or other divalent cations in the system. In order to avoid wetting of flour products during storage, the filling should have a low water activity, that is, the minimum content of unbound moisture [1].

The increase in the content of flour confectionery products (FCP) dietary fiber contributes to the possibility of partial or complete replacement of solid fats for liquid vegetable oils, because, despite its good technological properties, solid fats are characterized by a high content of trans fatty acids, and in liquid vegetable oils a mass fraction the latter does not exceed 1,5% of total fat [5].

The concern of the world community about the dangerous effects on the human body of trans fatty

acid isomers has led to the development of alternative technologies for the production of margarines, shortenings and other specialty fats. However, due to the high cost of production, it is not yet possible to go to work with these fats. The use of liquid vegetable oils in the production of FCP is limited, since they lead to destabilization of the food system, as a result, the volume of products decreases and the oil migrates to the packaging material during storage. The functional and technological properties that characterize the interaction of raw materials with oil include the ability of prescription components to bind and retain oil, which plays a significant role in shaping the quality of semi-finished and finished products [6].

According to the data obtained, pectin and fiber have the best fat binding capacity. Pectin is an anionic polysaccharide and is characterized by surface activity. In this regard, the interaction of pectin hydrophobic groups with oil is possible and the oil is adsorbed onto the surface of solid particles. The high fat-binding capacity of fiber is due to the unique natural capillary structure of the fibers, which makes it possible to retain fat not only due to functional groups, but also by adsorption. In this case, adsorption occurs not only on the external, but also on the internal surface of the adsorbent [7].

Recently, interest in vitamin preparations from natural raw materials has increased due to their higher physiological activity, since natural vitamins are stereospecific for the human body historically adapted to them. As a rule, natural vitamin complexes are more stable than individual synthetic vitamins. The solution of this problem in relation to the production of flour products has been associated in recent years with the use of fruit, berries and vegetables, as well as the products of its processing [8].

The science of nutrition regards these raw materials as vital food products, giving them functional properties. Range of products from fruit and berry and vegetable raw materials, including secondary, represents significant prospects for use in the manufacture of confectionery, helps reduce the consumption of the most expensive prescription components, the rational disposal of production waste and, consequently, increase its profitability. The use of fruit and vegetable additives in the production of flour confectionery products will increase the resistance of foams and emulsions due to the formation of protein – polysaccharide complexes, which act as surface active substances, by means of electrostatic attraction forces arising between polyelectrolytes, which are pectin substances and proteins, and also enrich products flavoring and aromatic substances, natural dyes and sweeteners, vitamins, minerals, dietary fiber and other vital nutrients [9].

Currently, technologies are being developed for the preparation and use of various types of multicomponent composite mixtures (MCM) for obtaining a wide range of products based on them. The development of new flour mixtures is a multi-faceted procedure, which includes a number of necessary and interrelated aspects and is carried out in stages (fig 1.) [10].

From the standpoint of a systematic approach to the development of the ISS, the following steps are envisaged [11]. At the first stage, the selection of raw materials is carried out, their functional properties are studied, the safety of the components in the food relation is clarified. The second stage includes the study of raw materials and improvers, their impact on the properties of the dough and the quality of the finished products. Raw materials are selected that are optimal according to the criteria that characterize their nutritional value. Criteria are selected depending on the purpose of the design – the functional purpose of the mixtures and products prepared on their basis. As optimization criteria when designing mixtures, the optimal content of amino acids, individual macro- and microelements, the ratio of basic nutrients and the provision of energy value are proposed.

At the third stage, when developing the technology for the preparation of mixtures and flour products, it is necessary to ensure the elimination of the negative influence of the components of mixtures on con-

sumer properties of products. This is possible when using special technological methods, which provide for the adjustment of technological parameters, or by making improvers and other food additives. The stage ends with the release of a pilot batch of mixtures and cooked bakery products using them. Thus, a flour mixture prepared by grinding a grain mixture of wheat and barley was developed for the production of FCP. Formulations of flour mixtures consisting of wheat flour, granulated sugar, potato and corn starch, dextrose, skimmed milk powder and whey, and dried vegetable oil are proposed. Products made on the basis of the developed mixtures are characterized by a reduced calorie content, a high content of polyunsaturated fatty acids and a low proportion of cholesterol in comparison with analogues. The polyfunctional properties of dry mixes can make it possible to eliminate undesirable components for the human body or to enrich food products with physiologically significant and scarce ingredients [10].

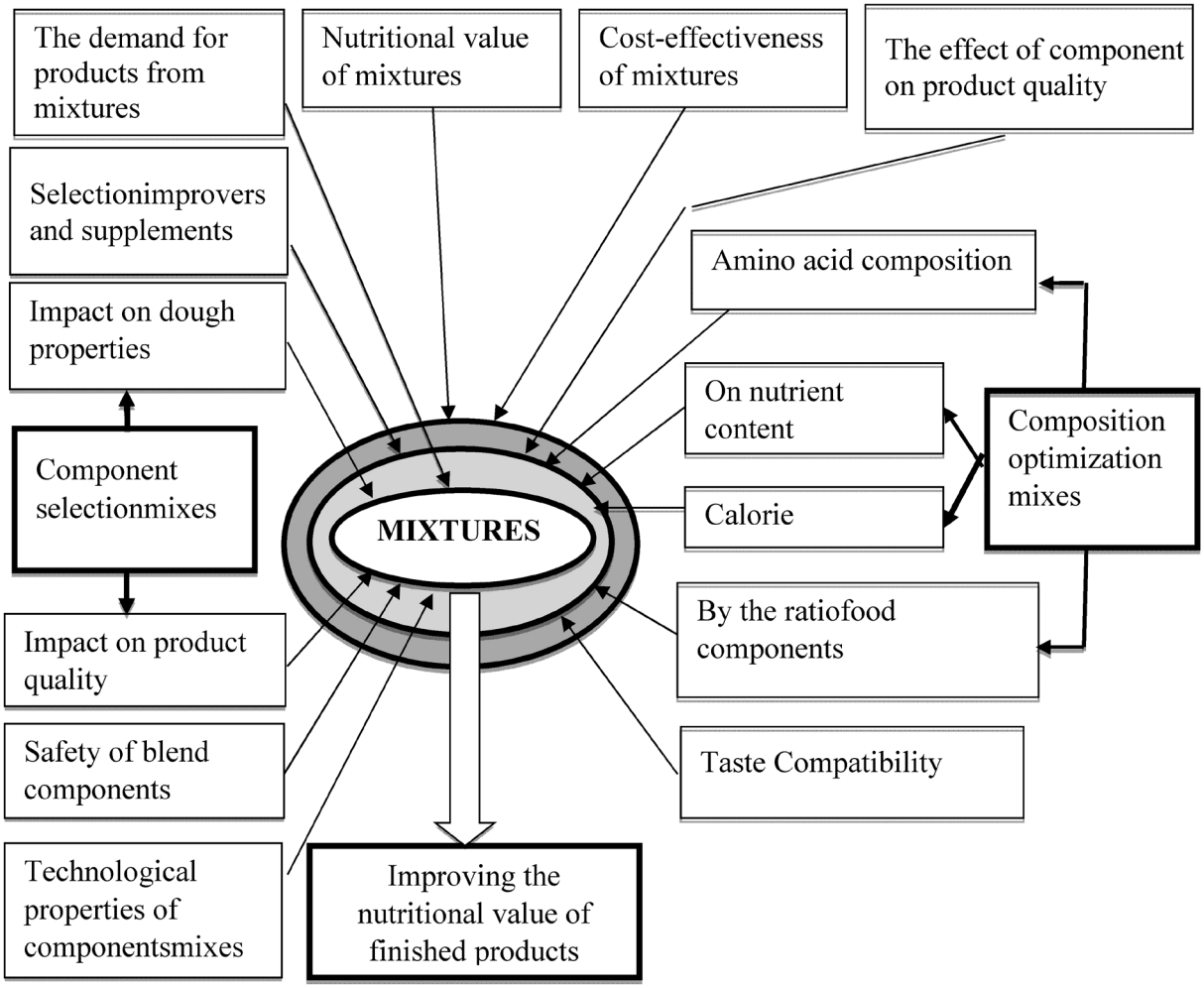

Figure 1. Scheme of an integrated approach to the development of flour mixtures

In science and industry, considerable experience has been accumulated in creating a range of enriched confectionery products, and their manufacturing techniques have been developed. However, the problem of forming a new assortment of these functional products cannot currently be considered solved. Successful solution of the tasks facing the confectionery industry is associated with the search for new natural functional ingredients, their more rational use, which will provide real prospects for reducing the deficit of functional products.

References:

1. Levchenko V. D. Pectin. Pectin prophylaxis / V. D. Levchenko, L. M. Timonov.– Krasnodar, 1992.– P. 21–23.
2. Andreev N. R. The use of starch products to improve the quality of bakery products / N. R. Andreev, N. D. Lukin, S. T. Bykova // GNU All-Russian Research Institute of Starch Products of the Russian Academy of Agricultural Sciences. Materials reports of the International Conference "Bakery production – 2014" / International Industrial Academy.– M., 2014.– P. 45–52.
3. Kulichenko A. I. Modern technologies for the production of confectionery products using dietary fiber / A. I. Kulichenko and others // Young scientist. 2014.– No. 4.– P. 203–206.– URL: https://moluch.ru/archive/63/9786 (access date: 10/31/2018).
4. Kurakina A. N. Functional ingredients in the production of confectionery / A. N. Kurakina [et al.] // Fundamental research. 2015.– No. 6–3.– P. 468–472. URL: http://fundamental-research.ru/ru/article/view?id=38643 (access date: 09/14/2018).
5. Kulakova S. N. Features of vegetable oils and their role in nutrition/ S. N. Kulakova [et al.] // Fat-and-oil industry. 2009.– No. 3.– P. 16–17.
6. Eingor A. B. The fat-absorbing ability of powdered raw materials of confectionery production / A. B. Aingor and others // Bakery and confectionery production. 1996.– No. 2.– P. 41–42.
7. Nechaev A. P. Fat products for healthy and therapeutic and preventive nutrition / A. P. Nechaev // International Conference "Technologies and Healthy Foods". Part 1 – M.: Publishing House MGUPP, 2003.– P. 93–98.
8. Bogatyryov A. N. The use of dietary supplements in food / A. N. Bogatyrev and others // Your food. 2000.– No. 1.– P. 17–20.
9. Blagodatskikh V. E. Investigate the patterns of structure formation of candy masses of pralines using beet fiber / V. E. Blagodatskikh, T. V. Savenkova // Materials nauch.-practical. conference "Food industry of the South of Russia. Environmentally friendly energy–saving technologies for the storage and processing of raw materials of plant and animal origin".– Krasnodar: KNIIKhP, 2000.– P. 32–34.
10. Koryachkina S. Ya. Innovative technologies of bakery, pasta and confectionery products: monograph / S. Ya. Koryachkina and others; Edited by Dr. Tech. sciences, prof. S. Y. Koryachkina.– Orel: Federal State Educational Institution of Higher Professional Education "State University–UNPK", 2011.– 265 p.
11. Stabrovskaya O. Classification of multicomponent mixtures for bakery products / O. Stabrovskaya, O. Korotkova // Bakery Products. 2009.– No. 8.– P. 48–49.

Section 5. Agricultural sciences

Khujakulova Nilufar Fayzullaevna,
prof. Majidov Kahramon Halimovich,
dost. Makhmudov Rafik Amonovich,
Bukhara Engineering-Technological Institute
E-mail: mega.sobirova@inbox.ru

QUALITY AND PHYSICAL AND CHEMICAL CHARACTERISTICS OF LOCAL WHEAT GRAIN KINDS

Abstract. The features of quality and technological properties of a new wheat variety have been studied. Modern methods of physical-chemical research were used in the studies. It has been established that the protein content in wheat ranges from 9.2 to 25.8%. The new grain variety has greater value than the optimal one, and it combines the most important biological and technological properties at a higher level.

Keywords: Wheat grain, "Istiklol" variety, chemical composition of grain, protein content, grain gluten, storage stability.

In connection with the development of breeding and seed farming in agricultural production, recently great attention is paid to the creation of new breeds and wheat kinds, which are resistant to cultivation in saline soil and climatic conditions [1–3]. One of these kinds of wheat grain is the Istiklol kind [4]. The cultivation of this type of grain expands in the conditions of grain fields. In this regard, the study of the features of the quality and technological properties of a new kind of wheat has both scientific and practical interest.

The work studies the quality and basic physical-chemical, technological characteristics of the wheat grain of the kind "Istiklol". To conduct research, modern methods of physical-chemical and biochemical analyzes have been used [4; 5].

In terms of food production, the most valuable part of the grain from which the best sorts of flour are obtained is the endosperm (table 1).

Table 1. – The chemical composition of the studied kinds of grain "Istiklol"

Crop	Water, g	Protein, g	Fats, g	Mono- and disaccharides, g	Starch, g	Cellulose, g	Ash, g	Energy value, kcal
winter soft	14.0	11.2	2.1	1.2	54.0	2.4	1.7	290
spring soft	14.0	12.5	2.3	0.9	53.0	2.5	1.7	291
durum	14.0	13.0	2.5	0.8	54.5	2.3	1.7	301

In table 2 data on the chemical composition of the grain by the constituent parts of the weevil are given

Table 2. – The chemical composition of the constituent parts of wheat grain "Istiklol",% dry matter

Name	Ratio of parts	Protein	Carbohydrates,%					Lipids,%	Ash content,%
			Total	including					
				starch	sugar	cellulose	pentosans		
Whole grain	100.0	16.06	78.25	63.07	4.32	2.76	8.10	2.24	2.18
Endosperm	81.60	12.91	85.23	78.82	3.54	0.15	2.72	0.68	0.45
Germ	3.24	41.30	37.32	–	25.12	2.46	9.74	15.04	6.32
Shell with aleurone layer	15.16	28.75	57.03	–	4.18	16.20	36.65	7.78	10.51

As can be seen from the data of (table 2), the protein content in wheat varies widely – from 9.2 to 25.8% (an average of 13.5). Durum wheat grain contains more protein than soft wheat grain.

Protein substances are unevenly distributed across individual tissues of wheat grain (Table 3). The aleurone layer is the richest in protein substances. A lot of protein is also in the germ. The protein content in the endosperm is less than in the whole grain. The sub-aleurone layer of durum wheat contains 45% protein, and the inner – 11%.

Table 3. – The protein content in the morphological parts of the grain of wheat "Istiklol"

Name	Kind – "Istiklol"	
	In each part of the grain,%	The ratio of the quantityby parts of the grain
Whole grain	16.07	100
Endosperm	12.91	65
Aleurone layer	53.16	22
Germ shield	37.63	8
Pericarp coat	10.56	5

Gluten is the most important factor in the baking value of wheat flour. It depends on the gas-holding capacity of the dough, and therefore, the volume and porosity of the bread. Strong gluten in normal flour makes the dough too tight, difficult to stretch with carbon dioxide. Weak dough badly keeps carbon dioxide, as its weak gluten cannot create the necessary strength of protein frame in the dough. Strong gluten during fermentation more steadfastly retains its inherent physical properties (Table 4).

Table 4. – Gluten composition of wheat grain kind "Istiklol"

Protein substances,%				Lipids,%			Carbohydrates,%				Ash content
Gliadin	Glutenin	Albumin and globulin	Total	Free	Bound	Total	Starch	Sugar	Cellulose	Total	
1	*2*	*3*	*4*	*5*	*6*	*7*	*8*	*9*	*10*	*11*	*12*
39.09	35.07	6.75	80.91	4.20	–	4.20	9.44	–	2.02	11.46	2.48
–	–	–	72.67	0.75	6.30	7.05	–	–	–	18.82	0.63
–	–	–	82.60	0.12	8.38	8.50	8.79	–	–	8.79	0.71
50.20	34.85	3.35	88.40	2.12	–	2.12	6.72	1.20	–	7.92	0.92

1	*2*	*3*	*4*	*5*	*6*	*7*	*8*	*9*	*10*	*11*	*12*
43.02	39.10	4.41	86.53	2.80	–	2.80	6.45	2.13	–	8.58	2.00
–	–	–	90.00	–	8.00	8.00	0.01	–	–	0.01	0.50
–	73.7	5.3	79.0	2.91	4.19	7.10	7.28	1.20	1.08	9.56	2.80
Average											
43.5	36.0	4.0	83.5	1.0	6.0	7.0	6.0	1.3	1.3	8.6	0.9

Wheat kind"Istiklol" is characterized by a complex of morphological, biological, and economic characteristics and properties, by which we understand yield, frost tolerance, resistance to disease and pest damage, requirements for soil and its composition, requirements for moisture, light, temperature, earliness, non-fall, resistance to lodging, size, shape and color of the grain, characteristic features of the chemical composition, storage stability. The new kind has greater value than the optimal one, and at a higher level combines the most important biological, economic and technological properties.

The valuable properties inherent in the kind "Istiklol" can appear only under certain growing conditions, on an agricultural background that provides the widest possible disclosure of the potential of the kind.

Thus, the established quality indicators and physical-chemical characteristics of the new wheat grain kind"Istiklol" allowed determining the possibilities and recommendations for its cultivation in the soil and climatic conditions.

References:

1. Кретович В. Л. Биохимиярастений.– М.: «Высшаяшкола» 1986.
2. Казаков Е. Д., Кретович Биохимиязерна В. Л. и продуктовегопереработки.– М.: Агропромиздат, 1989.
3. Кутыга О. Н., Вострикова О. В. Лабораторныйпрактикумпобиохимии.– Учебноепособие.– Волгоград, 2011.
4. Орехович В. Н. Современныеметоды в биохимии.– М.: Медицина, 1977.
5. Ермаков А. И. Методыбиохимическогоисследованиярастений.– Ленинград. Колос. Ленингр. отделением, 1972.

Section 6. Technical sciences

Makhmudov Nazirila,
Agzamov Avaz,
Ermatov Navruz,
Mukhammadiyev Khamidillo,
Karshi engineering-economics institute
E-mail: makhmudov.nazirila@bk.ru

ASSESSMENT OF THE DEGREES OF INFLUENCE OF GEOLOGICAL AND PHYSICAL AND TECHNOLOGICAL FACTORS ON THE EFFICIENCY OF WATER FLOODING OF OIL DEPOSITS IN THE FERGANA DEPRESSION OF THE RESERVOIR TYPE

Abstract. This article describes some data on geological and physical influence, as well as ways of modernizing the oil filed development procedures in the Fergana regional reservoirs. Moreover, some scientific analysis have been conducted at the territories of valley fields of Uzbekistan.

Keywords: efficiency, water flooding, oil deposits, injection, displacing, maintenance, depletion, development, residual, narrow, strata, creeping, saturation, predominant.

The effectiveness of modern oil field development systems is largely due to the use of the artificial water-flooding method, due to which currently about 90% of the total world oil production is being produced [1, 10].

Along with testing and introducing other methods, waterflooding has become the main method of influencing oil deposits. Due to the availability of water, the relative ease of injection and the high efficiency of oil displacing water, conventional water flooding will be widely used for a long time. According to the results of research by scientists and specialists, the maintenance of reservoir pressure by flooding made it possible to increase: the average design oil recovery (relative to development systems for depletion) by about 2 times; oil production rates (current annual production); well flow time [1; 6; 7; 10].

Water flooding as a separate development method with favorable physico-geological conditions allows achieving oil recovery ratio of 0.65–0.7. However, when watering fields with hard-to-recover reserves (high oil viscosity, low permeability and large reservoir heterogeneity), oil recovery coefficients decrease to 0.3–0.35 with increasing frequency of flushing from 0.8–1 to 5–7, and with oil viscosity 25–30 MPa·s Water flooding becomes ineffective. Therefore, the oil industry is faced with the problem of enhanced oil recovery, which is to increase the efficiency of water flooding as the main technology and to select residual oil from already watered zones and deposits that are developed under other depletion or repression regimes [3; 4; 8; 9].

However, the widespread use of this method of developing oil fields is unthinkable without its further improvement. In this regard, the study of the

features of artificial flooding of deposits in various geological and physical conditions and the search for ways to improve it have been and are being given considerable attention. Such studies, as is known, on the one hand, make it possible to use the accumulated experience in the exploitation of deposits during artificial flooding in the design process of developing new fields: on the other, they contribute to the effective development of depleted objects, in which huge material and technical resources have been invested [2].

Oil recovery is a complex function of many parameters of the reservoir and its saturating fluids, as well as development and flooding systems. At the same time, when studying the characteristics of the development of a particular group of fields, it is possible, as a rule, to single out the predominant influence on the oil recovery of a certain number of natural and technological factors and to estimate their share in the formation of current and final oil recovery. This is evidenced by numerous statistical (regression) dependencies of oil recovery on geological, physical and technological factors.

Oil deposits of the objects under study are confined to narrow asymmetrical folds, the length of which is 10–15 km, the width does not exceed 2–3 km, the dip angles are 20–30 º and more. Oil deposits are mainly of the reservoir-vault type. In cases of complications due to their disturbances, tectonically screened deposits are observed (Fig. 1).

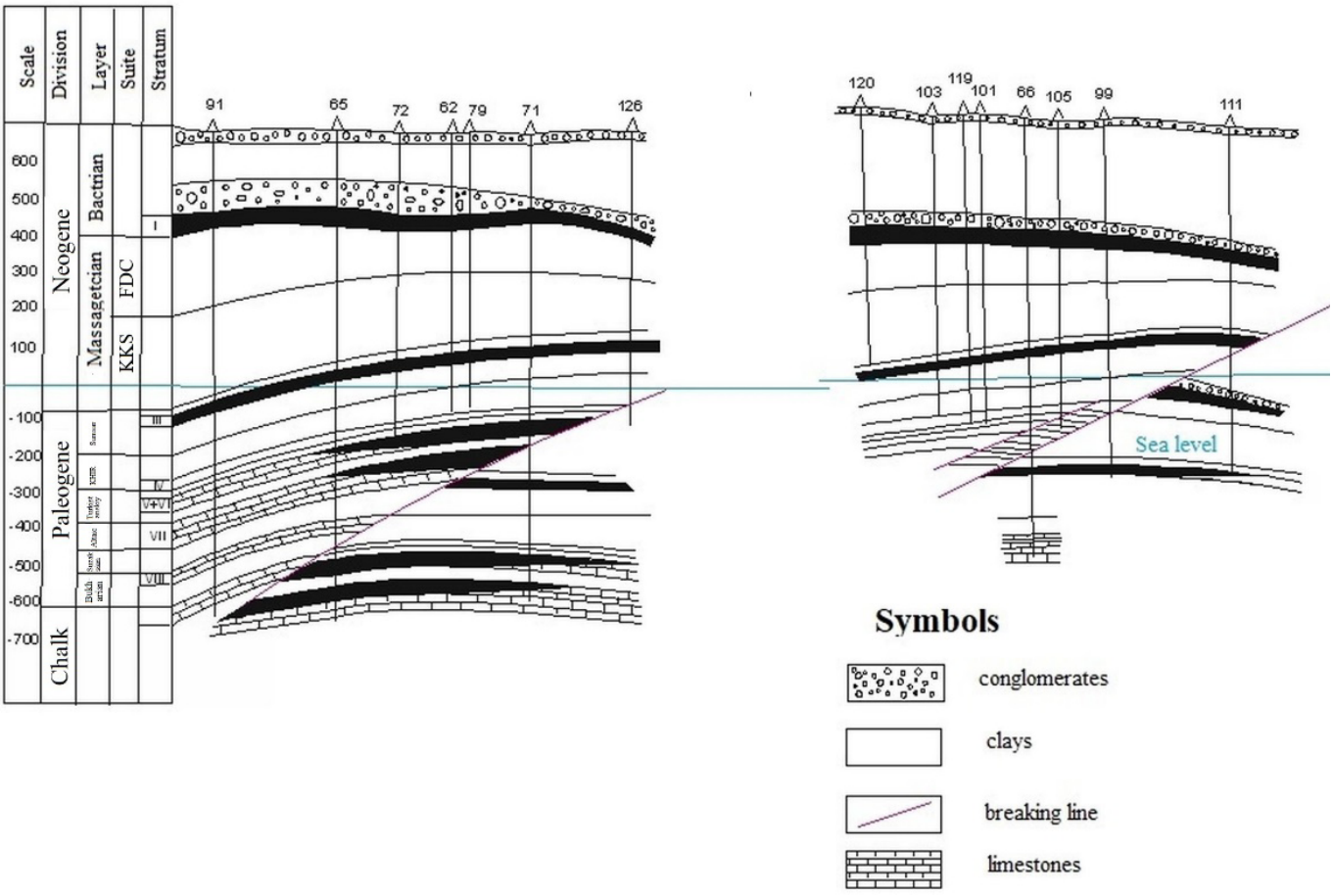

Figure 1. Cross-section geological profiles of the Andijan deposit

Oil-bearing fields are mainly represented in the Paleogene (productive horizons VIII, VII, VI, V, IV, III) and Neogene (sandstone brick-red and pale pink formations and horizon I) deposits. Oil

deposits in carbonate reservoirs (limestone and dolomite) are confined to the V, VI, VII, VIII, IX horizons of Paleogene sediments.

The oil of productive sediments is mainly light, low-sulfur, paraffin, high resin. The viscosity of reservoir oils is low 0.5–6 MPa • s, the initial gas saturation is up to 100–150 m^3/t. Oil deposits are characterized by an insignificant thickness of productive strata, a small difference between the initial reservoir pressure and the oil saturation pressure of gas.

All objects were drilled on the creeping system, the wells were placed on a triangular grid. Duration of drilling was mainly 5–7 years. Various waterflood systems were implemented (contour, boundary, contour, areal, focal and other modifications), gas was bypassed with simultaneous water injection, a 2–3 reservoirs were combined into one development object, a dense grid of wells was used (up to 3–5 ha well).

These facilities are currently in the final stages of development, which make it possible to evaluate the effectiveness of the technological solutions adopted, including the value of the final oil recovery factor.

To determine the degree of influence of various geological and physical and technological factors on the flooding of oil deposits in the Fergana Depression, in this work, methods of non-parametric statistics are used, namely: U is the Mann-Whitney criterion, X is the Van der Warden criterion and the Kullback measure [5].

Investigation of the influence on the current ηт and the expected final – oil recovery $\eta_к$, subjected to the following parameters: $(kh)/\mu_н$; $(k\delta_н)/m$; $P_{current.}/P_{true}$; S_{max}; S_{medium}; $Q_ж/Q_{ball}$; Q_{fin}/Q_{ball}; d_{max}; d_{medium} (where k, h, m – permeability, thickness and porosity respectively; $\delta_н$ и $\mu_н$ – initial oil saturation and oil viscosity; $P_{current\ and}$ P_{true} – the current pressure at which water flooding begins and the saturation pressure of oil with gas; S_{max} and S_{med} – maximum and average well density; $Q_ж$ and Q_{fin} – accumulated volumes of fluid and water pumped into the reservoir; Q_{ball} – balanced oil reserves; d_{max} and d_{med} – the maximum and average for the entire development period of the reservoir, the ratio of the number of oil and water injection wells). The results of the calculation of the informativeness of the listed parameters are given in (table 1).

As can be seen from the table according to the degree of influence on the final and current oil recovery, the studied parameters are arranged in the following sequence: $P_{current}/P_{true}$ (4,1); S_{max} (3,14); $kh/\mu_н$ (1,98); $Q_ж/Q_{ball}$ (1,76); Q_{fin}/Q_{ball} (1,29); $k\delta_н/m$ (0,44); d_{med}(0,21).

Table 1.

Geological-, physical and technological parameters	Criteria		Measure Kullback
	U- Manna-Whitney	X van der Warden	
$\eta_к = P_{current}/P_{pump}$	informative	Informative	4.10
$\eta_к = (S_{max})$	informative	Non-informative	3.14
$\eta_к = (kh)/\mu_н$	informative	Informative	1.98
$\eta_т = (Q_ж/Q_{ball})$	informative	Informative	1.76
$\eta_т = (Q_{fin}/Q_{ball})$	indefinite decision		1.29
$\eta_к = (k\delta_н)/m$	indefinite decision		0.44
$\eta_к = (d_{med})$	indefinite decision		0.21
$\eta_т = (S_{med})$	indefinite decision		–
$\eta_к = (d_{max})$	indefinite decision		–

Consequently, the most informative, (that is, the degree of influence on oil recovery) has the parameter $P_{current}/P_{true}$, which is associated with a reasonable time to start artificial flooding. Specified, of course, for the fields of the Fergana depression, the artificial flooding of which was started after a certain time of

their operation in the natural, most often dissolved gas, mode. The effect of this parameter on the final oil recovery can be clearly seen from (Fig. 2), where the optimum ratio is $P_{current}/P_{true}$, at which flooding should begin, lies for deposits of the Fergana depression in the range of 60–80%. In passing, we note that for the deposits of the platform type, this interval is somewhat already – 80–90% [1; 3]. At the same time in the fields where oil viscosity does not depend a lot on pressure; oil recovery with partial degassing of oil (about 20% of $P_{current}$) is 5–10% higher than with conventional water flooding [1]. These data are in good agreement with those observed in the fields of the Fergana depression.

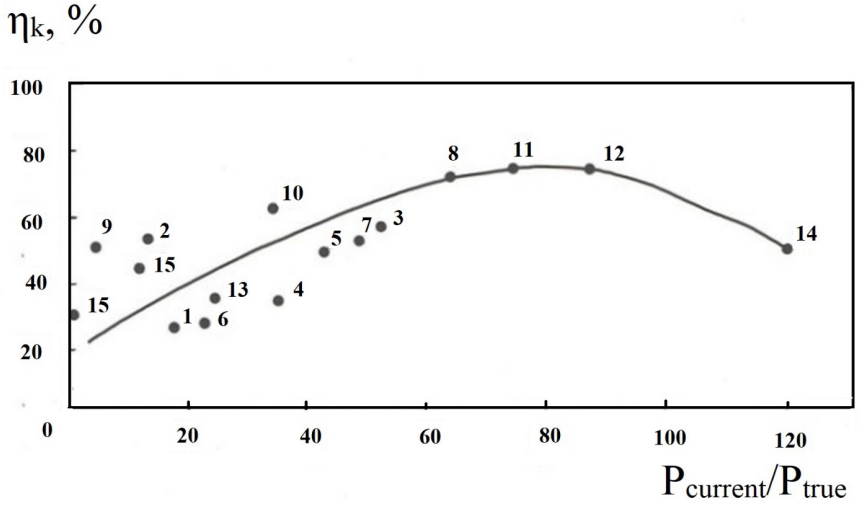

Figure 2. Dependence of the expected final oil recovery on the current reservoir pressure at which waterflooding is started, expressed in fractions of the oil saturation pressure of gas in the fields of the Fergana depression: 1, 2, 3 – Khodjiabad (III, VII, VIII); 4, 5, 6, 7 – South Alamyshik (I, KKC, III, V + VI + VII); 8 – Boston (III); 9, 10 – Andijan (III thrust and east field); 11 – Chongara-Galch (VI); 12 – Northern Sokh (VIII); 13, 14 – Palvantas (III, VII); 15, 16 – West Palvantash (III, VII) the horizon is shown in parentheses

At first glance, analyzing the values of informativeness and the Kullback measure of the Smax and kh/μ_H parameters, it can be concluded that the final oil output of the productive horizons of the Fergana Basin fields is weakly dependent on these parameters. However, given the relatively narrow range of changes in the hydraulic conductivity of horizons (in 60% of cases from 0.1 to 0.4 $\mu m^2 \cdot m^2$/mPa • s) and, in particular, the density of the grid of wells (in 72% of cases from 4 to 5 hectares / SLE) to draw such a conclusion, apparently, is not quite competent. Under these conditions (at practically fixed values $kh/\mu_н$ and S_{max}), the final oil recovery, which is natural, was largely formed under the influence of other parameters of the reservoir – in this case $P_{current}/P_{true}$.

References:

1. Surguchev M. L. Secondary and tertiary methods for enhanced oil recovery – M.: Nedra, 1985.– 308 p.
2. Ivanova M. M. Dynamics of oil production from deposits.– M.: Nedra. 1976.– 247 p.
3. Regulation of the development of oil fields / B. T. Baishev. V. V. Isaychev. S. V. Kozhakin et al.– M.: Nedra 1978,– 197 p.
4. Irmatov E. K., Agzamov A. Kh. Waterflooding of oil fields with complicated geological and physical conditions and ways to increase its efficiency.– Tashkent: Fan, 1992.– 53 p.

5. Runyon R. Reference book on nonparametric statistics (modern approach). Translated from English by E. Z. Demydenko.– M.: Finance and statistics. 1982.–198 p.
6. Problems of residual oil recovery by physicochemical methods / N. I. Khisamutdinov, Sh. F. Takhautdinov, A. G. Gelin, T. I. Zainetdinov.– M.: VNIIOEKG, 2001.– 184p.
7. Vladimirov I. V., Khisamutdinov N. I., Gaziev M. I. Problems of development of oil and partially flooded areas of oil fields.– M.: OJSC "VNIIOEKG", 2007.– 360 p.
8. Ibragimov L. Kh., Mishchenko I. T., Cheloyants D. K., Intensification of oil production.– M.: Science 2000.– 414 p.
9. Lysenko V. D., Graifer V. I., Rational development of oil fields.– M.: LLC Nedra – Business Center, 2005.– 607 p.
10. Methods for extracting residual oil / M. L. Surguchev, A. T. Gorbunov, D. P. Zabrodin and others.– M.: Nedra, 1991.–347 p.

Dadaev G'ani Toshxodjayevich,
Tashkent state technical university,
researcher, deputy dean
of the machine-building faculty
Safarov Jasur Esirgapovich,
Tashkent state technical university,
dean of the machine-building faculty
E-mail: jasursafarov@yahoo.com

IMPROVING ENERGY-SAVING SOLAR DRYING PLANT FOR DRYING DIETARY FOOD HERBS — MOTOR (ALLIUM MOTOR)

Abstract: The article describes the improvement of energy-saving solar drying plant for drying dietary food herbs — motor (Allium motor). The value of the equilibrium moisture content significantly affects the estimates of drying intensity indicators. At the same time, the asymptotic value looks reliable, which is especially evident when comparing empirical points and approximated graphs of the drying rate. Taking into account the neglect of the initial accelerating stage, the graphs of the drying curves and the drying speed do not reveal periods of constant and falling drying speed and the curves have the appearance similar to those known in the literature on the drying of herbaceous materials.

Keywords: drying, dietary food herbs, solar dryer.

According to the UN Food and Agriculture Organization, in 2050, to meet the demand for food, the annual volume of world crop and livestock production should increase by 60% compared to 2006 [1]. In the world each year, due to spoilage, losses of grain products by 30%, root crops, fruits and vegetables by 40–50%, oilseeds, meat and dairy products by 20% and fish by 35% [2].

In the years of independence, special attention is paid to the cultivation and effective development of the industry processing agricultural products. As a result of the program activities carried out in this direction, including the provision of quality processing of agricultural and forestry products, tangible results have been achieved in the production of import-substituting and export-oriented food and pharmaceutical products.

Scientific research on the development of technology and hardware design processes for drying and processing dietary food herbs were engaged in: A. V. Lykov, A. S. Ginzburg, B. S. Sazhin, S. G. Ilyasov, V. V. Krasnikov, M. Akkurf, D. Bahrus, B. Bala, A. K. Atyhanov, K. M. Hazimov, B. J. Babayev, N. R. Avezova, S. A. Lutpullaev, R. A. Zakhidov, N. R. Yusupbekov, O. F. Safarov, J. N. Mukhitdinov, A. A. Artikov, Kh. S. Nurmuhamedov, J. P. Mukhiddinov, H. F. Juraev, J. M. Kurbanov, K. O. Dodaev, Z. S. Iskandarov, K. T. Norkulova and others. Their research and development is aimed at improving installations and drying processes in order to obtain high-quality end products.

They developed the scientific basis for the processes of drying capillary-porous materials, gave practical recommendations for the introduction of modern technologies for drying materials of plant origin.

At the same time, the use of installations for drying dietary and food grasses with the intensification of the technological process makes it possible to obtain the final product with preservation of biological active components.

Analysis of the kinetics of drying dietetic food herbs motor (Allium motor) [2–4]. Table 1 presents the experimental values of the weight of the sample and the temperature in the drying unit.

Table 1. – Experimental values of the sample weight and temperature in the drying unit

Time, t *min*	0	10	20	30	40	50	60	70	80	90	100	110	120	130	140	150	160	170	180	190	200	210
Temperature, T, ^{0}C	24	30	57,7	60	60	60	60	58	58,5	59	60,7	63	62	64,2	63	65	67	67	67	70	72	72
Weight, P, g	229	225	216	197	170	151	133	108	90	75	72	56	47	39	37	35	34	33	32	30	27	27

In order to go from weight to moisture and moisture content, it is necessary to have data on the limit of moisture content achieved at infinity, or the weight of absolutely dry material. For leveling the experimental errors, we estimate the desired value as the horizontal asymptote to the graph (Fig. 1) of the function $P=f(t)$.

We assume that the maximum weight corresponds to the weight of the dry material under the assumption that an equilibrium moisture content of zero is reached. The basis of this assumption is low relative humidity and high temperature.

The nature of the graph P=f(t) corresponds to the formula $P = a_1 e^{b_1 t} + a_2 e^{b_2 t} + a_5$.

With this $a_2 < 0$, $a_4 < 0$, a $a_5 > 0$

Given the initial conditions

$$\begin{cases} P(0) = P_0 \\ P(0) = 0 \end{cases} \Rightarrow \begin{cases} a_1 + a_3 + a_5 = P_0 \\ a_1 a_2 + a_3 a_4 = 0 \end{cases} \Rightarrow \begin{cases} a_5 = P_0 - a_1 - a_3 \\ a_4 = -a_1 a_2 / a_3 \end{cases}$$

The results of the approximation with large specific coefficients of the end points are shown in Fig.1.

Asymptotic estimate $P(\infty)$ with the use of large specific coefficients to the end points and subject to the above limitations gives $a_5 = P(\infty) = 22{,}76$ г.

With this $a_1 = -4{,}3236 \cdot 10^3$, $a_2 = -0{,}0296$, $a_3 = 4{,}5299 \cdot 10^3$, $a_4 = 0{,}0283$, $a_5 = 22{,}688$.

Figures 2 and 3 show the drying curves, where the ordinate is expressed in moisture content by the formula $W_s = \frac{(P - a_5)}{a_5}$ and through the moisture formula $W = \frac{(P - a_5)}{P} 100\%$

Repeated approximation already with the known $P(\infty)$ and the same specific coefficients on the points gives: $a_1 = -9{,}9398 \cdot 10^4$, $a_2 = -0{,}0281$, $a_3 = 9{,}9604 \cdot 10^4$, $a_4 = -0{,}0281$.

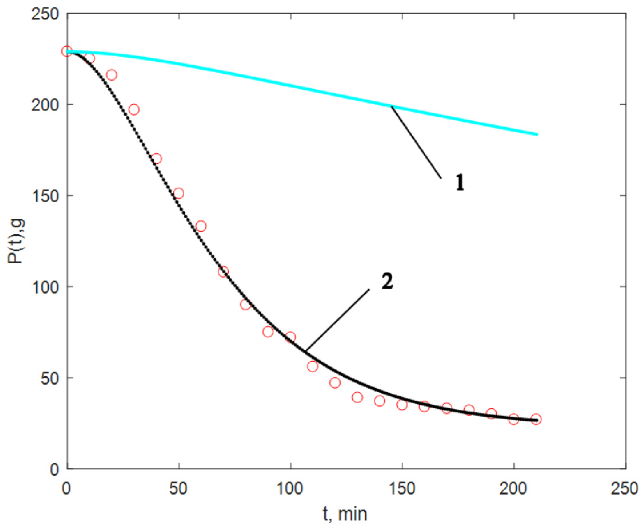

1 – initial approximation; 2 – approximating function.

Figure 1. Approximation result P=f(t)

Calculations on new values of parameters, and drying curves, and drying speed curves do not differ significantly from calculations on asymptotic parameters.

In fig. Figure 4 shows the curve for the rate of grass drying; the motor in terms of moisture content is the drying rate, and in fig. 5 shows the drying rate curve, expressed in the coordinates of the humidity — the drying rate.

In fig. 5 are marked by dots of grass drying rate motor, obtained as $\frac{dW}{dt} = \frac{\Delta W}{\Delta t}$ according to experimental data.

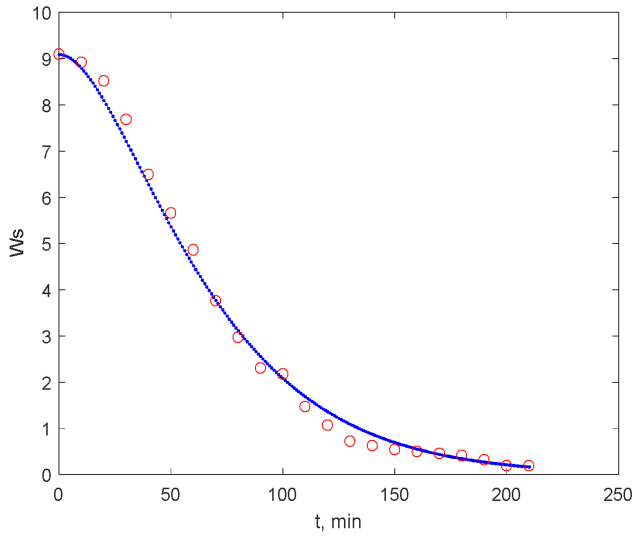

Figure 2. The change in moisture content over time

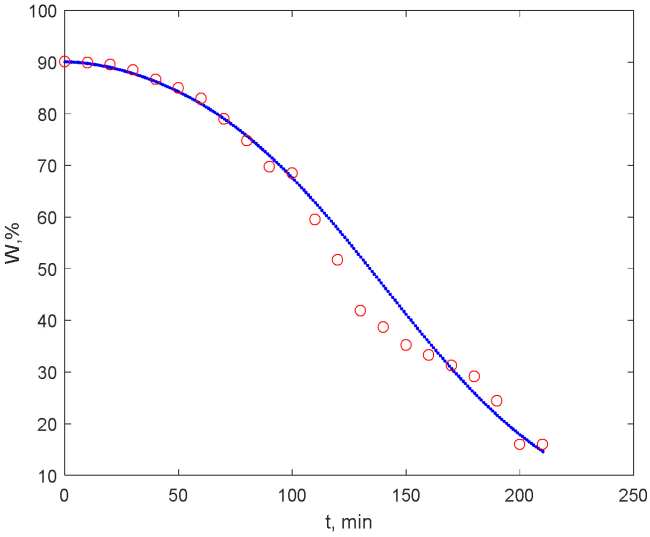

Figure 3. Change in humidity over time

Analysis of the results allows us to conclude:

– the value of the equilibrium moisture content significantly affects the estimates of drying intensity indicators. At the same time, the asymptotic value looks reliable, which is especially evident when comparing empirical points and approximated drying rate graphs;

– even taking into account the neglect of the initial accelerating stage, the graphs of the drying curves and the drying speed do not reveal periods of constant and falling drying speed and the curves look similar to those known in the literature on the drying of herbaceous materials;

– the impossibility of applying traditional methods of calculation and design, based on the presence of two specific periods, in this case is aggravated by the unpredictable weather parameters of the natural energy source of solar thermal plants that change in advance.

We proceed to the analysis of the ratios of internal and external resistance to moisture transfer in the process of drying the materials in question.

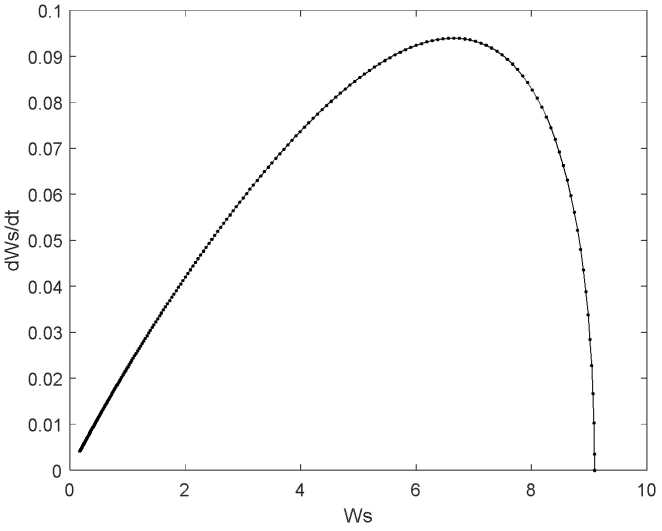

Figure 4. Drying speed curve

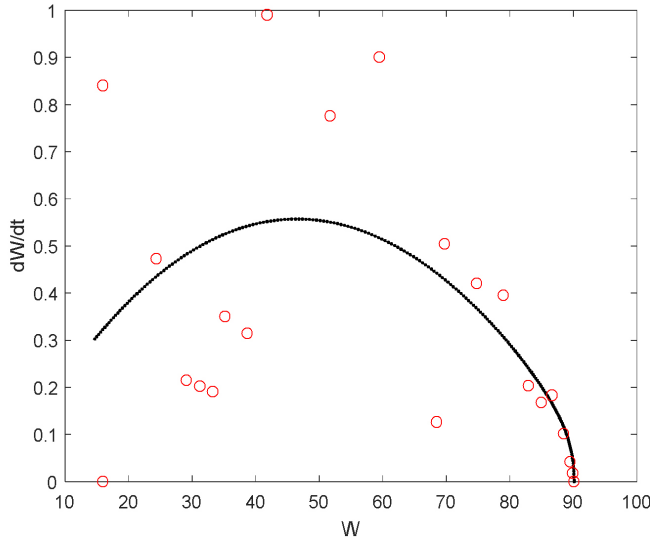

Figure 5. Moisture Drying Curve

Reference:

1. Food and Agriculture Organization of the United Nations. The state of food and agriculture. Climate change, agriculture and food security. Rome, 2016.– 210 p.
2. Food and Agriculture Organization of the United Nations.Global initiative on food loss and waste reduction 2015.Rome, 2015.– 8 p.
3. Safarov J. E., Dadayev G. T. The results of an experimental study of the accumulation of energy in a solar drying plant. // Austrian Journal of Technical and Natural Sciences.–Austria. 2017. № 9–10.–P. 60–64.
4. Safarov J. E., Dadaev G. T. The study of the drying process of the motor plant (Allium motor). // Chemistry and chemical technology.– Tashkent, 2017. № 5.– P. 35–38.

Rakhmatov Norkobil,
Associate professor of technical science at the department
"Hydrotechnical construction and engineering structures"
Tashkent institute of irrigation and agriculture
mechanization engineers (TIIAME), Uzbekistan
E-mail: rnr08@yandex.com

WATER RESOURCES MANAGEMENT OF SIRDARYA RIVER

Abstract. The Syrdarya water basin association is an intergovernmental coordinating organization which is part of the interstate commission (ICWC) on Aral Sea rescue in the role of "Executor". Transboundary waters are distributed to Kyrgyzstan, Kazakhstan, Tajikistan and Uzbekistan with the help of hydraulic structures within the association.

In order to avoid disagreements between "water consumers" in distributing the transboundary waters of Syrdarya, the operating organization should have up-to-date information on the amount of water flowing into Syrdarya River and on consumption of water distributed among users.

This article describes the experience of Syrdarya Basin Water-Management Association in improving data collection and management of hydrosystems within its balance.

Keywords: river, basin, water management, consumption, transboundary water, hydraulic engineering structure.

In 1988, the Syrdarya Basin Water-Management Association was established and limited water consumption was introduced to control the water management complex of the Syrdarya river.

The objectives of Basin Water-Management Association are to supply water to the consumers in accordance with the limits of regime control of the Naryn-Syrdarya cascade, water run provision in Chardara reservoir, monitoring the ecological state and river water quality.

The water management complex of the Basin Water-Management Association delivers of waterworks facility system, water intake of hydraulic structures on the Naryn, Syrdarya, Karadarya, Chirchik rivers, and also interrepublican canals, "Dustlik", Yujnogolodostepsky and the head section of the budget and finance committee with facilities (49 km). The Basin Water-Management Association serves along the stem stream from Toktogulsky to Chardara reservoir over 1000 kilometers (Fig. 1). The hydraulic structure 198 are on the balance of the Basin Water-Management Association, including three large river waterworks facility.

The discharge tolerance of the facilities is 20 … 2500 m^3/s, the hydraulic performance of "Dustlik" and Yujnogolodostepsky canals and the head section of the budget and finance committee reaches up to 400 m^3/s. 243 pumping stations and small backings are under control of the Basin Water-Management Association.

Table 1.

Irrigated area	ths.ha
Syrdarya	3200
Naryn-Syrdarya	1770.7
Kyrgyzstan	59.9
Kazakhstan	491
Tajikistan	185.3
Uzbekistan	1039.5

Water intakes from rivers and subordinate canals are counted in 445 points: at 21 head intakes, 36 stationary pumping stations, 172 temporary

pumping stations and branches from main canals. Under centralized management until 1991, the Naryn-Syrdarya reservoir cascade operated in irrigation mode with agricultural priority. The development of irrigated agriculture in the Syrdarya basin was carried out at the expense of measures for the economical and rational use of local water resources. It is considered that the further development of irrigation will lead to the complete exhaustion of water resources in 2000. In terms of the formation five sovereign states "Syrdarya" in Central Asia in 1991, it has become an "international watercourse" according to modern terminology. There was to organize use of "transboundary water resources" as river basin and as the whole basin of Aral Sea. The Inter-State Commission for Water Management was established in 1992 and pick up the management of Aral Sea basin water resources.

The Inter-State Commission for Water Management preserving continuity in management has to be one of the executive bodies of Basin Water-Management Association. The Inter-State Commission for Water Management annually approves water withdrawal limits for each water-consuming country and water supply volume for Aral Sea. In accordance with the Intergovernmental Agreement of Central Asia on the complex exploitation and protection of Syrdarya water resources water intakes are limited from 1992.

Annual water withdrawal limits normal water content in Countries; Kazakhstan- 8.2 km^3 (38%), Kyrgyzstan-0.22 km^3 (1%), Tajikistan-2.0 km^3 (9%) and Uzbekistan-11.15 km^3 (52%). In case of water content changes (water shortage or high water year), the amount of water intake limits is adjusted with the appropriate justification and approval of the Inter-State Commission for Water Management. Having the forecast from Hydromet Chiefs and preliminary proposals on water withdrawal limits from each basin state via canals and pumping stations, the Basin Water-Management Association makes calculations of Naryn-Syrdarya reservoir cascade operating mode and several options taking into account the water content of the year and offers the Inter-State Commission for Water Managementas the best one.

The delivered project of Naryn-Syrdarya reservoir cascade regime submitted by the Inter-State Commission for Water Management contains a summary information calculations and date explanation of irrigation consumptive water use by canals and pumping stations. The project is submitted 10 days before the meeting to each member of Inter-State Commission for Water Management for studying and giving subsequent comments and suggestions.

The collective decision of the Inter-State Commission for Water Management members is approved only with the consent of all members. The approved project is recommended for further discussion by the working group of power engineers, water workers and preparation the intergovernmental agreement on water and energy resources exploitation for a certain period.

Implementation of decisions the Inter-State Commission for Water Management is carried out by the Basin Water-Management Association and its territorial departments. The Basin Water-Management Association, shall have the right to adjust the limits within ± 10% on the basis of official notification of this water users depending on water situation and rivers content. If situation so requires a larger adjustment of the Basin Water-Management Association, the Inter-State Commission for Water Management delivers relevant calculations and a new adjusted regime of Naryn-Syrdarya reservoir cascade. After agreement the Inter-State Commission for Water Management provides the official guidance document for the Basin Water-Management Association.

Despite a high degree of regulation (93%) of Syrdarya runoff makes possible to effectively supply water to irrigated agriculture, industry, energy, utilities. The implementation of limits has some difficulties caused difference of macroeconomic interests in Central Asia.

The Toktogul reservoir has been operating as an energy regime since 1995. Water pass in autumn-winter period sometimes up to 8.5, in vegetation period 5–6.5 km^3. Due to the increased passes in autumn-winter period, the Kayrakkum and Chardara reservoirs are prematurely filled. However, an excessive discharge of water into the Arnasai depression is allowed, farmlands and settlements are flooded. In 1992–2002, more than 27 km^3 of water was dumped into Arnasay.

In autumn-summer period, artificially created shortage of water resources leads to reduction of limited water supply in the Republic of Kazakhstan, Tajikistan and Uzbekistan, causing damage to agricultural production. In continuation of Toktogul reservoirs, the operation regime of the Kayrakkum and Chardara reservoirs were completely deformed.

Average annual natural river flow in autumn-winter periods at the Toktogul hydroelectric station is 2.5 km^3, actually reaches 8.5 km^3, or more than 3 times the natural indicator. Summer mode changed in the opposite direction: average long-term runoff 9–10 km^3, reservoir passes 4.5–6.5 km^3, or 1.4–2.4 times less than the natural value. This is largely responsible for floods in winter and in summer for artificial water shortage.

The signed agreements among Kazakhstan, Kyrgyzstan and Uzbekistan on compensatory energy supplies for Toktogul reservoir pass in vegetation period are often led to water shortage for water consumer. Additional complication of water management that, paid water by other countries entraps in Kayrakkum reservoir in Tajikistan without passing to Kazakhstan and Uzbekistan. The absence of a long-term interstate agreement forces out of follow by seasonal agreements only.

In connection with above mentioned conditions, necessity arises to develop an agreed position to prevent a possible violation of joint management and cooperation on rivers. The main guiding principle should be strict adherence the norms of international water law, where natural flow is accepted and relevant water management principles.

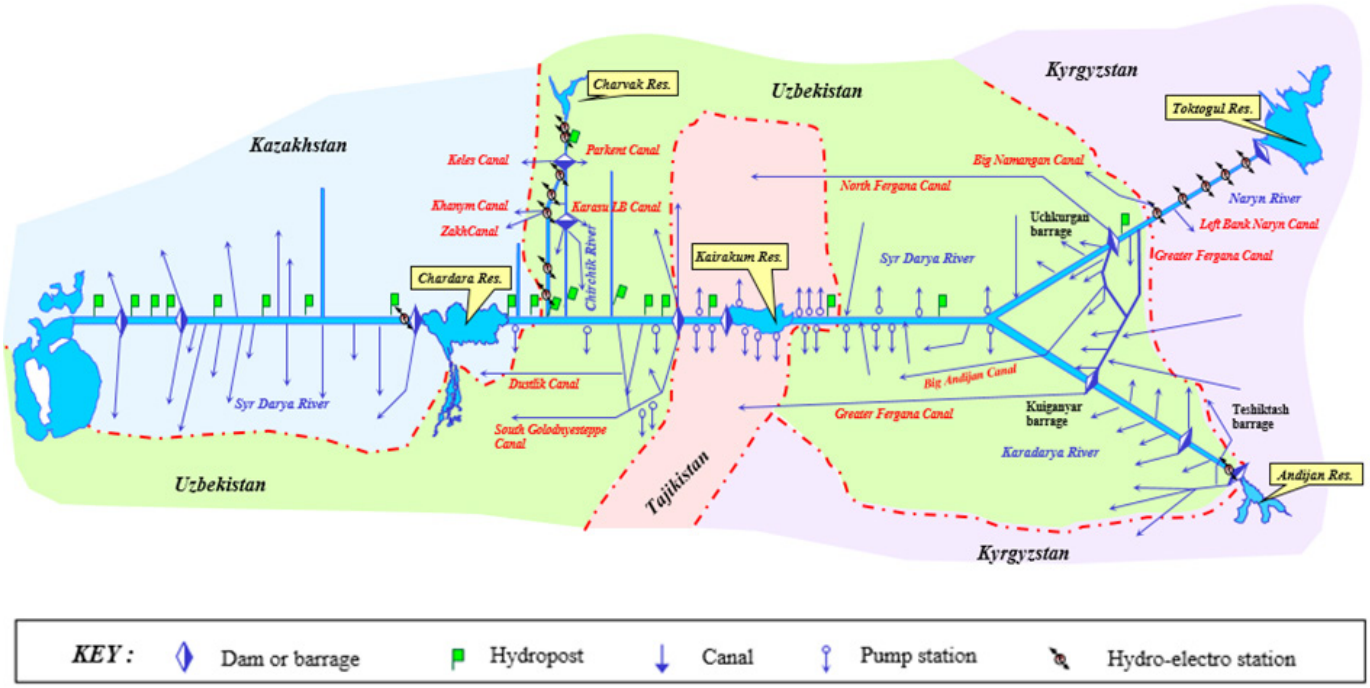

Figure 1. Schematic of the Syr Darya River

References:

1. Rakhmatov N. Management system improving of transponder water recourses of Sydarya basin. Regional consultative seminary «Сотрудничество в области совместного использования водных ресурсов в Центральной Азии: опыт прошлого и проблемы будещего» – Almata, 26–28 сентябрь 2002.– P. 235–237.
2. Rakhmatov N. Правовые вопросы обеспечения безопасности ГТС на трансграничных водных объектах бассейна Сырдарьи. Узбекский журнал «Irrigatsya va melioratsiya».– Tashkent, 2017.– № 4 (10),– P. 31–32.
3. Rakhmatov N. Маълумотлар базасини яратиш йўлидаги Сирдарё ҳавзаси сув хўжалик бирлашмасининг тажрибаси. Узбекский журнал «Irrigatsya va melioratsiya».– Tashkent, 2018.– № 2 (12).– P. 31–33.

Tymkiv Oleksandr,
National University Odessa Maritime Academy,
postgraduate student, Marine Engineering Faculty
E-mail: dvg.smc@gmail.com

WAYS TO IMPROVE SHIP POWER PLANTS

Abstract. The article considers a method for evaluating the effectiveness of potential and actual capabilities of vehicles and systems utilization. It is shown that for ships, the reserves for improving the use of the transport potential associated with ship power plants are characterized by such an parameter as the loss factor of the transport work from incomplete use of speed.

Keywords: reliability of power plants, transport potential, transport performance

Modern ship companies are constantly increasing demands on the safety of navigation. It is possible to meet their demands by increasing reliability of ship power plants (SPP) that work in specific and extreme conditions (oscillating motion, storm, lack of professional assistance from onshore repair bases, etc.). Improving the reliability and safety of SPP is a complex task that is solved both during manufacture and during operation. Timely detection of the deviations from the operational value and prevention of failure accidents are one of the most important component for SPP technical operation [1].

The long-term trend for increase in energy prices predetermines a share of fuel costs escalation in total operating costs of ship owners. Concurrently, environmental safety requirements are toughening, which makes it necessary to prevent even economically insignificant failures of the SPP if they are associated with a risk to the vessel and the environment. In this regard, the SPP technical operation development is a range of important scientific and technical issues.

An overview of the development trend of SPP technical operation in historical retrospect shows that the effectiveness of their solution is largely determined by the mutual compliance of technological and information processes. Ensuring such compliance is particularly important [2].

An analysis of the current state of these issues have revealed that they are solved at the level of individual technical issues: fuel and oil economy; technical condition maintenance of various technical equipment and systems of the ship; reduction of maintenance and repair complexity, etc. Despite the wide scope of research conducted in this direction by domestic and foreign experts, their overall progress is not very high [3].

There are many reasons that determine this predicament, but one of the most crucial is the contradiction between the high complexity and diversity of SPP equipment, high amount of information on its functioning and technical condition on the one hand, and the limited capabilities of shipboard specialists to analyze this information. As a result of the consistent reduction in the number of ship crews and the need to combine the professions of the deck and machine teams, these opportunities are on decrease.

For further analysis of the SPP technical use and their importance for the overall improvement of the efficiency of the fleet, it is necessary to be able to comprehensively evaluate this effectiveness. The performed transport work to the theoretically possible transport work in the case of full use of the passport characteristics of the vehicle ratio. For brevity, this ratio is called the transport potential utilization factor γ. Its analytic form can be obtained on the following basis [4].

It is known that the system of transport meters can be constructed on the basis of three basic units:

1) transport mass Q; 2) transport route L; 3) transport time T.

Then the characteristic of the transport system of any level can be considered the transport work A.

$$A = QL.$$

For the subsequent analysis it is more convenient to express L in terms of speed V and time T. Then the dependence is as follows

$$A = QVT. \quad (1)$$

On a practical level the factual transport work is expressed as:

$$F = Q^f V^f T^f = \rho^{Q^p} \delta^{V^p} \alpha\beta \cdot (1-\lambda)T,$$

where Q^p is the nominal tonnage, tonn;

V^p is the nominal speed, km/h;

T – transport uptime, h;

T^f – factual transport operation time, h;

Q^f – factual used tonnage (cargo performance), tonn;

V^f – vehicle technical speed, km/h;

$\rho = \frac{Q^f}{Q^p}$ – is the tonnage factor;

$\delta = \frac{V^f}{V^p}$ – is the speed utilization factor;

$\alpha = \frac{T^f}{T}$ – is the uptime utilization factor;

$\beta = \frac{T^m}{T}$ – is the steaming time utilization factor (T^m – is the ship motion time, h);

$\lambda = \frac{T^b}{T^m}$ – is the ballast passage factor (T^b – is the ship ballast passage time, h).

Without losses (i.e. in the ideal case)

$$\rho = 1, \quad \delta = 1, \quad \alpha = 1, \quad \beta = 1, \quad \lambda = 0,$$

and potential transport work will be described by

$$P = Q^p V^p T,$$

with identical structure to (1).

Then the transport potential utilization factor:

$$\gamma = F/P.$$

For a single vehicle (ship) it is obviously:

$$\gamma = \rho\delta\alpha\beta \cdot (1-\lambda). \quad (2)$$

For n same type vehicle system the transport potential utilization factor will be calculated by the following formula for general case:

$$\gamma = \sum_{i=1}^{n} \gamma_i I_i = \sum_{i=1}^{n} \rho_i \delta_i \alpha_i \beta_i (1-\lambda) I_i,$$

where $I_i = \frac{Q_i^p V_i^p T_i}{\sum_{i=1}^{n} Q_i^p V_i^p T_i}$ – weight factor of i vehicles.

The proposed factor allows you to quantify effectiveness of the operation of both potential and actual capabilities of vehicles and systems. The case of a transportation system with γ=1 can be considered a pipeline through which oil or gas is continuously pumped over the period T at a design rate [5]. Low values of the transport potential utilization in the general case will indicate the irrational use of transport and the insufficiently substantiated design of vehicles. For a single vehicle, the method of calculating ρ, δ, α, β and λ factors is obvious by definition. They are similar to the known load factor ρ, speed utilization factor δ, uptime utilization factor β etc., which are widely used in the reporting documentation and in statistical reviews. As a result, for n transports with different nominal parameters we get:

$$\rho = \sum_{i}^{n} \rho_i I_i; \quad \delta = \sum_{i}^{n} \delta_i I_i; \quad \alpha = \sum_{i}^{n} \alpha_i I_i;$$
$$\beta = \sum_{i}^{n} \beta_i I_i; \quad \lambda = \sum_{i}^{n} \lambda_i I_i. \quad (3)$$

In general, the analysis of transport work parameters is performed for the reporting period. In this case, the transport uptime for all transport units is the same and the weight factors in formulas (3) are reduced to

$$I_i = \frac{Q_i^p V_i^p}{\sum_{i=1}^{n} Q_i^p V_i^p}.$$

The calculations show that evaluation of the transport potential utilization of the main types of general-purpose transport range from 4% for river transport to 20% for maritime transport (Table 1).

Table 1.– Estimates of the potential utilization of different transport types

Parameter	Transport types,%			
	river	road	railroad	sea
Transport potential utilization factor	4.1	5.4	7.4	18.0
Potential losses of:				
tonnage	16.4	10.7	–	22.6
speed	23.4	33.8	40.1	17.1
uptime	17.4	–	–	–
steaming time	21.9	33.5	52.5	23.3
ballast passage	15.0	16.6	–	19.0

From the analysis of the data in (Table 1) and the structure of formula (2) it follows that for sea ships, the reserves for improving the transport potential are characterized by the loss rate of the transport work due to under-utilization of speed. The mean value is 17%.

These reserves are indirectly and partially associated with the loss of transport work from under-utilization of tonnage and the loss of transport work from non-compliance of the operating time with the uptime (decommissioning the vessel to repair SPP if necessary). However, their quantitative evaluation of available data is difficult.

References:

1. Golikov V. A. A simple technique for identifying vessel model parameters / V. A. Golikov, V. V. Golikov, Ya. Volyanskaya, O. Mazur, O. Onishchenko // 4th International Scientific Conference SEA-CONF 2018. IOP Conf. Series: Earth and Environmental Science 172 (2018) 012010 doi:10.1088/1755–1315/172/1/012010.
2. Kuropyatnyk O. A. Reduction of NO_x emission in the exhaust gases of low-speed marine diesel engines / O. A. Kuropyatnyk //Austrian Journal of Technical and Natural Sciences,– Vienna-2018.– No. 7–8 (July-August).– P. 37–42. doi.org/10.29013/AJT-18–7.8–37–42.
3. Тымкив А. В. Методы и средства диагностирования судовой энергетической установки / А. В. Тымкив, В. Г. Денисов // Судовые энергетические установки: науч.-техн. сб., 2013.– Вып. 32.– С. 113–123.
4. Тымкив А. В. Мониторинг процесса изнашивания судовой энергетической установки / А. В. Тымкив, В. Г. Денисов // Судовые энергетические установки: Одесса, 2014.– Вып. 33.– С. 88–96.
5. Sagin S. V. Improving the performance parameters of systems fluids / S. V. Sagin // Austrian Journal of Technical and Natural Sciences,– Vienna-2018.– № 7–8 (July-August).– P. 55–59. doi.org/10.29013/AJT-18–7.8–55–59.

Section 7. Physics

Aminov Nusrat,
Faculty of Electronics and Automatics,
State Technical University, Tashkent, Usbekistan
Sultanova Yulduz,
Faculty of Electronics and Automatics,
State Technical University, Tashkent, Usbekistan
Khujaniyazova Azizakhon,
Faculty of Electronics and Automatics,
State Technical University, Tashkent, Usbekistan
Mavlyanov Abdulaziz,
State Technical University – affiliated Uzbek-Japan Innovation Center of Youth
E-mail: microelectronics74@mail.ru

PHOTOCONDUCTIVITY SPECTRUM OF SILICON DOPED BY MANGANESE AND SULFUR

Abstract. The spectral dependences curve of the photoconductivity of manganese and sulfur-doped silicon Si <MnS> is presented. For experiments the initial silicon sample was single-crystalline boron-doped silicon with ρ = 1 Ω cm. Over the entire energy range of $h\nu$ = 0.226 ÷ 1.28 eV in the Si <MnS> sample, the current increases by three orders of magnitude. From the analysis of the curve, the levels E_1 = 0.226 eV and E_2 = 0.86 eV were detected.

Keywords: single-crystalline silicon, energy of ionization, photoconductivity, dark current, resistivity.

1. Introduction

Photoconductivity of sulphur-doped silicon was studied in [1, P. 262–266]. As authors report in the paper, the original *p*-type silicon wafers had ρ = 20 Ω cm resistivity. After doping with sulfur at temperature of 1200 °C, the initial *p*-type silicon wafer turned into an *i*-type one with $\rho = 10^5$ Ω cm resistivity and an *n*-type with $\rho = 10^3$ Ω cm resistivity, respectively. The photoconductivity measurements were performed an IKS-21-type infrared (IR)-spectrometer at temperature of 77K. The dark photoconductivity of $\rho = 10^3$ Ω cm samples launches at $h\nu$ = 0.3 eV and was characterized by a small maximum at $h\nu$ = 0,38 eV. In the *i*-type samples with $\rho = 10^5$ Ω cm, the dark spectrum was monotonic. In these samples, the dark photoconductivity grew monotonically starting at $h\nu \geq 0.5$ eV.

2. Main Part

Sulphur in silicon is believed to manifest large variety of ionization energies E_i, determined by various authors as shown in (Table 1.) Such variety of ionization energy values and the occurrence of the ionization energy band in the range of $h\nu$ = 0,28÷0,38 eV,

the authors in [1; P. 262–266] are inclined to explain by the fact that sulphur in silicon is a relatively small single-charged donor, and the formation of deeper impurity levels may be due to the fact that sulphur comparatively easily forms associations of closely spaced singly-charged atoms and thus the ionization energy of electrons is determined not only be potential of ionization of isolated sulphur atom, but also by the Coulomb force of the ions present in the association.

Table 1.– Ionization energy levels E_i of sulfur determined by different authors by using different techniques

E_1	E_2	Centers and bands	Technique	Authors
E= 0.18 eV	E= 0.37eV			R.O. Carlson, R. N. Hall et al. J. Phys. Chem. Sol., 8,81 (1959)
E= 0.1 eV	E= 0.61eV		Optical spectroscopy	W.E. Krag, H. J. Zeyger et al. J. Phys. Soc Japan (Suppl), 21, 230 (1966)
E= 0.1 eV	E= 0.19eV		Temperature dependence of the Hall coefficient	D.L. Camphausen et al.Am. Phys. Soc, 13, 406 (1968)
E= 0.275 eV	E= 0.53eV		Photocapacitance	C.T. Sah, L. L. Rosier at al. Appl. Phys let,15,316 (1969) C. T. Sah, L. L. Rosier at al. Sol. St. Electron.,14, 41 (1971)
E= 0.18B	E= 0.37eV	Band E=0,28÷0,38eV E_t= 0.5eV	Photoconductivity and IR-quenching	A.A. Lebedev, A. T. Mamadalimov and N. A. Sultanov, FTP, 5, 22 (1971)
E= 0.26B	E= 0.48eV		Encyclopedic data	M.K. Bakhadirhanov and I. B. Ortikov, Encyclopedia/Semiconductor materials.: TasGTU, 2006.– p.132–135
	S_1 = 0.318 eV, S^+_1= 0.614 eV $S_{2=}$=0.188 и S^+_2=0.37 eV S_X=0.06–0.1 eV	S_1, S_2, S_X	Temperature dependence of the Hall coefficient	Yu. Astrov and et al. FTP, 2013, vol. 47, no. 2. p.211–215.

3 Experimental

We carried out doping with sulfur and manganese by using diffusion doping technique in vacuumed (10^{-4} bar) and sealed quartz ampoules at a temperature of 1260 °C and 1200 °C, respectively, for a duration sufficient for uniform doping. The initial samples were Si wafers doped with boron, with an initial specific resistance in the range of ρ = 1 Ω cm. After doping with Mn and S, the initial silicon remained of *p*-type, but the resistivity increased to $\rho = 2.4 \cdot 10^4$ Ω cm.

In order to study the photoconductivity curve of the silicon sample doped with Mn and S, the authors had performed measurements at IKS-21 spectrometer equipped with a cryostat, which allows one to study photoconductivity in a wide temperature range (T = 77 ÷ 350 K). To study the impurity photoconductivity only, a double filter of polished

monocrystalline silicon wafer was used, which was installed before the cryostat window after the infrared light emitter of IKS-21.

The (Fig. 1) shows the spectral dependence of photoconductivity of Si <Mn, S> samples (initial silicon doped with boron –1 with ρ = 1 Ω cm) in the dark and under background light (source is a conventional incandescent lamp with a power of 2 V). As is clear from (Fig. 1), the photoconductivity in silicon samples doped with Mn and S in the dark launches at $h\nu \approx 0.226$ eV. In the range of $h\nu$ = 0.226–0.42 eV, with an increase in the photon energy, the photoconductivity increases continuously and then the saturation region of the photocurrent gradually begins to manifest itself. At $h\nu$ = 0.42 eV, a sharp decrease in photoconductivity occurs, and a further increase in the photon energy leads to a noticeable decrease in photoconductivity value with a relatively deep minimum at $h\nu \approx$ 0.45–0.46 eV. The non-monotonous photoconductivity in the region $h\nu$ = 0.226–0.46 eV, apparently, is due to the fact that there is a non-monotonous dependence of the ionization cross section, which is given in the theory of G. Lukovsky [2; P. 299–302].

In [1, P. 262–266] for the silicon samples doped with sulfur, the dark photoconductivity in samples with $\rho = 10^3$ Ω cm begins at $h\nu$ = 0,3 eV, whereas in [3: P.140–142] in samples of silicon doped with manganese with resistivity $\rho = 7 \cdot 10^3$ Ω cm, the photo-response begins at $h\nu$ = 0.4 eV.

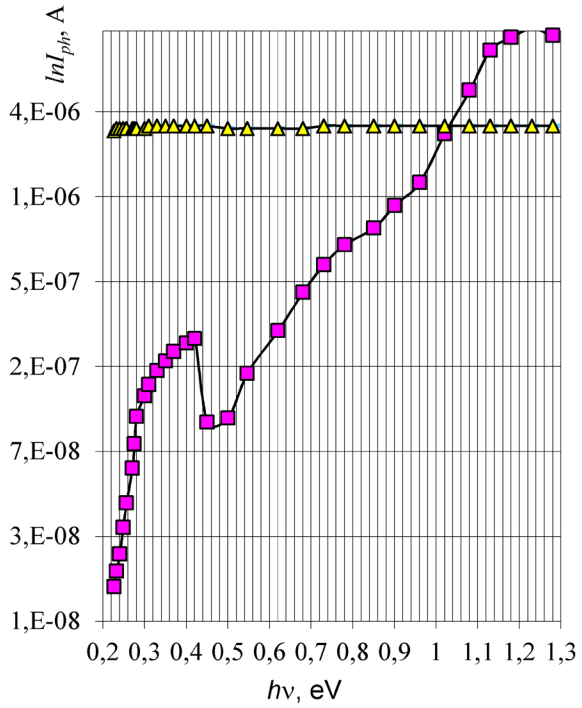

Figure 1. Spectral curve of photoconductivity of sample Si<MnS> (initial wafer silicon doped with boron-1 with ρ = 1 Ωcm) in dark and at constant background light at T = 77K

4. Conclusion

Based on the analysis of literature data and the results of experiments photoconductivity, it can be argued that Si <MnS> samples manifest impurity photoconductivity in the wavelength range λ = 1.4–5.4 μm.

Overall, over the entire energy range of $h\nu$ = 0.226 ÷ 1.28 eV in the Si <MnS> sample, the current increases by three orders of magnitude. From the analysis of the curve, the levels E_1 = 0.226 eV and E_2 = 0.86 eV were detected, and the second level should most likely be measured from the bottom of

the conduction band and might represent either a deep donor level (which is unlikely) or a local level associated with transitions between impurities of manganese and sulfur.

References:

1. Lebedev A. A., Mamadalimov A. A. and Mahkamov Sh. "Research of photoconductivity and IR quenching in Si<S> A. A. Lebedev Лебедев А. А., Мамадалимов А., Махкамов Ш. Исследование ФП и ИК гашение в Si<S> // ФТП. 1974.– № 8.– С. 262–266." Physics and Technology of Semiconductors,– No. 8. 1974.– P. 262–266.
2. Lucovsky G. V. "On the photoinization of deep impurity centers in semiconductors". Sol. St. Commun.,– No. 3. 1965.– P. 299–302.
3. Bakhadirkhanov M. K. and Isamov S. B. "IR photodetectors that operate in the presence of background light, Бахадырханов М. К., Исамов С. Б. ИК фотоприемники, работающие при наличии фонового освещения. ЖТФ, 2016. – том 86. – Вып. 3. – С. 140–142." Journal of Technical Physics, 2016.– том 86. – Вып. 3.– P. 140–142.

Zikrillayev Nurilla,
Saitov Elyor,
Botirov Bozorbek,
Nasirdinov Bakhodirw,
Kurbanov Yunus,
Turayev Farxodjon,
Shodiyeva Nozina,
Faculty of Power Engineering,
Tashkent State Technical University, Tashkent, Usbekistan
E-mail: gelyor.satov@gmail.com, elyor.saitov@yandex.ru

STUDY OF THE RESULTS OF DIFFUSION DOPING TECHNIQUE FOR PRODUCING HETEROSTRUCTURES (Si-Ge) USING MICROPROBE ANALYSIS

Abstract. Large-scale application of solar power in all areas of the economy is mainly determined by the efficiency, reliability, and cost factors of solar cells. Currently, solar cells based on silicon have exhausted their peak capacity, the efficiency ratio of such elements is believed to hit 20%. Silicon – germanium solid solutions are widely used in electronics and especially in nanoscale electronics technology. The unique properties of this material make it possible to create devices with parameters superior to those manufactured on the basis of $A^{III}B^{V}$ compounds. It is known that solid solutions of $Si_{1-x}Ge_x$ is mainly produced by liquid-phase epitaxy or during cultivation. However, the above techniques barely allow to obtain solid solution on the crystal surface with desired thickness and composition. Neither allows it to engineer nanoscale structures on the basis of germanium in the silicon lattice.

Keywords:

Introduction

The technique of building nanoclusters of impurity atoms in the crystal lattice of semiconductors with desired concentration and structure is a fundamentally new approach in engineering nanoscale structures.

In compare to the existing techniques of creating nanoscale structures using expensive equipment in the process of complex technological operations, the diffusion doping technique for building nanoclusters of impurity atoms is believed to manifest several advantages among them are are the ability to create nanoscale structures across the entire bulk of the crystalline material, capacity to control their size and structure, and the ability to create magnetic and multiply charged nanoclusters.

The development of new materials for solar power absorption, namely based Si with Ge clusters, is of particular importance due to natural obstruction related to the process of photonic-induced generation of carriers and thus the width of the forbidden band. This restriction is mainly due to the inability to use for photonic-induced generation of charge carriers with energy $h\nu < Eg$ (representing the wider infrared

solar spectrum λ = 1.2÷3 μm), which is almost ~40% of solar energy.

The ultraviolet (UV) and visible solar spectra (where *hv* > Eg) due to the effect of thermal photon-induced generation of hot charge carriers, also results in the loss of solar energy. The existing production technology of silicon photocells virtually does not allow to eliminate these losses.

Although the above problem is partially solved by using multi-stage (sandwiched) photocells based on semiconductor compounds such as Ga As, Al Ga As, nevertheless, the production technology of such photocells is not only rather complicated, but also requires the availability of expensive equipment.

Besides that, their price does not allow for large-scale application and the creation on their basis of high-power solar stations. Therefore, this problem can be successfully solved only on the basis of the development of novel class of semiconductor materials or on the basis of new physical phenomena.

Elements of AIII and AV subgroups are inserted in[to] the lattice of germanium and silicon, mainly replacing the atoms of the main substance, and at the same time behave in accordance with their valence. The atom of the AV subgroup element allocates four valence electrons to form a chemical bond, and one of its electrons can be transferred to the conduction band.

The atom of AIII subgroup element gives three valence electrons to form a chemical bond and can attract one electron, which will lead to the formation of a hole in the valence band. Thus, the elements of the AV subgroup behave as simple donors do, and the elements of the AIII subgroup do as simple acceptors do, forming shallow energy levels in the forbidden band. The ionization energy levels of impurities of the elements of the AV and AIII subgroups, and of lithium in lightly doped Si and Ge determined via the "conductivity as a function of temperature" curve are given in (Table 1).

Table 1. – Thermal ionization energy of impurities of the elements AV, AIII of the subgroups and Li in Si and Ge

Silicon				**Germanium**			
Donors		**Acceptors**		**Donors**		**Acceptors**	
Atom	***Ei*, eV**	**Atom**	***Ei*, eV**	**Atom**	***Ei*, eV**	**Atom**	***Ei*, eV**
Li	0.033	B	0.045	P	0.0120	B	0.0104
P	0.044	Al	0.057	As	0.0127	Al	0.0102
As	0.049	Ga	0.065	Sb	0.0096	Ga	0.0108
Sb	0.039	In	0.16			In	0.0112
Bi	0.069	Tl	0.26			Tl	0.01

From (table 1) it is clear that the ionization energy of A^{III} and A^{V} subgroups' impurities in germanium differ from each other significantly less than those in silicon. In germanium, the ionization energy of impurities from different subgroups differs negligently to the level of 0.01 eV, which is predicted by the hydrogen-like model for impurity atoms [1].

A small difference in the ionization energies of different impurities in this case shows that for impurities of the A^{III} and A^{V} subgroups in germanium, a hydrogen-like model gives a a rather satisfactory approximation. In silicon, the situation however is different: there is a large difference in the ionization energies of impurities, even from the same subgroup than in germanium for impurities from different subgroups.

The stark contrast in the values of ionization energies of impurities from the A^{III} and A^{V} subgroups in Si and Ge from the values predicted by hydrogen-like model is due to the fact that at interatomic distances the potential created by the impurity ion differs significantly from the potential of the point charge and depends on the chemical nature of the impurity.

This short-acting portion of the impurity potential creates an additional potential to the magnitude of the ionization energy predicted by the hydrogen-like model, the so called the displacement of the impurity level, otherwise known as chemical shift. Due to the chemical shift, the impurity levels of different impurities differ from each other.

The practical significance of impurities that give shallow energy levels in the band gap of a semiconductor is that they have low ionization energies (for example, in germanium at temperatures of 10 K, almost all atoms of these elements are believed to be completely ionized) and dissolve well in the doped material, have high coefficients of solubility, and low diffusion coefficients, therefore, by embedding them into semiconductors, one can widely vary the concentration of electrons and holes in them (from the intrinsic up to 10^{21} cm^{-3}).

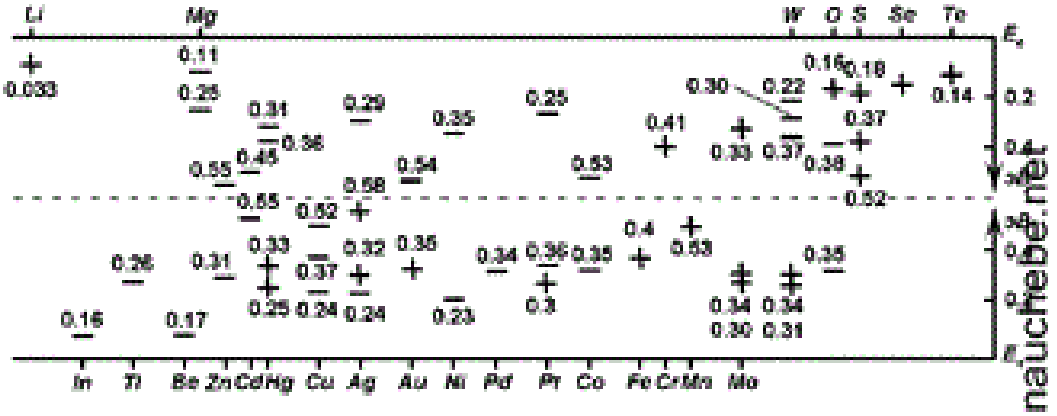

Figure 1. Energy levels of impurities in Si. The symbols "+" and "-" denote donor and acceptor levels, respectively

The behavior of impurities in silicon and germanium becomes more complicated as they are placed further in the periodic system from the elements of the A^{IV} subgroup. Most of the impurities from groups I, II, VI and transition metals in lightly doped silicon and germanium are substitutional impurities, although some of them can be placed in the lattice of the basic material and (or) in the interstices. For example, cuprum in germanium. Cu atoms enter both nodes and interstices in the Ge lattice. Magnesium, calcium, strontium and barium in silicon and germanium can also be placed both in the nodes and in the interstices of the crystal lattice [2].

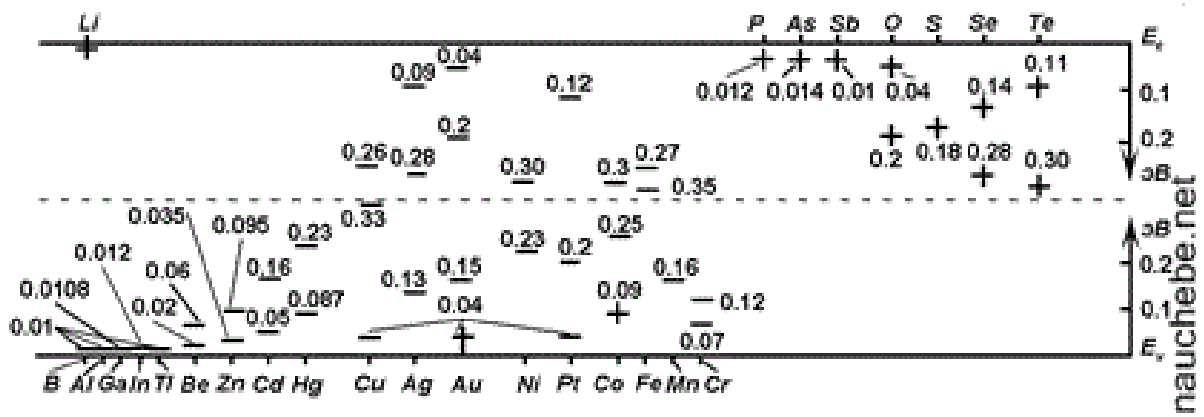

Figure 2. Energy levels of impurities in Ge. The symbols "+" and "-" denote donor and acceptor levels, respectively

Impurities of I, II, VI groups and transition metals form several alternative deep local energy levels in the forbidden band of silicon and germanium. Deep states, as a rule, occur when the main contribution to the binding energy is not of electric attraction nature weakened by the dielectric constant (hydrogen-like approximation), but of a short-acting potential, which is determined by the chemical nature of the impurity.

Shallow donor states can be seen as split off from the conduction band, and shallow acceptor states from the valence band. Deep states equally belong to both bands and can be both of donor and acceptor nature. The position of the experimentally determined energy levels of some impurities from these groups in the silicon and germanium bandgap are shown in (Figures 1 and 2), respectively.

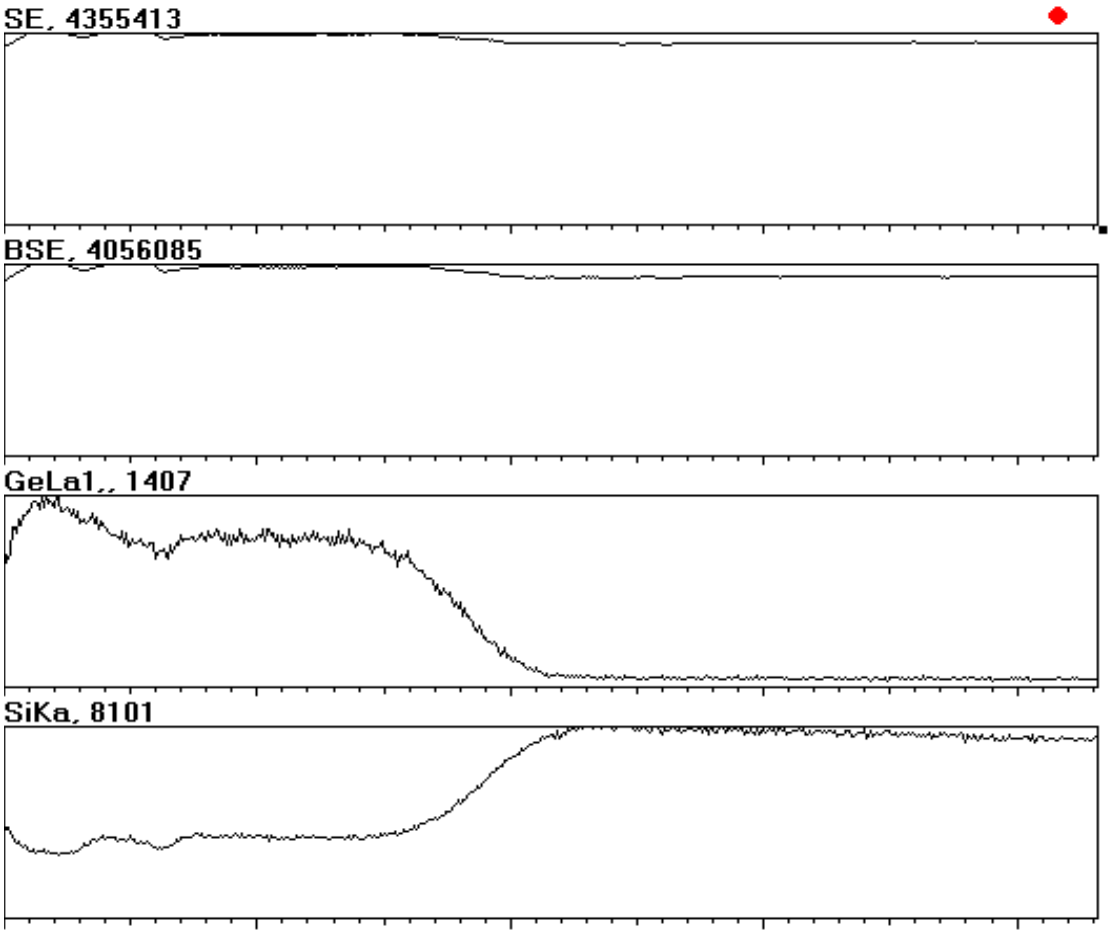

Figure 3. Diagram of the distribution of germanium atoms
in the near-surface region of siliconIt can be assumed that the behavior of substitution impurities that form deep levels in Si and Ge corresponds to their valences

On the outermost orbital of atoms from this group, there are two electrons ns^2, whereas all valence electrons participate in the formation of tetrahedral bonds, and in the case of elements of group VI, four valence electrons participate in the formation of these bonds and two valence electrons can be transferred to the conduction band. In the semiconductor lattice in the ionized state, these impurities are present in the form of multiply charged ions.

It should be noted that the behavior of transition metals from groups VII, VIII and with an unfilled 5*d*- shell in Si and Ge is studied in less detail than of impurities of other groups (see Fig. 1 and Fig. 2). Most often they form several deep levels in the

forbidden band. As noted above, if these impurities are placed in the nodes of the Si or Ge crystal lattice, then their behavior, as a rule, corresponds to their valence, i.e. they are doubly charged acceptors [3].

Amphoteric impurities in silicon and germanium can be atoms with an unfilled 5*d*- – orbital, can be donors or acceptors in one of the crystalline positions, or those that can be placed both in the nodes and interstices of the crystal lattice, showing the donor and acceptor properties depending on their location [4].

Experimental and Discussion

The diffusion process was carried out in stages by gradually increasing the temperature, starting from room and rising it to the diffusion temperature. The diffusion temperature would increase from room temperature and in 3 hours would reach 1200 °C, and then the samples were kept at this temperature for 2–4 hours. This experiment was repeated several times and each time five samples were used.

The concentration profile of germanium atoms and their distribution across the depth was studied using X-ray microprobe analysis of Joel super probe JXA-8800 R/RL. (Figure 3) shows the distribution of germanium atoms (as well as the distribution of silicon atoms) in the near-surface region of silicon (the diffusion was carried out at temperature T=1180 °C).

As can be seen from the figure, to depth of d ~ 0.6 μm on the silicon surface, the concentration of germanium atoms is greater than that of silicon, i.e. $Si_{1-x}Ge_x$ solid solution is being formed at x > 0.5, then the concentration of germanium atoms decreases sharply, and at d > 3 μm it decreases to a substantial degree, that due to the limited sensitivity of the device, their concentration is even difficult to determine.

Thus, in this case, one can obtain a continuous solid solution $Si_{1-x}Ge_x$, where x varies in the range of 0 ÷ 0.5. Figure 4 shows the microstructure of this sample from the front and surface sides. The figure clearly shows the boundary between Ge and Si, as well as the thickness of the doped Ge layer, which is quite accurately consistent with the results shown in (Figure 3).

An analysis of the above results reveals the following important phenomena. The maximum penetration depth of germanium atoms under these diffusion conditions should be roughly d~ 0.5–0.6 μm.

This value is almost 6–8 times less than in the experimental data obtained (Figure 3), i.e. This means that according to the new doping technology, the diffusion process of germanium atoms is significantly accelerated, and, accordingly, the diffusion coefficient of germanium increases by 6 ÷ 8 times.

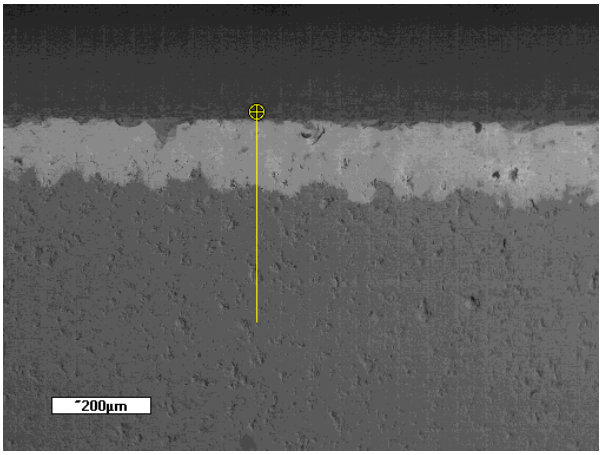

Figure 4. Pictures of the microstructure of the butt side of sample received on Joel super probe JXA-880 R / RL with clusters of impurity atoms of Ge atoms at T = 300K

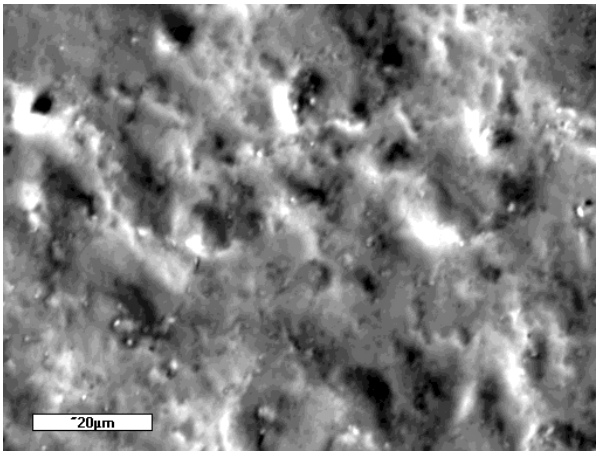

Figure 5. Pictures of the microstructure of the surface of sample received on Joel super probe JXA-880 R / RL with clusters of impurity Ge atoms at T = 300K

To identify such significant discrepancies, the authors carried out diffusion of germanium into silicon at T = 1200 °C using the conventional diffusion technology. As shown by the results of research using the X-ray microprobe microanalysis method, in such samples the depth of penetration of germanium is almost consistent with the reference diffusion coefficients.

The data in (Fig. 3) allow us to make an important conclusion that the diffusion process of germanium atoms in silicon can be significantly accelerated using the new technology.

By controlling the heating rate between the stages and choosing the parameters of the stages in the diffusion process, it is possible to obtain a Si1-xGex solid solution with the required thickness and composition. It is possible to obtain in a sufficiently thin near-surface region of silicon a continuous solid solution type Si1-xGex with a value of $x = 0 \div 1$[5].

It has been revealed that the proposed low-temperature multi-stage technique of doping semiconductors with impurities is a practically new technical solution of the diffusion process. This technique has the following advantages over high-temperature diffusion:

1) Eliminates the erosion of the crystal surface during the diffusion of impurities (Mn, Ni, Se, Te, …), which always takes place during high-temperature diffusion;

2) Eliminates the formation of various types of alloys, silicides and other compounds Si + impurity, which also occurs during normal diffusion;

3) It significantly stimulates the diffusion process, which provides not only time and energy savings, but also more uniform doping of samples.

4) The new multi-stage low-temperature doping method developed by the authors ensures the formation of clusters of impurity atoms in the bulk of the crystal. By varying doping conditions, one can control the parameters of clusters of impurity atoms.

Conclusion

Thus, it can be argued that the silicon with heterostructure-nature clusters is the material of future energy, since it will be possible to create sandwich-shape photocells on a single crystal on the basis of such materials and the need for complex technological operations and expensive AIIIBV and AIIBVI semiconductor materials is substantially eliminated. Of great practical interest is the information on the use of clusters such as micro and nanoscale heterojunctions to create new classes of microelectronic devices, as well as photocells.

The team of authors is grateful to Academic Bakhadyrkhanov M. K. for his valuable advice and discussion of the experimental results.

References:

1. Случинская И. А. Основы материаловедения и технологии полупроводников, – М., 2002.
2. Risa Suryana, Osamu Nakatsuka, Shigeaki Zaima. Jpn J. Appl. Phys., 50, 05EA09–12011.
3. Bakhadyrkhanov M. K., Isamov S. B., and Zikrillaev N. F. IR Photodetectors in the Range of λ = 1.5–8μm, Based on Silicon with MultichargedNanooclusters of Manganese Atoms, Microelectronika – Vol. 41.– No. 6. 2012.– P. 433–435.
4. Abdurakhmanov B. A., Bakhadirkhanov M. K., Saitov E.B and other // Formation of Clusters of Impurity Atoms of Nickel in Silicon and Controlling Their Parameters Nanoscience and Nanotechnology,– Vol. 4.– No. 2. 2014.
5. Abdurakhmanov B. A., Bakhadirkhanov M. K., Iliyev H. M., Saitov E. B and other // Silicon with Clusters of Impurity Atoms as a Novel Material for Photovoltaic // Nanoscience and Nanotechanology,– Vol. 4.– No. 3. 2014.

Section 8. Chemistry

Le Thanh Son,
Facutly of Chemistry, Ha Noi University of Natural Science, VNU
Nguyen Thi Huong,
Institute for Chemistry and Material, Viet Nam Academy of Military science and Technology, Viet Nam
E-mail: nguyenhuong0916@gmail.com

PREPARATION AND CHARACTERIZATION OF ORGANOPHOSPHATE FUNCTIONALIZED MORDENITE ZEOLITE FOR REMOVAL OF BENZEN VAPOUR IN THE AIR

Abstract. The organophosphate functionalized H-MOR materials were synthesized with a organic agent (TBP or TCP)/zeolite ratio of 10/100 (wt%) in n-hexane solvent. The obtained materials exhibited a uniform thin film structure on the surface of zeolite particles. The structure and porosity of the materials were studied by Field Electronic Scanning Emission Microscope (FESEM), X-Ray Difraction (XRD) and Brunauer-Emmett-Teller (BET) adsorption method. Chemical bondings were characterized by Fourier Transform Infrared Spectroscope (FT-IR). Adsorption of benzene vapor by the functionalized zeolite materials was investigated in a fixed-bed column with low benzene concentrations. The effects of factors such as empty bed contact time (EBCT), inlet concentration of benzene vapor, temperature (30°C to 50°C) and gas flow rate (0.15 L/min to 0.60 L/min) on the absorption capacity of the organophosphate functionalized zeolite were studied. The results showed that these absorbents are suitable for application of benzene vapour treatment in the air environment.

Keywords: Mordenite zeolite, functionalized, Organophosphate, Adsorption, Benzene.

1. Introduction

Zeolites are microporous aluminosilicates which are widely used as adsorbents and catalysts in the chemical industry. In chemical engineering, zeolites, zeolite membranes are used as catalytic to remove gases and volatile organic compounds (VOCs) by combustion reactions (Bilge Yilmaz et al. [4]; Huanhoa Chen et al. [12]).

In the field of adsorption, especially adsorption of VOCs in general and benzene in particular, there are many research results on the adsorption mechanism and the distribution of benzene molecules on some types of zeolites such as: HY (Fabien Jousse et al. [9]), MFI, CHA, BEA, STT (Coseron A.F et al. [6]), toluene adsorption on zeolite ZSM-5, MOR, and their composites such as mordenite modified with Cs, ZSM-5 zeolite membrane/PSSF (Statoshi Yamazaki, Kazuao Tsutsumi [21]; Ramiro M. Serra [20]; Huanhao Chen et al. [13]). The influence of the zeolite particle size, gas mixtures to the VOCs

adsorption process were researched and published by many authors (Ichiura. H et al. [14]; Shuai Ban [23]; Guillaume Rioland et al. [10]). When using zeolite HY as a benzene adsorbent in the air, the benzene adsorption process of zeolite HY makes up a relatively stable mixture of HY-benzene, which is still under physical adsorption; two complex forms are formed by binding of benzene to H and by the Van der Wan (vdW) interaction of benzene inside the 12-T or 4-T ring of zeolite (Shuai Ban [23]). The benzene adsorption process on zeolite HY mainly depends on the interaction of benzene with the four hydroxyl groups of four faces in a cellular unit. Typically, these H groups can be determined through IR spectrometry method (Dongjiang et al. [8]). Using the infrared spectrum for studying adsorption process of benzene in zeolites Na-Beta and H-MOR, the group of Bao-Lian Su concluded that all of the hydroxyl groups (Si-OH, Al-OH, Si-OH-Al) of the zeolites are interacting with benzene. However, only the hydroxyl groups on the 12-sided frame of the zeolite interact with benzene and the groups on the 4-sided frame are less likely to interact (Bao-Lian Su [3], Valérie Norberg 1998 and 2001).Recently, in order to increase the selective adsorption of volatile organic compounds, such as benzene, zeoliteSBA-15 has been organofunctionalized with silicon mechanics, at the aim of addition of aromatic ring groups to the zeolite substrate improving the interaction between the π electrons of benzene and the eπ elements of the aromatic ring (Qin Hu et al. [19]).

Our research work has been focus on the zeolite hybrid materials with organic agents that make them have both hydrophobic and organic properties, micro/mesoporous capillary effects. These zeolite properties are able to increase selective absorption and interaction with VOCs (Nguyen et al. [18]).This paper describes the fabrication and property characterization of the organophosphate functionalized H-MOR zeolite material using TBP, TCP as organophosphate agents. Additionally, their benzene vapor adsorption ability is also studied.

Experimental

Functionalized zeolite preparation Material samples were synthesized according to the literature (Nguyen et al. [18]): 1 g of H-MOR zeolite (HS-690, Wako-Japan; SiO_2/Al_2O_3: 240 mol/mol; crystal size: 0.1 × 0.5 μm) was added to 50 ml of n-hexane withvigorous stirring. Next, … g tributyl phosphate (TBP, 0.979 g/ml, Aldrich) or …g tricresyl phosphate (TCP, 1.16–1.175 g/ml, Aldrich) taken in 50 ml of n-hexane was added dropwise to the mixture. Subsequently, the mixture was continuously ultrasonicated for 3 hours at 70° C (50W, 20 kHz) under airtight conditions to avoid evaporation of n-hexane. Finally, the products were obtained via vacuum and dried at 75° C for 1 hour. The obtained materials have been designated as $CM_{PH.TBP}$ and $CM_{PH.TCP}$ corresponding to the organic agent used TBP and TCP. The chemical bonding characteristics of $CM_{PH.TBP}$ and $CM_{PH.TCP}$ materials were evaluated by Fourier Transform Infrared Spectroscope (FT-IR, GX-Perkin Elmer, USA), the materials structure was determined by Field Emission Scanning Electron Microscope method (FESEM, Jeol 6610LA, Japan). Nitrogen adsorption – desorption isotherms were performed at 77 K in Tristar 3000-Micromeritics equipment, USA, using static adsorption proceduce. Samples were degassed at 150°C and 10^{-6} Torr for minimum 12 h prior to analysis. BET surface areas were calculated from the linear part of BET plot according to IUPAC recommendation. Pore size distributions of the samples were calculated via the conventional BJD model.

Adsorption of benzene vapor

* *Adsorption column:* 0.5 g of functionalized zeolite and 2.0 g of sand were mixed well together then packed in a 1.0 cm diameter quartz column. The length of the adsorption material packed column was 2.9 ml. In two ends of the column were blocked by layers of glass fiber. For experimental performance, the column was inserted into the themostate room as shown in (Figure 1).

* *The research equipment:*

– Figure 1 is diagram of the equipment for organic solvent vapor adsorption investigation with themostate room setting temperature with vibration of ± 0.1 °C.

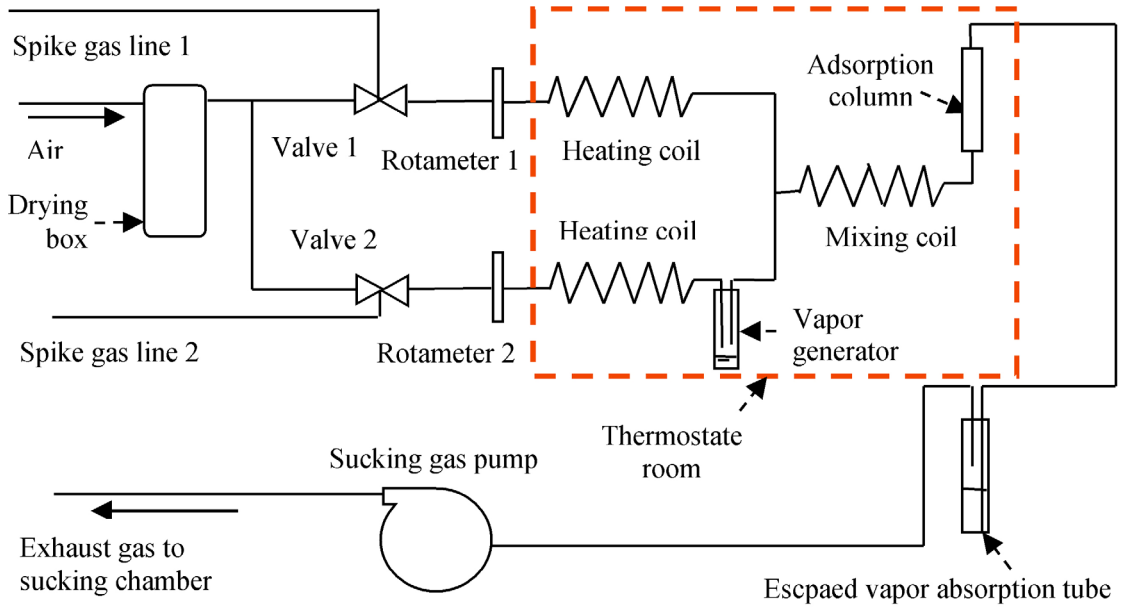

Figure 1. Diagram of vapor adsorption research equipment

The equipment is operated under the principle of vacuum pressure generated by a vacuum pump. Air flow is pumped through a silicagel tube which can dry the air. The tee valve 1 and Rotameter 1 are used to regulate dried air flow which does not flow through VOCs equipment. Once the temperature of the thermal-insulated tank obtained the specific and stable value, tee valve 2 and Rotameter 2 are used to quickly drive VOCs vaporized flow to the value point of interest. The air flow carrying VOCs vaporized compounds is gone through the mixer and the column which contains 20-ml adsorption solvent subsequently. The VOCs vapor left will flow through the absorption tube and all these VOCs vapors will be grasped by activated carbons (200-g). This will ensure that exhausted gas to be emitted from the system is clean and environment-friendly.

* *Benzene concentration determination* (Abdulrahma Bahrami et al. [1]; L. Zoccolillo et al. [15]): The inlet and outlet benzene vapor concentrations were determined through analysis of benzene absorbed in acetonitrile – water mixture with volume ratio of 3:1 before and after adsorption respectively by the HPLC Model HP 1100, using column C18-Zobax and DAD detector series. Dynami acetonitrile: water ratio 70:30% W; 0.005% H_3PO_4; 0.1% $HClO_4$; Flow rate: 1.0 ml / min; λmax: 255 nm; cooling temperature in the pump system: 4 °C; Sample time: 3.

The content of adsorbed benzene vapor on the column over the time was calculated by the formula: $m_B = m_I - m_t\,(mg)$. In which: m_I is the amount of input benzene vapor (mg); m_t is the amount of output benzene vapor (mg) in the time *t*. The equilibrium adsorption capacity of the material is calculated according to the formula: $q = \frac{m_B}{m_Z}(mg/g);$); In which m_Z is the adsorbent mass (g).

Results and discussion

Characteristics of zeolite composite materials

The functionalized zeolite materials are composed of two types: $CM_{PH.TCP}$ and $CM_{PH.TBP}$. The formation of the functionalizedzeolite is shown by the following equation:

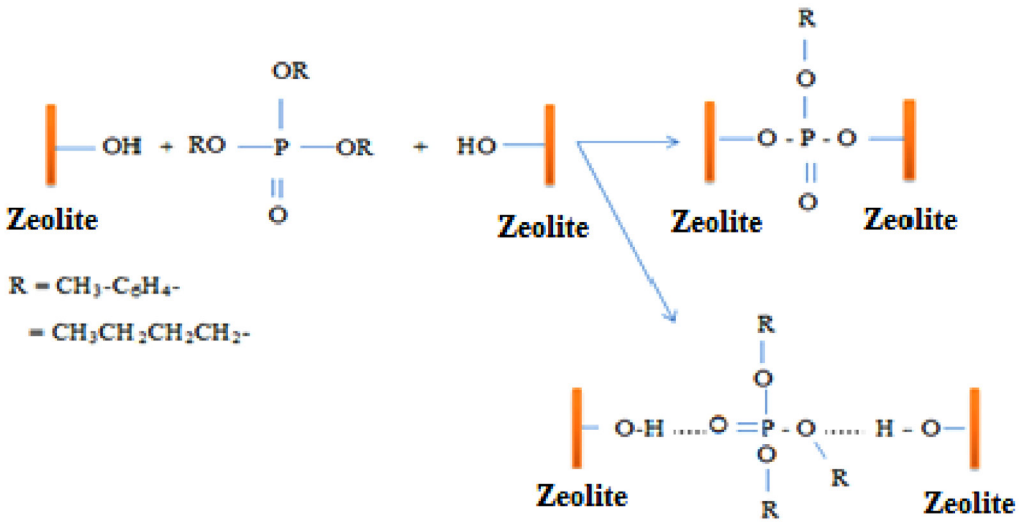

Functionalized zeolite materials have characteristics of organophilic as they contain CH_3 -C6H_4 – or CH_3 CH_2 CH_2 CH_2 – and of hydrophilic because of having zeolite.; in addition, it can be seen that the material is capillary, a type of capillary is formed by the zeolite and another type is the medium capillary due to the structure of the formed hybrid material.

The infrared spectra of $CM_{PH.TBP}$ and $CM_{PH.TCP}$ are shown in (Figure 2). The broad peak at 3662 cm^{-1} to 3490 cm^{-1} is characteristic of the vibration of the OH group of the zeolite. However, the peak intensity is weak due to the presence of physical adsorbed H_2O on the surface of zeolite, so the hydrogen bridge bonds between oxygen of water and the OH group of the zeolite surface. It was also demonstrated by the presence of peaks at 1632 cm^{-1} ($CM_{PH.TBP}$) and 1633 cm^{-1} ($CM_{PH.TCP}$) (H. Robsin [11]). The peaks at 2834 cm^{-1} and 2978 cm^{-1} characterize the C-H vibration of the CH_3 group in the tributylphosphate of $CM_{PH.TBP}$, while $CM_{PH.TCP}$ has peaks appeared at 1471 cm^{-1} and 1433 cm^{-1}, this shows that in the $CM_{PH.TCP}$ there is a characteristic vibration of aromatic cyclic structure.

In the wave numbers from 1200 cm^{-1} to 400 cm^{-1}, there appeared characteristic peaks for framework structural bonds of zeolite, both samples have the appearance of three smaller peaks around wave number 600 cm^{-1}, characterized the vibration of framework structure and distortion vibration of group O-T-O of zeolite. For example, the occurrence of the peaks1055 cm^{-1} and 1058 cm^{-1} which characterize the oscillation of the Si-O, Al-O bonds in the TO_4 tetrahedron of the zeolite. In addition, the wave number area less than 600 cm^{-1}, the presence of the peak at wave number 592 cm^{-1} ($CM_{PH.TBP}$) and 547 cm^{-1} ($CM_{PH.TCP}$) characterizes asymmetrical and symmetrical vibration of the five-sided ring, which is also the characteristic of distortion vibration of the double ring in the framework structure of zeolite type mordenite (Mohamed Mkhtar Mohame et al. [17]). In addition, both materials have the appearance of two peaks at wave number characterized the valence vibration of group P=O, P-O-C aliphatic for $CM_{PH.TBP}$ (1275 cm^{-1}, 1055 cm^{-1}) and P=O, P-O-C aromatic for $CM_{PH.TCP}$ (1177 cm^{-1}, 1043 cm^{-1}) (Shruti Mishra et al. [22]). These two groups indicate the presence of phosphate functional group in the structure of the functionalized zeolite.

Surface morphology of MOR, $CM_{PH.TBP}$ and $CM_{PH.TCP}$ is expressed in FE-SEM image (Figure 3). the original zeolite structure consists of almost unconnected grains with the form of rectangular blocks and the size of several μm to dozens μm. While the functionalized zeolite showed that in the grains surface likely appeared covered sticky layer. However, the surface and grains size of all three materials are almost the same as that of original zeolite. In which, the presence of P on the surface of both materials and

the carbon content of the substrate, corresponding to carbon content of 4.44% ($CM_{PH.TCP}$) and 3.80% ($CM_{PH.TBP}$), the material structure is also not sharp as with the zeolite background. But the materials covered organic agents hopefully increase ability of VOCs separation and absorption of materials, because organic agents have the role of both absorber and conductor in interaction with VOCs.

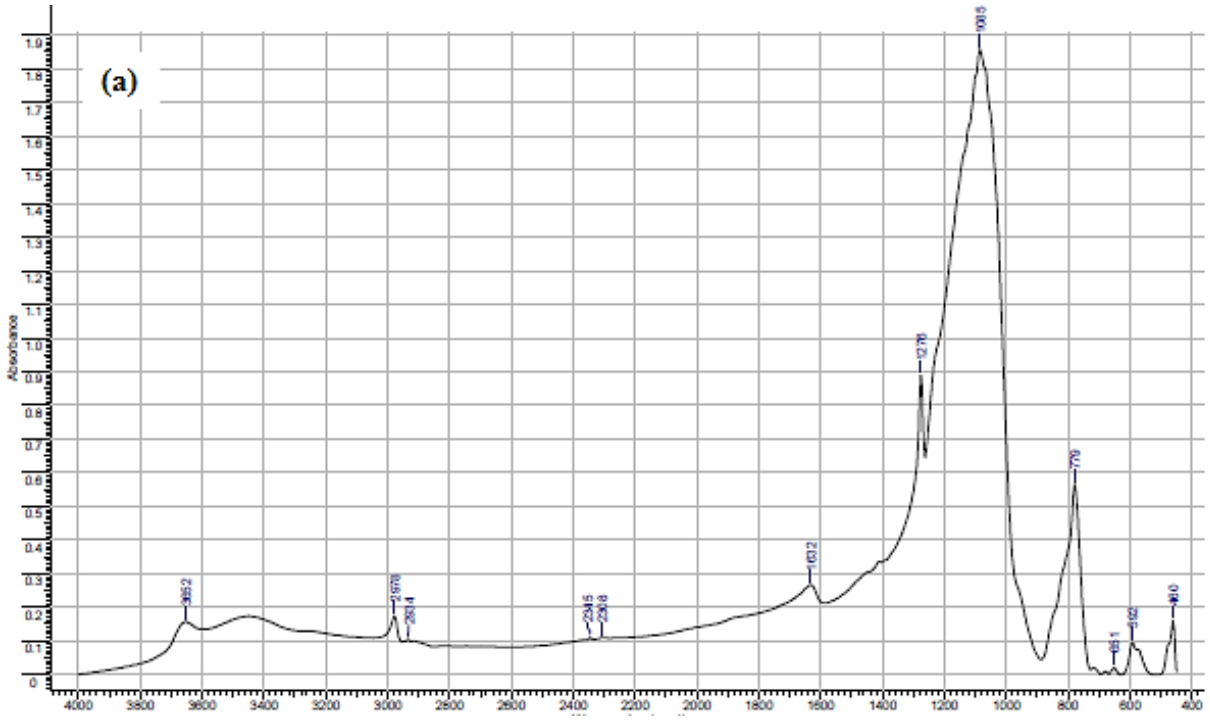

a)

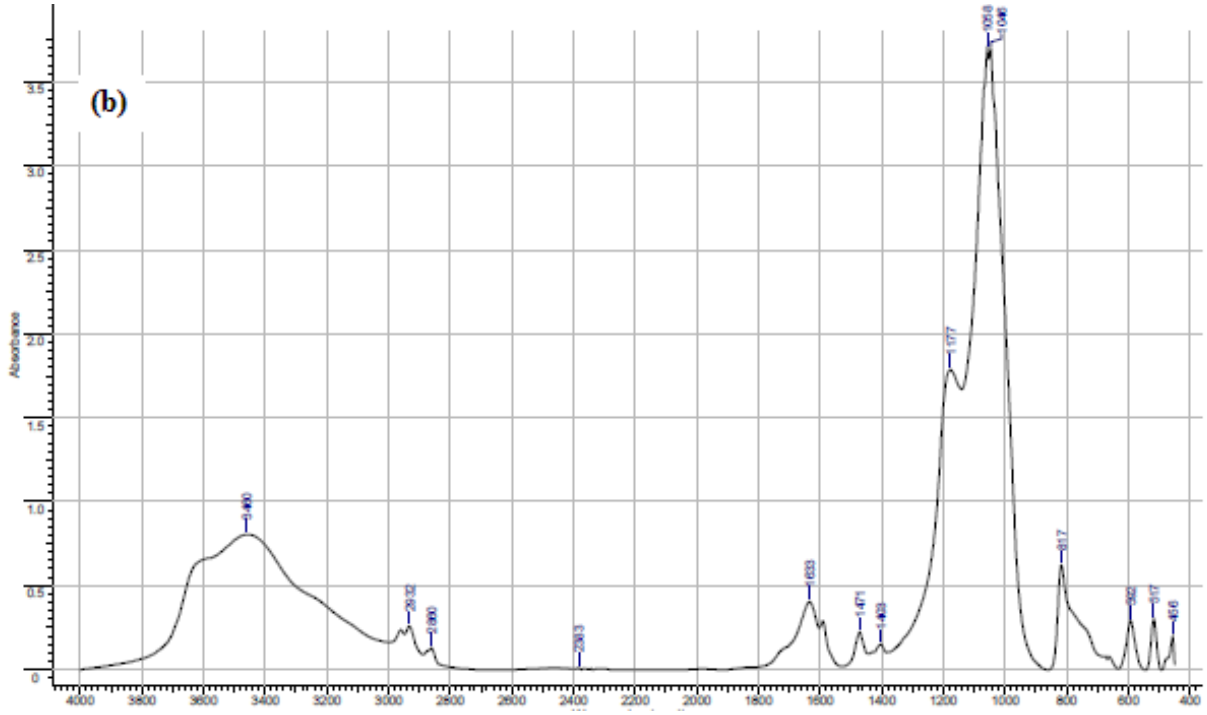

b)

Figure 2. Infrared spectrum of $CM_{PH.TBP}$ (a) and $CM_{PH.TCP}$ (b)

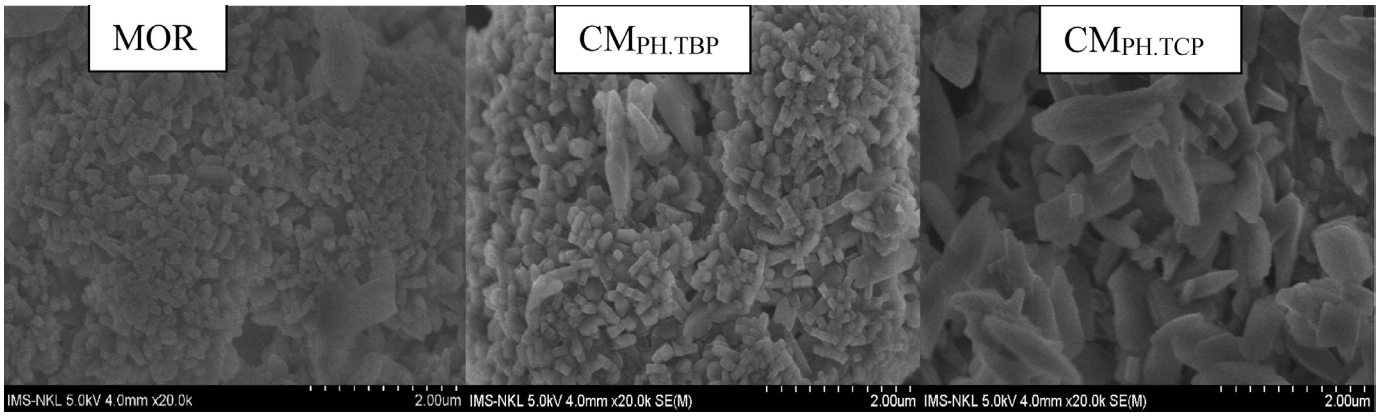

Figure 3. The FE-SEM image of sample MOR; $CM_{PH.TBP}$ and $CM_{PH.TCP}$

For better understanding the changes in the structure of the functionalized zeolite materials, the porosity of the materials was studied via the the nitrogen isothermal adsorption method. The N2 adsorption-desorption isotherms of all sample are presented in (Figure 4).

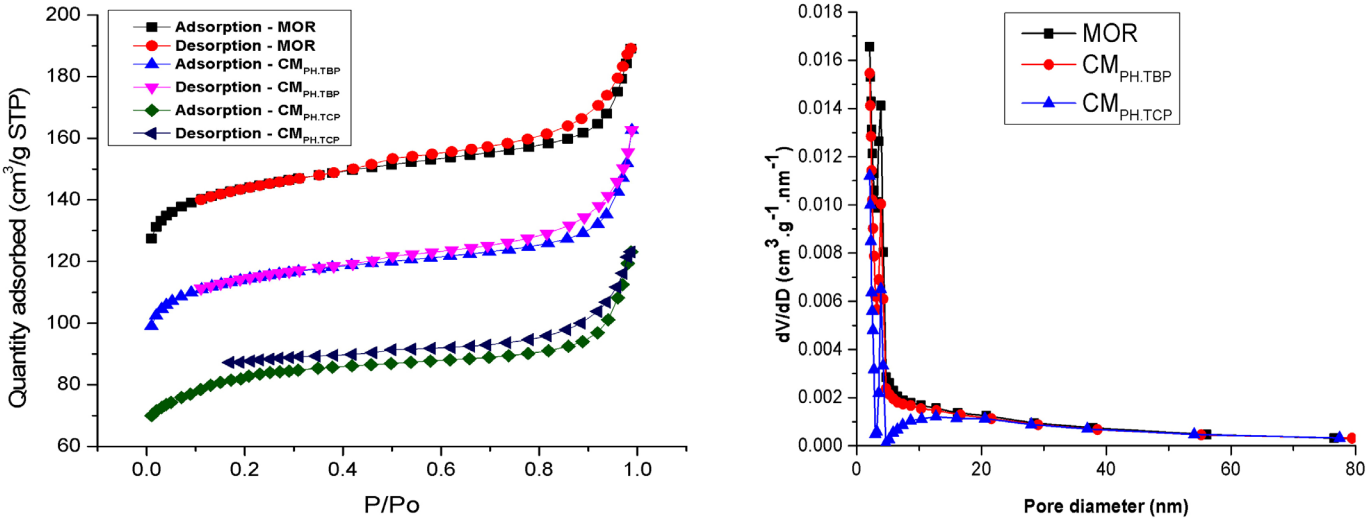

Figure 4. Diagram of the nitrogen isothermal adsorption-desorption line and capillary size distribution of $CM_{PH.TBP}$ and $CM_{PH.TCP}$

Study on the surface properties of functionalized zeolite materials, based on the BET method shows that the nitrogen isothermal adsorption-desorption line of all three samples was of type IV and has hysteresis loop type H2 (as sorted by IUPAC). The belong to materials have medium capillary with hollow both ends cylinders, and corresponding to the Barret-Joyner-Halenda (BJH) hole size distribution.

Figure 4 also shows that desorption line of the samples were relatively smooth, in which the sample $CM_{PH.TBP}$ has the nitrogen isothermal adsorption-desorption line started condensation in the relative pressure P/P_o about 0.5–1.0 demonstrates that the material has a relatively large capillary diameter.

While $CM_{PH.TCP}$ sample of late loop is not closed loop at low pressure of P/P_o, indicating the presence of organic agents in the sample alters TCP ring latency, as well as changes in the distribut ion of the capillary size of the sample than the sample of $CM_{PH.TBP}$ (Dongjiang Yang et al. [8]).

In which, the specific surface area and average capillary diameter of sample MOR; $CM_{PH.TBP}$

and $CM_{PH.TCP}$ are 474.47 m^2/g; 329.65 m^2/g; 385.40 m^2/g and 2.4614 nm; 2.6479 nm and 2.5878 nm respectively. Based on the above results, the $CM_{PH.TCP}$ material has the smallest surface area, with the largest average capillary size, indicating a greater percentage of capillary size than the percentage of large capillary size of both MOR and $CM_{PH.TBP}$ material. This shows that the functionalized zeolite material based on MOR zeolite and TCP organic matter, TCP acts as a framework for the formation of large capillary sizes and also as a VOCs vapor conductor when applied in later processing.

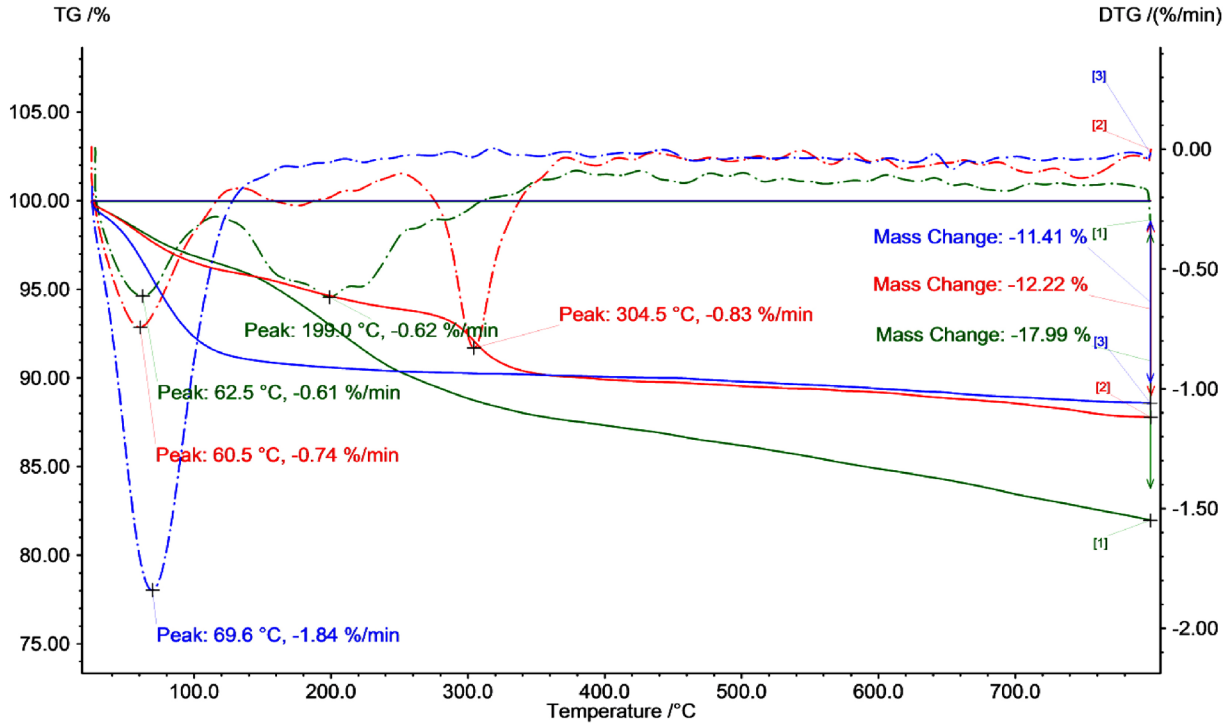

Figure 5. TG and DTA plots of$CM_{PH.TCP}$ [1]), $CM_{PH.TBP}$ ([2]) and MOR ([3])

TG and DTA curves (figure 5) show that, when rising room temperature to 300° C, the sample mass decreases rapidly. In both samples, the effect of heat recovery was 199.0 ° C ($CM_{PH.TBP}$) and 304.5° C ($CM_{PH.TCP}$). This effect may be the escape of organic solvent or water vapor in the capillary structure of the studied materials. Continuously increasing the temperature to more than 300° C, the studied materials have reduced mass, but the $CM_{PH.TCP}$ and $CM_{PH.TBP}$ have more mass reduction than the MOR.

From the results of the study, there are differences in the thermal effect at these two temperatures, due to the different physicochemical properties of the two compounds. In particular, the TCP agent has a molecular weight of 368.37 g/mol and a flammability temperature of 220° C. The TBP agent has a molar mass of 266.32 g / mol and is particularly flammable at 146° C is much lower than the TCP counterpart, so the thermal effect of the material $_{PH\ PH.TCP}$ occurs at a higher temperature than the thermal effect occurs with the material $CY_{PH.TBP.}$

Noteworthy, the particle size of the material is almost the same as that of the zeolite substrate, which shows that the film on the surface of the material is rather thin, with the organic matter deposited on the substrate surface to increase its ability to adsorb subtraction and gas separation of the material, as organic agents both act as carriers and interact with VOCs (Qin HU et al. [19]; Mohamad et al. [16]).

Adsorbability of benzene vapor on zeolite composite materials

Benzene vapor adsorption by the functionalized zeolite matertals was conducted with the gas flow rate from 0.15 L/min to 0.6 L/min at 40 °C, the inlet benzene concentration of 21.8 ppmv and the bed volume of 2.9 mL.

Empty bed contact time is one of the important parameters of an adsorption system. Assuming the flow is ideal, the empty bed contact time is calculated by the following formula (Chaiwat et al. [5]; William et al. [24])

$$EBCT = \frac{V}{f}$$

where *EBCT* is empty bed contact time, s

V – is empty bed volume of the column, L.

f – is the gas flow rate through the column, L/s.

The results are given in table 1 and (Figure 6).

Table 1.– Influence of gas flow rate to the adsorption capacity of $CM_{PH.TBP}$, $CM_{PH.TCP}$

The gas flow rate (L/min)	Contact time (s)	Adsorption capacity of $CM_{PH.TBP}$ (mg/g)	Adsorption capacity of $CM_{PH.TCP}$ (mg/g)
0.15	1.16	1.0607	1.5014
0.30	0.58	1.1005	1.4832
0.45	0.32	0.9973	1.4075
0.60	0.29	0.9012	1.3297

As results showed in (table 1), with the same inlet benzene concentrations, but with lower contact time (about 0.29 s), the adsorption capacity began decrease. It demonstrates the rate of gas flow significantly affects to the adsorption capacity of the materials. Particularly, when the contact time is too short, it shall not guarantee that gas molecules can diffuse through the absorbed material surface. From the above review, we conducted the survey of benzene vapor adsorption process of the materials in the two flow rate 0.15, 0.3 and 0.45 L/min.

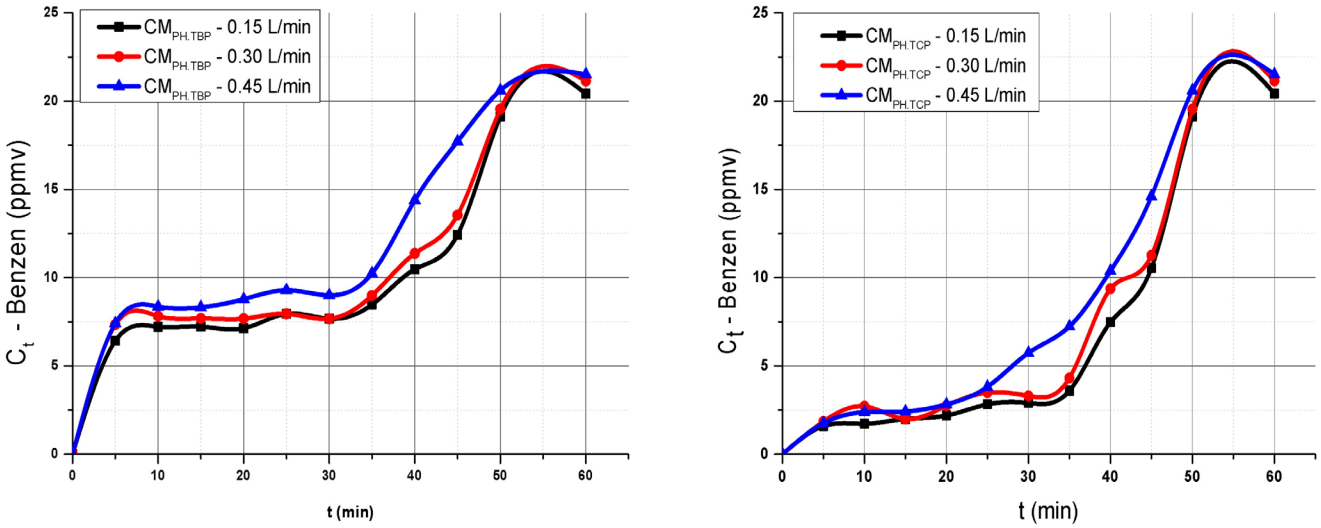

Figure 6. Breakthrough curve of benzene vapor through zeolite composite column at 40 °C

The results also showed that at the flow rate of 0.15 and 0.45 L/min, the adsorption capacity of the materials varied not so much. However, adsorption breakthrough curve is different. The breakthrough curve at a flow rate of 0.45 L/min is more sloping than those of 0.15 L/min and 0.30 L/min. However, the difference of adsorption capacity appeared by the different organophosphorous component in the

material. The composite material with tributylphosphate showed higher adsorption capacity than those with tricresylphosphate.

The investigation was carried out at 40 °C and 50 °C; the initial benzene concentration of 21.8 ppmv and 32.6 ppmv; air flow rate 0.3 L/min; the adsorption fractions were measured after every 5 min.The cumulative curves of benzene vapor on the functionalized zeolite materials are given in (Figure 7).

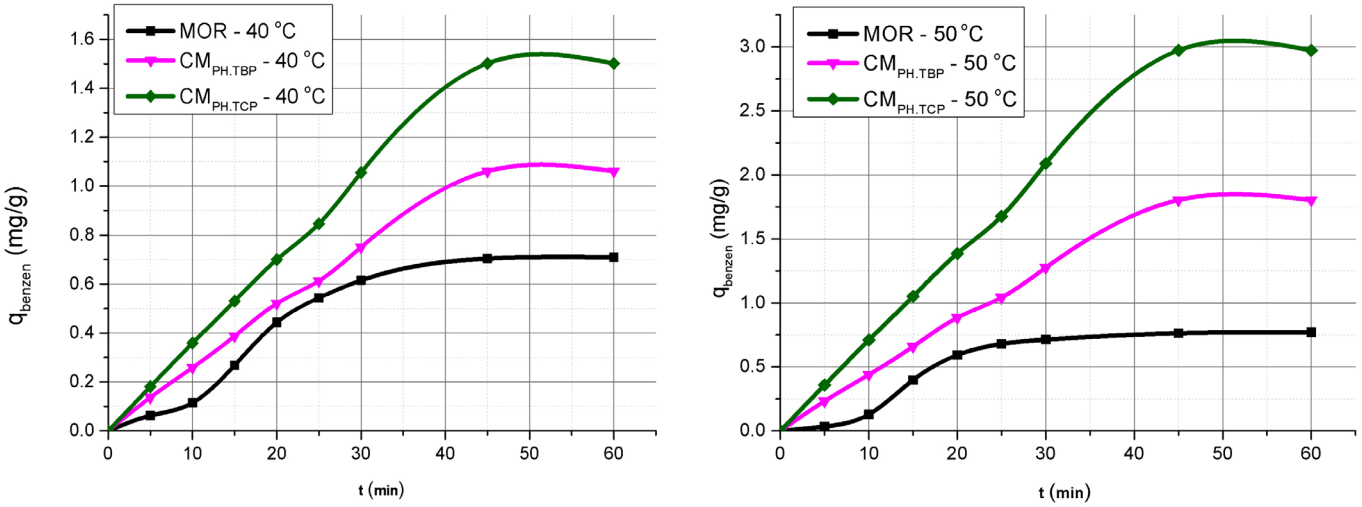

Figure 7. Cumulative curves of benzene vapor on the zeolite composites at 40 °C and 50 °C

The results showed that, increasing of temperature from 40 °C to 50 °C, the adsorption capacity of $CM_{PH.TBP}$ and $CM_{PH.TCP}$ increased, and after maximum 60 min contacted the adsorption process of all materials reached equilibrium state. The adsorption capacity of $CM_{PH.TBP}$ reached 1.0917 mg/g and 1.8031mg/g, and those of $CM_{PH.TCP}$ were 1.5014mg/g and 2.9725 mg/g respectively. This phenomenon seems unaccordant to the adsorption kinetics (temperature increased, the adsorption capacity decreased). In this case, it can be explained by better diffusion of benzene through organophosphorous layer to zeolite core under high temperature and holed in zeolite structure. But actually, the threshold of higher temperature was not determined yet. The adsorption capacity of benzene vapor on $CM_{PH.TCP}$ was better than that on $CM_{PH.TBP}$ and original zeolite. The reason can be explained by that, the IR study showed that the $CM_{PH.TCP}$ has interaction of benzene ring in the TCP agent with benzene vapor, so the dynamic equilibrium adsorption capacity of this material was greater than that of $CM_{PH.TBP}$. According to Qin Hu et al. 2009, the presence of aromatic cyclic agent in the material, its adsorption ability changed, and this was explained by the interaction of electron-π of benzene or phenyl when studied adsorption of benzene on different materials.

Conclusion

This article presents new experimental results on functionalized zeolite material. This material is prepared from zeolite MOR with tributylphosphate ($CM_{PH.TBP}$) and tricresylphosphate ($CM_{PH.TCP}$). As a result, two materials of $CM_{PH.YBP}$ and $CM_{PH.TCP}$ having large specific surface area of 329.65 m^2/g and 385.40 m^2/g with current pore data around 2.6479 nm to 2.5878 nm respectively were obtained. The BET surface area, TG, FT-IR spectra of the functionalized zeolite showed strong interaction between zeolite base and organophosphate substances.

Adsorption of benzene vapor in fixed-bed columns on functionalized zeolite materials, in quite low concentration from 20 ppmv to 40 ppmv and the adsorption time of 0.29 s to 1.16 s, the equilibrium adsorption capacity of $CM_{PH.TBP}$ reached 1.0917 mg/g and 1.8031mg/g, and those of $CM_{PH.TCP}$

were 1.5014mg/g and 2.9725 mg/g corresponding with 40 °C and 50 °C in the adsorption conditions of gas flow rate of 0.3 l/min and input benzene concentration of 21.8 ppmv and 32.6 ppmv.

References:

1. Abdulrahman Bahrami, Hosien Mahjub, Marzieh Sadeghian, Farideh Golbabaei. Determination of Benzene, Toluene and Xylene concentrations in Air using HPLC developed method compared to Gas chromatography. International Journal of Occupational Hygiene 3(1): 2011.– 12 p.
2. Bao – Lian Su, Valérie Norberg. Adsorption behavior of benzene ni NaBeta zeolite: An in-situ Infrared study of molecular recognition. Langmuir 14: 1998.– P. 7410–7419.
3. Bao-Lian Su, Valérie Norberg. Quantitative characterization of H-Mordenite zeolite structure by infrared spectroscopy using benzene adsorption. A: Physicochemical and Engineering Aspects 187–188: 2001.– P. 311–318.
4. Bilge Yilmaz, Ulrich Müller. Catalytic applications of zeolites in chemical industry. Top Catal 52: 2009.– P. 888–895.
5. Chaiwat Rongsayamanont, Khaornak Sopajaree. Modification of synthetic zeolite pellets from Lignite Fly Ash B: Treatability study, World of coal ash, Covington Kentucky – USA. 2007.
6. Coseron A. F. and et. Adsorption of volatile organic compounds in pure silica CHA, BEA, MFI and STT-type zeolites. Microporous and mesoporous materials 173: 2013.– P. 147–154.
7. Dombrowski Jürgen Hoffmann, Johanna Fruwert. Infrared spectroscopic investigation of Hydroxy-group siting in H. Faujasites. J. Chem. Soc., Faraday Trans 1(82): 1995.– P. 2257–2281.
8. Dongjiang Yang, Junping Li, Yao Xu, Dong Wu, Yahan Sun, Huaiyong Zhu, Feng Deng. Direct formation of hydrophobic silica – based micro/mesoporous hybrids from polymethylhydrosiloxane and tetraethoxysilane. Microporous and Mesoporous Materials 95: 2006.– P. 180–186.
9. Fabien Jousse, Scott M. Auerbach, Daniel P. Vercauteren. Adsorption sites and diffusion rates of benzene in HY zeolite by force field based simulations. J. Phys. Chem B104: 2000.– P. 2360–2370.
10. Guillaume Rioland, Habiba Nouali, T. Jean Daou, Delphine Faye, Joel Patarin. Adsorption of volatile organic compounds in composite zeolites pellets for space decontamination. Journal of the internation adsorption society 23(2–3): 2017.– P. 394–403.
11. Robsin H. Verified synthesis of zeoliteic materials, Elsevier Science B.V: 2001.– P. 69–71.
12. Huanhao Chen, Huiping Zhang, and Ying Yan Catalytic combustion of volatile organic compounds over a structured zeolite membrane reactor. Ind. Chem. Res 52(36): 2013.– P. 12819–12826.
13. Huanhao Chen, Huiping Zhang, Ying Yan. Preparation and characterization of a novel gradient porous ZSM-5 zeolit membrane/PSSF composite and its application for toluene adsorption. Chemical engineering journal 209: 2012.– P. 372–378.
14. Ichiura H., Nozaki M., Kitaoka T., Tanaka H. Influence of uniformity of zeolite sheets prepared using a papermaking technique on VOC adsorptivity. Advances in Environmental research 7: 2003.– P. 39–979.
15. Zoccolillo L. Alessandrelli M., Felli M. Simulataneous determination of Benzene and total aromatic fraction of Gasoline by HPLC-DAD. Chromatographia 54: 2001.– P. 659–663.
16. Mohamad H. Kassaee, David S. Sholl, Sankar Nair. Preparation and gas adsorption characteristiecs of zeolite MFI crystals with organic – functionalized interiors. The Journal of Physical chemistry 115: 2011.– P. 19640–19646.

17. Mohamed Mkhtar Mohame, Tarek M. Salama. Effect of mordenite dealumination on the structure of encapsulated molybdenum catalysis. Journal of Colloid and interface science 249: 2002.– P. 104–112.
18. Nguyen Thi Huong, Vo Hoang Phuong, Tran Hong Con, Le Thanh Son, Dang Thi Uyen. Removal posibility of benzene vapour in the air by zeolite HY composite. Austrian journal of technical and Natural sciences 1–2: 2018.– P. 63–71.
19. Qin Hu, Jin Jun Li, Zheng Ping Hao, Lan Dong Li, Shi Zhang Qiao. Dynamic adsorption of volatile organic compounds on organofunctionalized SBA-15 materials. Chemical engineering journal 149: 2009.– P. 281–288.
20. Ramiro M. Serra, Eduardo E. Miró, Pablo Bolcatto, Alicia V. Boix. Experimental and theoretical studies about the adsorption of toluene on ZSM5 and mordenite zeolites modified with Cs. Microporous and Mesoporous Materials 147: 2012.– P. 17–29.
21. Satoshi Yamazaki, Kazuao Tsutsumi. Adsorption characteristic of synthesized mordenite membranes. Adsorption 3: 1997.– P. 165–171.
22. Shruti Mishra, Jaya Dwivedi, Arma Kruma and Nalini San Karamakrishnan. The synthesis and characterization of tributyl phosphate grafted carbon nanotubes by the floating catalytic chemical vapor deposition method and their sorption behavior towards uranium. New. J. Chem 40: 2016.– P. 1213–1221.
23. Shuai Ban – Utrecht University, Utrecht, Netherlands. Computer Simulation of zeolites: Adsorption, diffusion and dealumination. 2009.
24. William F. Naylor, Dennis O. Rester. Determining activated carbon performance, Pollution Engneering: 1995.– P. 28–29.

Urinov Ulugbek Komiljonovish,
associate professor
Tashkent chemical-technological institute
Maksumova Oytura Sitdikovna,
Doktor of Chemistry, professor
Tashkent chemical-technological institute
E-mail: omaksumovas@mail.ru

COPOLYMERIZATION OF ACRILONITRILE WITH DIFFICULT ETHERS (MET)ACRYLIC ASIDS

Abstract. This article presents the results of the study of fiber-forming copolymers based on N-morpholine-3-chloroisopropyl acrylate and isohexyl methacrylic ester with acrylonitrile.

Keywords: copolymer, unsaturated esters, acrylonitrile, radical polymerization, initiator.

Introduction

Chemical, textile, aircraft and mechanical engineering and a number of other industries are in dire need of structural materials based on carbon fibers, one of which is polyacrylonitrile fibers. The mechanical properties of PAN fibers are very close to wool, and in this respect they are superior to all other chemical fibers. Polyacrylonitrile fibers have a good range of consumer properties. Polyacrylonitrile fibers, in particular nitrone, attracts the attention of many researchers due to their availability. They are often called "artificial wool". They have maximum light resistance, high strength and relatively high tensile properties (22–35%). The disadvantages of polyacrylonitrile (PAN) fibers are their low hygroscopicity, relatively high rigidity and electrification [1, 19–22; 2, 26–30].

Findings and their discussion

It is known that an effective method of imparting specific properties to chemical fibers is an includation modification carried out in the process of their production. In this regard, we were interested in the synthesis of binary fiber-forming copolymers on the bases of acrylonitrile with heterofunctional compounds. As the nitrogen and oxygen-containing reagent selected unsaturated ester – N-morpholine-3-chloroisopropylacrylate (MHIPA) [3, 88]. Its synthesis was carried out according to the following reaction: and as the oxygen-containing isohexyl methacrylic ester (IHMEA) [4, 260–261]. The scheme of its formation was carried out according to the following scheme:

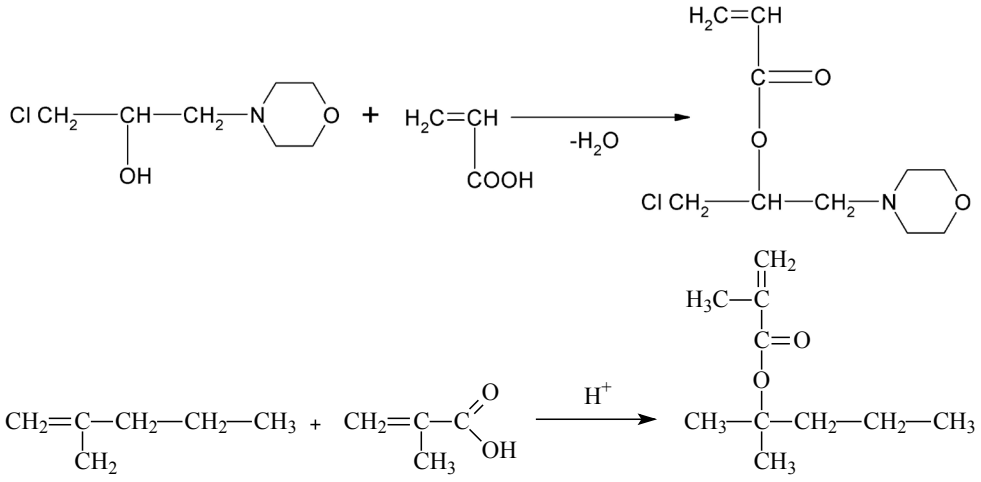

The structure of the obtained compounds was determined by IR-spectral analysis (table 1).

Table 1. Results of IR-spectr of the synthesized connections

№	Name of compound	IR-spectrum		
		C=C	C=O	C-O-C
1.	MHIPA	1642	1728	1297
2.	IHMEA	1636	1730	1280

The copolymerization of acrylonitrile with N-morpholine-3-chloroisopropyl-acrylate and isohexylmethacrylic ester was carried out in organic solvents in the presence of dinitrilazobisisobutyric acid initiator (DAK). In the technology of producing nitron fibers, aprotic solvents are most widely used: dimethylformamide, dimethylacetamide, dimethyl sulfoxide, 51.5% aqueous solution of NaSCN. However, dimethylformamide and dimethylsulfoxide are the most promising solvents in the copolymerization of acrylonitrile, since they are the most accessible and less toxic in comparison with aqueous solutions of sodium thiocyanate. In this regard, dimethylformamide and dimethyl sulfoxide are chosen as the solvent.

The copolymerization of acrylonitrile with the above comonomers was investigated by the gravimetric method at temperatures of 50–70 °C. The influence of the duration of the copolymerization reaction on the yield of the resulting copolymer was studied (fig. 1).

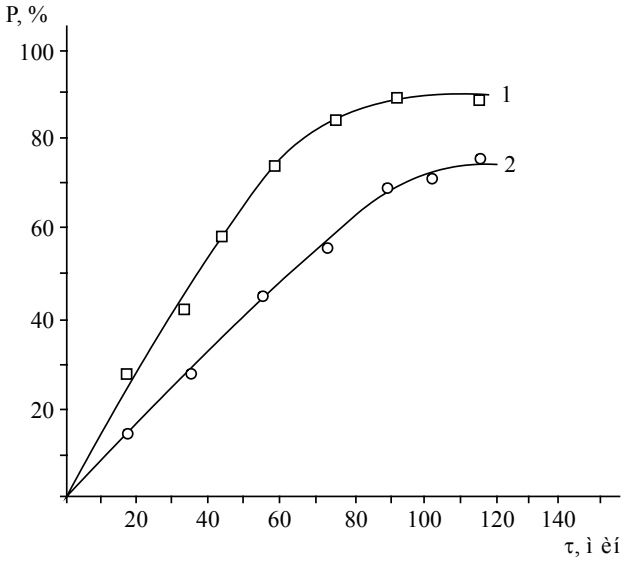

Figure1. Dependence of the yield of copolymer based on acrylonitrile with isohexyl methacrylate ether at a ratio of: 1–0.97: 0.03; 2–0.95: 0.05 mole fraction, T = 60 °C; DMSO solvent

As can be seen from the figure, with a ratio of acrylonitrile: IHMEA equal to 0.97:0.03, the highest reaction rate is observed.

In studies, the duration of the polymerization process was changed (60, 120, 150, 180 min.) and the composition of the copolymer – AN: MHIPA and AN: IHMEA = 0.95: 0.05; 0.97: 0.03 mole fraction (table 2).

The samples were obtained in the form of films by dissolving the copolymer in dimethylformamide, followed by casting. Analysis of the results showed that the optimum polymerization time is 150 minutes. During this period, when the content in the reaction mass was 0.03 mole fraction of the indicated esters, the copolymer yield was 95–97%. It was experimentally established that radical polymerization

of acrylonitrile with N-morpholin-3-chloroisopropyl acrylate and isohexylmethacrylic ether proceeds at high speed in the presence of DAA in dimethyl sulfoxide condition.

Table 2. Dependence of the composition of acrylonitrile copolymers on the ratio of monomers in the initial mixture. DAK = $5 \cdot 10^{-2}$ mole/l, T = 60 °C, DMFA

The initial ratio of monomers, mole fraction		**Yield,%**	**Composition of copolymer, mole fraction**	
M_1	**M_2**		**m_1**	**m_2**
AN: IHMEA				
0.95	0.05	97.0	0.86	0.14
0.97	0.03	86.0	0.90	0.10
AN: MHIPA				
0.95	0.05	98.5	0.81	0.19
0.97	0.03	97.0	0.88	0.12

The main parameters of polymerization in solution: temperature, 50–70 °C; duration, h: 2–4. Synthesis of a binary copolymer based on acrylonitrile with isohexyl methacrylate ether proceeds by a chain radical polymerization mechanism in three stages using as the initiator – DAA. The homogeneous copolymerization of acrylonitrile in solution is well described by the general scheme of radical polymerization, which includes the stages of initiation, growth, transfer, and chain termination.

1. The formation of an active radical. At the initiation stage, free radicals are formed in the reaction system, which are capable of adding monomer molecules:

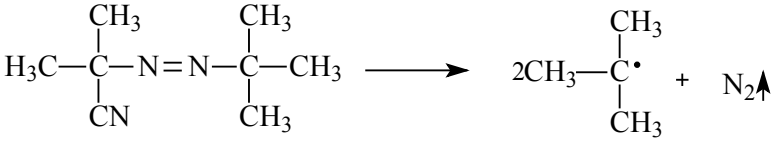

2. Chain growth occurs as a result of sequential addition of monomer molecules first to the primary radical formed at the initiation stage, and then to the growing chain:

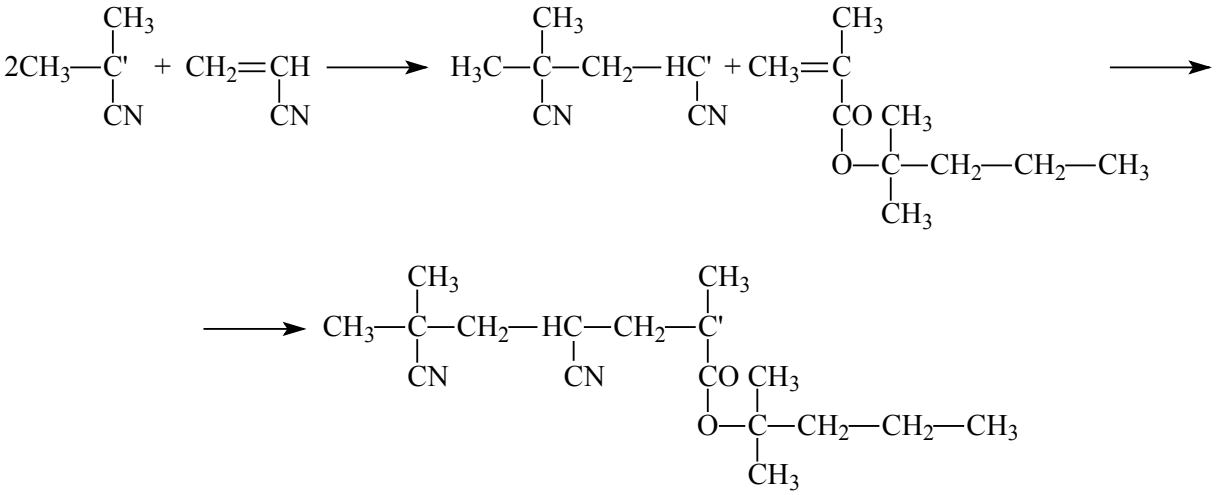

3. Chain breakage occurs during the bimolecular interaction of macroradicals by the recombination mechanism and the structure of the copolymer can be represented as follows:

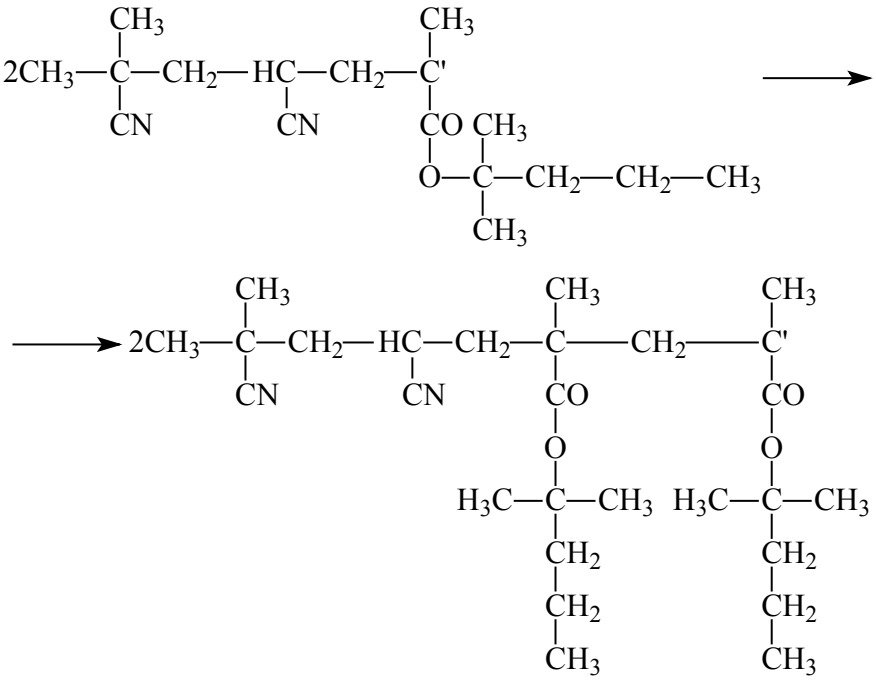

The chemical structure of the obtained copolymers is confirmed by the data of IR-spectral analysis. In the IR-spectra of copolymers based on acrylonitrile with isohexylmethacrylic ether, absorption bands were found in the region of 2900–3000 cm^{-1}, which belong to methylene and methyl groups. The characteristic absorption bands of the nitrile groups (CN) are in the region of 2250–2260 cm^{-1}, the stretching vibrations of the ester group in the region of 1100 and 1300 cm^{-1}, and the absorption bands in the region of 1655 cm^{-1} correspond to the stretching vibrations of the carbonyl group. The absence in the spectra of the absorption bands of double bonds C=C at 1600–1670 cm^{-1} indicates that the reaction proceeds beyond the opening of the double bonds of both monomers.

Conclusion

The radical copolymerization of acrylonitrile with N-morpholine-3-chloroisopropylacrylate and isohexylmethacrylic ester was studied. The influence of the ratio of the initial monomers on the yield of the final product was studied

References:

1. Mukhamedjanova M. Yu., Shirshova N. Yu., Nikonovich G. V. Structural, physicomechanical and sorption properties of fibers from acrylonitrile terpolymers // Chemical fibers.2000.–No. 3.–P.19–22.
2. Serkov A. T., Budnitsky G. A., Radishevsky M. B., Medvedev V. A., Zlatoustova L. A. Ways to improve the technology of carbon fiber production // Chemical fiber, 2003.–No. 2.– P. 26–30.
3. Maksumova O., Urinov U. Synthesis of Derivatives of morpholinium with acrylic and metakrilovy asids // International conference on thermophysical and mechanical properties of advanced materials, 2014. Izmir, – Turkey.– 88 p.
4. Makhmudova F. A., Maksumova O. S. Search for the availability of olefins // The Regional Central Asian international conference on chemical technology of KhT-12. on March, 27–28, 2012. – Tashkent, 2012.– P. 260–261.

Contents